Facile Fabrication of Meso-to-Macroscale Single-Molecule Arrays for High-Throughput Digital Assays

by

Rishabh Manoj Shetty

A Dissertation Presented in Partial Fulfillment
of the Requirements for the Degree
Doctor of Philosophy

Approved July 2019 by the
Graduate Supervisory Committee:

Rizal F. Hariadi, Chair
Ashwin Gopinath
Arvind Varsani
Mehdi Nikkhah
Stephen Helms Tillery
Ye Hu

ARIZONA STATE UNIVERSITY

August 2019

ABSTRACT

One of the single-most insightful, and visionary talks of the 20th century, “There’s plenty of room at the bottom,” by Dr. Richard Feynman, represented a first foray into the micro- and nano-worlds of biology and chemistry with the intention of direct manipulation of their individual components. Even so, for decades there has existed a gulf between the bottom-up molecular worlds of biology and chemistry, and the top-down world of nanofabrication. Creating single molecule nanoarrays at the limit of diffraction could incentivize a paradigm shift for experimental assays. However, such arrays have been nearly impossible to fabricate since current nanofabrication tools lack the resolution required for precise single-molecule spatial manipulation. What if there existed a molecule which could act as a bridge between these top-down and bottom-up worlds?

At ~100-nm, a DNA origami macromolecule represents one such bridge, acting as a breadboard for the decoration of single molecules with 3-5 nm resolution. It relies on the programmed self-assembly of a long, scaffold strand into arbitrary 2D or 3D structures guided via approximately two hundred, short, staple strands. Once synthesized, this nanostructure falls in the spatial manipulation regime of a nanofabrication tool such as electron-beam lithography (EBL), facilitating its high efficiency immobilization in predetermined binding sites on an experimentally relevant substrate. This placement technology, however, is expensive and requires specialized training, thereby limiting accessibility.

The work described here introduces a method for bench-top, cleanroom/lithography-free, DNA origami placement in meso-to-macro-scale grids using tunable colloidal nanosphere masks, and organosilane-based surface chemistry modification. Bench-top DNA origami placement is the first demonstration of its kind which facilitates precision placement of single molecules with high efficiency in

diffraction-limited sites at a cost of $1/chip. The comprehensive characterization of this technique, and its application as a robust platform for high-throughput biophysics and digital counting of biomarkers through enzyme-free amplification are elucidated here. Furthermore, this technique can serve as a template for the bottom-up fabrication of invaluable biophysical tools such as zero mode waveguides, making them significantly cheaper and more accessible to the scientific community. This platform has the potential to democratize high-throughput single molecule experiments in laboratories worldwide.

I dedicate this thesis to my pillars of strength and sanity—my family, and friends—but first, to some standout mentions starting with Sabita M. Shetty, and Manoj R. Shetty, my parents. The former may not always understand what I do or why I do it but empowers me to soldier on regardless, standing by me and my decisions no matter what. I have grown more through learning from your evolution than anything else in this world, and I am immensely proud of you and your journey. The latter gives me the strength to face any challenge through his omnipresence, constantly enveloping me with the knowledge that while it may not always seem that way, as long as I am honest and keep at it, everything will eventually be okay. Lastly, I dedicate this to my brother, Advait Krishna, who now understands how much I have always loved and looked up to him. Unintentionally, he taught me that it's not how long you live, but how well you do. Papa, and Anna, I am grateful for your constant guiding presence. You two embody the impermanence of life and have shown me that we are human first, much before we are our standing in the material world. I thank the three of you for affirming that some things transcend distance, borders, time, even life and death. For everything else, there's MasterCard.

I would be lost without the following people- my family in the US, my cousin, Deepti aka mummy. My best friend for over ten years, and roommate for five, Meryl. I am grateful that we have shared this journey together and grown through it. My childhood friend, Sheron, who has been my pillar through thick and thin; without judgement. Akshay, and Anup, you have my heart. Mansa, you have been a great source of inspiration. Baatli, and Rach, thanks for always making me smile. Pouya, Farzaneh, Sway, Sam, Kalyani, and Harpinder- thanks for reminding me that the little things and breaks matter. Tapappa, Ammamai, Di, Nandita, Bina periammai, Krishna periappa, thank you for being patient with me on my visits back. I will never know if living so many years away from home was worth not spending much time with all of you. I love you all unconditionally.

ACKNOWLEDGMENTS

Unless one is exemplarily gifted in the art of stoicism, I believe it is nearly impossible to endure the long, and arduous journey of graduate life alone. A journey such as this allows you the freedom to fall to pieces and put yourself back together multiple times. The people you meet along the way are integral to this process. I would like to take this opportunity to thank all those who have played a part, big or small, in shaping my present.

First, I thank my adviser, Dr. Rizal F. Hariadi, who took a chance on me during a time that I needed it most. I hope that I have repaid his faith with the work presented in this dissertation. He has my respect first and foremost as a person, and for his child-like enthusiasm, open-mindedness, out-of-the-box thinking, and a unique passion for merging art with science. I have learnt a lot from him about scientific philosophy, the rewards of collaboration, and the importance of mentoring future scientists. The last two years would not have been the same without your guidance, support, and belief in me and this project.

Next, I would like to thank Ashwin Gopinath for helping accelerate my development as a scientist and instilling a healthy sense of apprehension about my data which helped me stay grounded and pragmatic about my work. I am very excited about exploring and tackling other important questions with you in the next phase of my career. Another person I cannot wait to work more with is Paul Rothemund. For someone like him to be so humble and approachable is inspiring beyond compare. I would also like to thank our collaborators at Stanford University- Dr. Manu Prakash, and Hongquan Li for their help with the low-cost microscope used in the diagnostics project.

I would like to gratefully acknowledge all of my committee members: Dr. Mehdi Nikkhah, Dr. Stephen Helms Tillery, Dr. Tony Hu, Dr. Arvind Varsani, and Dr. Vikram Kodibagkar for their insightful comments and guidance related to my research.

It has been one of the greatest pleasures of my life as a graduate student to be part of the Hariadi lab. I thank my fellow graduate students, Franky Djutanta, Swarup Dey, and Devika Kishnan for their help and support. I am also grateful to have had the opportunity to mentor Sarah Brady, Eric Le, Kenna McRae, Gabby Hirneise, Tal Sneh, and Maeve Kennedy during my time in the lab. I feel extremely proud to see them mature into curious scientists, ready to take responsibility of a project and see it through to the end.

I would like to thank all the members of the Center for Molecular Design and Biomimetics but especially Jia-Ming Li, Kristen Lee, and Shuoxing Jiang. Jia-Ming, you are the star of this show. Mike Dodson, thank you for being such a joy to work with. The Biodesign Institute is a special place and having worked in the building for over seven years, it feels like home. I am thankful for the kindness and generosity of everyone, from the security guards, IT/RTS, facilities, HR, to the leadership teams, and all the centers.

I would like to thank the wonderful staff in the Center for Solid State Electronic Research (CSSER) for all their help over the years; a special shout-out to Carrie Sinclair, and Stefan Myhajlenko for being so wonderful.

I would also like to thank all of the faculty and staff in my home department, the School of Biological and Health Systems Engineering, but especially Laura Hawes, and Dr. Christopher Buneo for their constant guidance, and support through difficult periods.

Even though my time at The Center for Biosignatures Discovery and Automation was a mix of highs, and lows, I would like to thank everybody for their contribution to my growth as a scientist, and person. I would like to especially thank Dr. Roger Johnson, and Dr. Laimonas Kelbauskas for their mentorship, and kindness.

Finally, I would like to acknowledge the support of the Arizona Biomedical Research Commission's New Innovator Award through which most of the work in this dissertation was funded. I sincerely apologize if I have forgotten to acknowledge anyone.

TABLE OF CONTENTS

Page

CHAPTER Page

CHAPTER Page

LIST OF TABLES

LIST OF FIGURES

Figure Page

PREFACE

This dissertation includes original research currently being prepared for submission by the primary author. Chapter 2, and 3 present a novel, bench-top single molecule nanoarray fabrication technology based on bottom-up self-assembly techniques and discuss its applications for high-throughput single molecule biophysics studies (R.M. Shetty, S. Brady, E. Le, M. Kennedy, P.W.K. Rothemund, R.F. Hariadi, A. Gopinath, "A facile, cleanroom-free DNA origami nanoarray platform for non-Poisson digital assays"). Chapter 4 presents results comprising a proof-of-concept of this platform as a low-cost diagnostic tool for the digital detection of nucleic acid biomarkers (R.M. Shetty, T. Sneh, S. Brady, A. Gopinath, R.F. Hariadi, "A DNA origami-based single molecule nanoarray platform for enzyme-free digital biomarker detection at the point-of-care").

CHAPTER 1* BACKGROUND AND RESEARCH OBJECTIVES

1.1 Introduction

1.1.1 DNA origami nanotechnology

In 2006, Paul Rothemund at Caltech first demonstrated the folding of long, single-stranded viral DNA scaffolds in solution with hundreds of short staple strands into programmed shapes ~100-nm across (Rothemund 2006). Subsequent work in the field of DNA nanotechnology has underlined the potential of DNA origami nanostructures to act as multifunctional breadboards or substrates. These nanostructures are capable of integrating electronic components such as carbon nanotubes (Maune, Han et al. 2010), optical components such as quantum dots (Ding, Deng et al. 2010) (Pal, Deng et al. 2010), and biological components such as myosin motors (Derr, Goodman et al. 2012, Elting, Leslie et al. 2013, Hariadi, Cale et al. 2014, Hariadi, Sommese et al. 2015, Tee, Shemesh et al. 2015) with unprecedented precision for their respective applications. Some origami-based techniques have already demonstrated their biological relevance as biosensors (Fu, Liu et al. 2012, Godonoga, Lin et al. 2016). While certain challenges, especially in terms of the size-limit of origami nanostructures remain (Pinheiro, Han et al. 2011), the advantages in terms of the technique's modularity and multi-functionality are evident. The ability to recruit relevant biological molecules conjugated to *ss*DNA linkers and bind these components to complementary linkers on the origami is a particularly powerful asset of this technology. Origami-bound, aptamer-mediated logic gates (Yang, Jiang et al. 2016) and biomarker detection (Godonoga, Lin et al. 2016) are examples of the breadth and diversity of DNA nanotechnology applications. Simply put, any molecule/ligand that can

* Some parts of this chapter appear in an unfunded NSF grant proposal, and two manuscripts in preparation.

be coupled to DNA, from small proteins to large aptamers, can be incorporated into a DNA origami macromolecule in a programmable and addressable fashion. Their size, modularity, and multi-functionality make DNA origami ideally suited for patterning on a substrate for single-molecule experimental assays – a technique that has heretofore required micro-or-nanofabrication technologies.

1.1.2 DNA origami placement (DOP)

Prior work from the Rothemund lab in collaboration with IBM overcame a severe limitation with the ability to use DNA origami breadboards for real-world applications (Kershner, Bozano et al. 2009). Briefly, owing to the solution-phase self-assembly of origami and its incorporated components, it is difficult to integrate them into larger assembly-level systems built on-chip or on glass surfaces with any control over their spatial addressability. The advent of DNA origami placement (DOP) technology (Kershner, Bozano et al. 2009, Gopinath and Rothemund 2014) enabled the precise, nanometer-scale positioning of DNA origami on a variety of technologically useful substrates such as silicon, silicon dioxide, silicon nitride, and quartz. This technology works through the application of nanofabrication techniques such as EBL to physically write binding sites onto an electron-beam sensitive chemical/resist. Standard chemical passivation strategies can be used to create negatively charged surfaces at these pre-defined binding sites – lithographically size-matched to immobilize the ~100 nm origami macromolecule. Positively charged magnesium ions (Mg^{++}) act as bridges between the two negative components: the placement substrate, and origami. Large-scale 2D arrays of DNA origami can thus be created on these surfaces, loading >95% sites with exactly one DNA origami nanostructure. Magnesium concentration required for immobilizing origami is dependent on the binding site chemistry and can be as low as 4-8 mM to as high as 125 mM. Photonic Crystal Cavities (PCCs) with precisely positioned DNA origami

devices (Gopinath, Miyazono et al. 2016) have been fabricated using this DNA placement technology. DNA origami has perhaps been accurately described as a “bridge” from the bottom to the top in recent years (Xu, Harb et al. 2017). Accessibility can be drastically improved by retaining the surface chemistry (Mg^{++} bridging two negative surfaces) characteristic of DOP but replacing the EBL technique with a more basic yet equally effective bottom-up, self-assembly-based technology. This will enable precision placement on a bench-top and allow device fabrication in any conventional laboratory setting.

1.1.3 Nanosphere Lithography (NSL)

The use of colloidal particles to form lithographic ("stone-writing" in Latin) masks in a technique known as Natural Lithography was first introduced in 1983 (Deckman 1983). For the first demonstration of a nanometer-scale Periodic Particle Array (PPA) fabricated via bench-top self-assembly of molecular materials in 1995, the technique was renamed Nanosphere Lithography (NSL) (Hulteen and Duyne). Because optical lithography was limited by diffraction, electron-beam lithography was the gold standard for nanofabrication (Craighead and Mankiewich 1982, Craighead and Niklasson 1984). However, its serial processing format was a severe limitation for commercially acceptable throughput, and a parallel processing paradigm such as NSL was highly desired. NSL is capable of patterning on a variety of substrates such as insulators, semiconductors, and metals with excellent inter-particle spacing/pitch. It is compatible with both inorganic and organic materials for formation of PPAs. Such a hybrid approach to lithography based on inexpensive self-assembly combines the advantages of both “top-down” and “bottom-up” paradigms to maximize its utility as a nanometer-scale precision patterning tool (Colson, Henrist et al. 2013).

In NSL, a flat, hydrophilic substrate (such as glass) is coated with a monodisperse colloidal suspension of spheres (e.g. Polystyrene), and upon drying, a hexagonal-close-packed (HCP) monolayer/bilayer called a Colloidal Crystal Mask (CCM) is formed. This mask is then used to selectively pattern the substrate by depositing the material-of-interest in the interstitial spaces between the close-packed spheres. Attractive capillary forces and convective nanosphere/microsphere transport are the dominant factors in the self-assembly process. However, the ordering and quality of the assembled arrays are substantially affected by the rates of solvent evaporation (Denkov, Velev et al. 1992, Kralchevsky and Denkov 2001). Control over the temperature and humidity of the system on a slightly tilted substrate can yield colloidal monolayers (Micheletto, H.Fukuda et al. 1995). Conversely, low control over this process often yields undesirable multilayers of colloidal particles. Methods such as spin coating (Colson, Cloots et al. 2011), Langmuir-Blodgett deposition (Grandidier, Weitekamp et al. 2013), and controlled evaporation (Zhang and Xiong 2007) have all been used to assemble large-scale monolayers of colloidal suspensions. A variety of nanostructures and devices can be fabricated by etching or annealing of these monolayers. Some of the applications of NSL structures are in optics, photonics (e.g. solar cell fabrication), plasmonics (e.g. biomolecular binding events in metal nanoapertures), optoelectronics, microelectronic engineering, and biomimetic surfaces (Vogel, Weiss et al. 2012, Cong, Yu et al. 2013, Geng, Wei et al. 2014, Lotito and Zambelli 2017). A modified NSL technique could potentially use the 0.2–0.3D (D = diameter of nanosphere) “footprint” of nanospheres as observed from previously published micrographs (Grandidier, Weitekamp et al. 2013) to exert precise control over single origami-binding comparable to that achieved via EBL.

1.1.4 Stochastic single-molecule biophysics (SMB)

Single-molecule methods are powerful tools that enable the study of dynamic molecular processes without the ensemble averaging inherent in bulk population measurements (Ritort 2006). Therefore, they allow heterogeneity within a population of molecules to be probed and reveal dynamic instability inherent in cellular processes (Coelho, Maghelli et al. 2013). These methods are capable of visualizing cellular processes with high spatial and temporal resolution down to nanometer- and tens to hundreds of milliseconds- precision owing to advancements in microscopy techniques, camera sensor technology, and image processing over the last few decades. Depending on the molecule-, process-, and cellular region-of-interest, single molecules can be observed using conventional widefield microscopy, or the more widely used Total Internal Reflection Fluorescence Microscopy (TIRF-M) for large populations of molecules. Sub-diffraction limit microscopy (Huang, Bates et al. 2009), however, relies on localization-based techniques which either modulate the Point Spread Function of the excitation beam – Structured Illumination Microscopy (SIM), or excite only a fraction of the molecules in a given sample – Photo-Activated Localization Microscopy (PALM), Stochastic Optical Reconstruction Microscopy (STORM), or Stimulated Emission-Depletion Microscopy (STED). Single-molecule Forster Resonance Energy Transfer (FRET) is a specialized technique which enables the detection of conformational changes in the same molecule or two molecules separated by a distance of <10-nm through non-radiative energy transfer between a donor and acceptor fluorophore in close proximity to each other. It has been used for a wide range of applications ranging from the study of Holliday Junction dynamics (Ha 2001, Roy, Hohng et al. 2008) to protein folding and unfolding. DNA-Points Accumulation for Imaging in Nanoscale Topography (PAINT) (Dai, Jungmann et al. 2016, Jungmann, Avendano et al. 2016, Schnitzbauer, Strauss et al. 2017, Stehr, Stein et al. 2019) is a DNA origami-based

stochastic super-resolution imaging technique which is decoupled from dye photophysics by the "blinking" events originating from transient interactions of short, fluorophore-labeled *ss*DNA strands in solution with strands hosted on immobilized DNA origami nanostructures on a glass substrate. This technique is primarily used for molecular counting and for revealing sub-diffraction patterns programmatically arranged on DNA origami molecules.

All of these *in vitro* SMB experiments are stochastic in nature and mostly facilitated through biotin-streptavidin mediated immobilization of single molecules on glass. This leads to the possibility of two or more molecules binding to the same diffraction-limited location and confounding data analysis. While this may present less of a challenge for a super-resolution technique such as DNA-PAINT, it has detrimental effects on most other diffraction-limited single-molecule experiments. DNA origami nanotechnology is modular, spatially-programmable, and capable of organizing various biological and non-biological molecules of interest. DNA origami placement therefore represents a straightforward route towards making traditionally stochastic SMB experiments more deterministic and high-throughput in nature through the controlled positioning of origami-associated Holliday Junctions, or DNA-PAINT "docking strands" on a chip-based substrate.

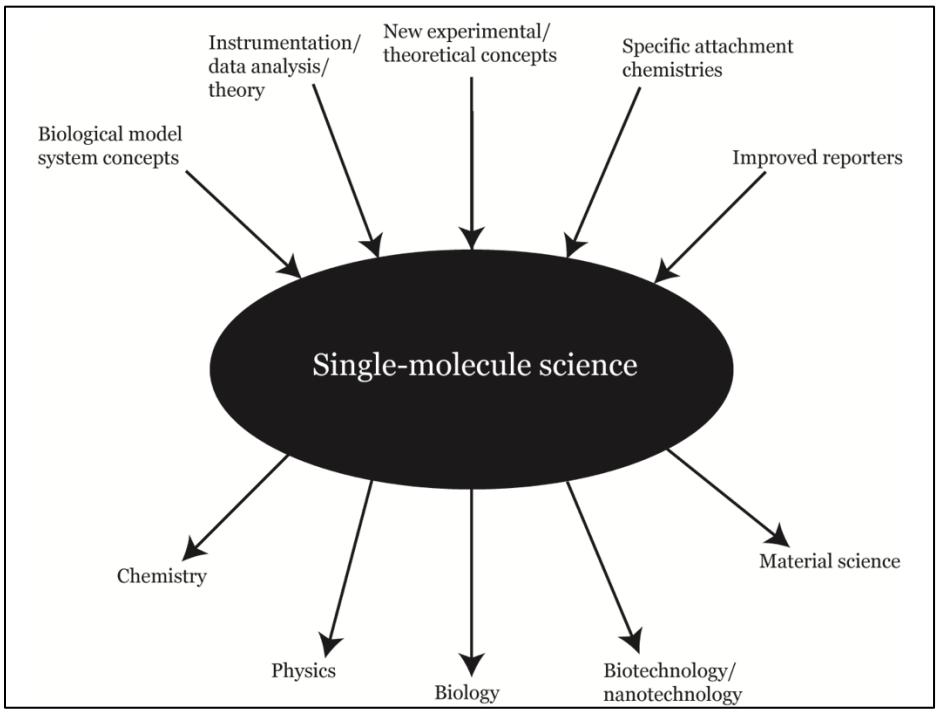

Figure 1*:* The component-parts and scope of single-molecule science [adapted from (Deniz, Mukhopadhyay et al. 2008)]

1.1.5 Low-cost, chip-based diagnostics

The current gold standard for quantitative nucleic acid detection is qPCR or droplet-digital PCR (ddPCR), which is limited, especially in low-resource settings, by its high equipment/reagent cost and the need for thermal cycling. With regards to its extension to an "on-chip" in situ device platform, qPCR is severely limited by the diffusion of products into solution (Nallur, Luo et al. 2001). High-throughput DNA microarray technology (Heller 2002, Thissen, McLoughlin et al. 2014) on the other hand suffers from an inherent limitation: while it is capable of sensitive *in situ* detection of microbe presence (using longer probes), it fails to quantify viral loads (Gardner, Jaing et al. 2010).

Several *in situ* isothermal approaches compatible with product localization (while demonstrating excellent sensitivity) such as Hybridization Chain Reaction and Rolling Circle Amplification, exhibit the potential to overcome these limitations (Dirks and Pierce

2004) (Lizardi, Huang et al. 1998, Nallur, Luo et al. 2001). The former uses DNA initiator/target strand-triggered amplification by setting up a chain reaction of fluorescently labeled DNA hairpin openings until all the hairpins involved have been exhausted. Exponential growth kinetics have been reported (Xuan and Hsing 2014, Bi, Chen et al. 2015) for rapid product amplification and detection. The latter technique, as the name suggests, performs a circular amplification in situ by using a primer, and padlock probes that circularize via ligation with a target DNA strand. Exponential RCA amplification has been demonstrated (Xu, Xue et al. 2017). DNA nanotechnology enables the self-assembly of origami nanostructures, capable of carrying active components (Bald and Keller 2014), into 2D and 3D conformations (Seeman 2010, Zadegan and Norton 2012). By extension, origami placement enables these nanostructures to serve as substrates for *in situ* isothermal amplification of bound nucleic acid targets. It thereby retains the advantages of highly sensitive isothermal amplification while facilitating broader functionality and addressability through precise origami placement on a chip-based platform. The programmable placement of functionalized DNA origami nanostructures on addressable substrates at the diffraction limit can be extended to serve as a portable, nucleic-acid-based digital assay platform for counting biomarkers bound to DNA origami biosensors.

Such a biosensor platform could be especially useful in the detection of endemic, epidemic, or pandemic viruses with known sequences to target conserved domains of their genome with high specificity. Target diseases could include Malaria, Zika, other flaviviruses, Ebola, Influenza A, B, C and a BLAST analysis would enable careful probe design. For example, rapid, point-of-care diagnostics (2-4 hours) based on nucleic-acid detection have been shown to be more sensitive than antigen-based serological tests with the ability to detect the virus much earlier in clinical samples. Specifically, an isothermal

amplification approach which utilizes *ss*DNA probes to serve as reporter molecules for capturing specific viral RNA sequences has demonstrated excellent sensitivity for detection of seasonal H1N1, H3N2, and pH1N1 viruses with an analytical sensitivity of 100,000 RNA copies/mL (Vemula, Zhao et al. 2016). A fungal infection such as Valley Fever which can take a long time to diagnose specifically and presents a significant average cost per hospitalization of $49,000 could also benefit from this type of low-cost, specific, nucleic acid-based digital assay (Tsang, Anderson et al. 2010). The DNA origami nanoarray platform, integrated with a low-cost visualization setup could also be deployed in areas where quick, reliable detection of human, animal, avian, or plant diseases are required in decentralized laboratories without sophisticated infrastructure or storage facilities in place and biomarker (DNA/RNA) load is in the nanomolar-picomolar range.

1.2 Analytical techniques

For the purpose of device and assay characterization, several surface analytical tools such as Total Internal Reflection Fluorescence Microscopy (TIRFM), Scanning Electron Microscopy (SEM), and Atomic Force Microscopy (AFM) were extensively employed during the process of data collection, and parametric optimization. They are briefly introduced here in the context of optical experiments.

1.2.1 Total Internal Reflection Fluorescence (TIRF) microscopy

In contrast with epifluorescence microscopy where the image superimposed on the camera sensor is a combination of light emission from a large volume of the sample and the numerous fluorophores the excitation beam impinges upon, TIRF microscopy, as the name suggests, relies on the total reflection of the excitation beam at the glass-sample interface. This results in an evanescent wave propagating ~100-nm into the sample volume from the glass surface, and a selective excitation of fluorescent molecules close to

the glass surface (Dulin, Lipfert et al. 2013). The advantage of this technique is therefore the high-contrast afforded by the exclusion of background fluorescence and consequently high localization-precision. A classic example of TIRF microscopy for cellular imaging is that of the plasma membrane which is an important barrier for all molecules entering or exiting the cell volume (Mattheyses, Simon et al. 2010). This interface is poorly imaged using confocal or epifluorescence microscopy owing to the high background characteristic of these techniques.

Briefly, the physical objective-TIRF setup involves an excitation laser beam focused off-axis at the back focal plane (BFP) of the objective lens. While exiting the objective lens, the light passes through the immersion oil and into the coverslip, which have matched refractive indices. When the excitation beam propagating through the coverslip encounters the interface with the aqueous medium of the sample, the direction of the beam is altered based on its angle of incidence at this interface. If the angle is greater than a critical angle, the light beam undergoes a phenomenon termed "total internal reflection (TIR)", which stops it from propagating any further, instead creating an evanescent excitation field in a small volume of the sample close to the glass surface; a consequence of some of the incident energy penetrating through the interface. The intensity of the evanescent field decays exponentially with the distance from the glass interface, i.e. a fluorescent molecule closer to the surface is strongly excited, whereas one further away from the surface is weakly or barely excited, resulting in high Signal-to-Noise ratios (SNR). The critical angle is given by Snell's law:

$$\theta_c = \sin^{-1}(n_1/n_2),$$

where n_1 and n_2 are the refractive indices of the sample and the coverslip, respectively. To achieve TIR, the sample refractive index must be less than that of the coverslip.

In this thesis, all fluorescence experimental data obtained in Chapters 3 and 4 were courtesy of an Oxford Nanoimager benchtop super-resolution microscope (Oxford, UK) capable of epifluorescence, TIRF, and Structured Illumination Microscopy (SIM). Samples were labeled primarily with Cy3-b, Alexa-546, and Atto-647 dyes, and excited using 532-nm, and 640-nm laser lines.

1.2.2 Scanning Electron Microscopy (SEM)

A conventional optical microscope is capable of a maximal 1000x magnification and is limited by diffraction of the visible wavelengths of light (Vernon-Parry 2000). Better resolution demands that the wavelength of imaging radiation be decreased. In electron microscopy, the electrons are usually accelerated to high energies of between 2 and 1000 keV, corresponding to wavelengths on the order of 0.027-00009 nm. In thin specimens, highly energized electrons are transmitted through the sample volume unabsorbed and used to form the image in a transmission mode, therefore the name Transmission Electron Microscopy (TEM). For thicker samples, electrons are not transmitted without interactions with the sample volume, and therefore result in particles such as x-rays, photons, and secondary electrons emerging from the surface and forming a consequent signal used as information for a "scanning" electron microscopy image.

SEM images can provide information about the surface topography, crystal structure, chemical composition, and electrical behavior of the top 1 μm of the sample. Hot, cold, and mechanical testing-compatible stages enable the probing of sample behavior under various experimental conditions. Some of the important advantages of SEM over optical microscopy include the large depth of field which allows most of the specimen to be observed in focus irrespective of surface roughness, magnifications of up to 1,000,000x (1-nm resolution), large specimen area observation, and gathering

information about crystal structure, and chemical composition by switching modes on the instrument. A basic SEM setup comprises incident electrons from an electron gun typically having energies between 2-40 keV, two or three electromagnetic condenser lenses to demagnify the beam into a fine probe which is scanned across a selected area-of-interest on the specimen by scan coils, an aperture, and a detection system specific to the type of electrons collected (secondary, backscattered, x-rays).

1.2.3 Atomic Force Microscopy (AFM)

AFM is a form of scanning probe microscopy (SPM) capable of achieving sub-nanometer resolution (Rao and Costa 2014). While super-resolution light microscopy techniques such as STED, STORM, etc. can regularly achieve resolutions of 50-100 nm, they do not depict the structure or morphology of individual molecules or sub-molecular details. Electron microscopy can provide ultra-high magnification but requires extensive sample preparation including fixation, and can distort soft biological samples, precluding the imaging of living cells and tissues. AFM is also agnostic to whether a sample is conductive or not, unlike electron microscopy. It relies on mechanically feeling the surface in order to sensitively record deflections over an entire scan area, rendering a high-resolution image of its topography. This is achieved using a nanofabricated tip at the end of a cantilever beam which is soft enough to sense piconewton forces. The tip is about 3-15 μm tall with an end radius of 10-50 nm and is made of silicon or silicon nitride. Owing to its ability to measure soft surfaces and compatibility with aqueous media, this technique has been widely used to image biological samples.

In general, as the AFM tip scans the surface, a diode laser focused on the reflective back surface of the cantilever deflects in response to surface topology and the information is transmitted to a detector which then maps the morphology being scanned. The two

common modes of operation are contact mode and tapping mode, each of which have their own advantages and disadvantages and should be chosen based on the sample and application of interest. Tapping mode is widely used for biological and liquid samples so as to limit sample damage and avoid moving particles that may cause damage to the tip itself. AFM has also been used as a manipulation tool in order to probe the force required to break naturally occurring biological bonds, and other interactions on the molecular level. Examples also exist of the technique being used in conjunction with FRET in order to reveal important functional information about conformational changes in single molecules.

In this thesis, AFM was used as the primary means of device characterization from quantifying the effect of binding site diameter on DNA origami occupancy to quantifying the single origami occupancy itself. Furthermore, prior to collecting experimental data on the patterned DNA origami nanoarray chip each chip was first benchmarked using AFM as a quality control measure.

1.3 Motivation and significance

Chip-based mesoscale grids of bio-molecules combine the unique advantages of microarrays and single-molecule experiments (SME). They facilitate high-throughput assays with low reagent consumption while probing heterogeneity often masked within bulk populations (Ritort 2006, Dulin, Lipfert et al. 2013). Over the last few years, miniaturization of reaction volumes to achieve confinement of analytes of interest has significantly enhanced the sensitivity and processing speed of analysis and detection methods (Walt 2013, Cohen and Walt 2017). Until recently, creating single molecule nanoarrays presenting a digital number of moieties-of-interest proved particularly challenging due to conventional top-down fabrication technologies lacking the resolution

for molecular manipulation. Moreover, traditional single molecule optical assays are qualitative rather than absolutely quantitative owing to the high probability of multiple single molecules binding to the same diffraction-limited spot. Exerting positional control over these molecules on experimentally relevant surfaces is therefore a constant area of interest.

DNA Origami Placement (DOP) (Gopinath and Rothemund 2014) addresses this issue through a synergistic combination of two powerful techniques: (i) DNA origami (Rothemund 2006), which provides a ~100-nm self-assembled template for programmable, single-molecule attachment, with a 3-5 nm resolution and (ii) Top-down lithography, which offers precise positional control over these origami, transforming them into functional nanodevices (Gopinath, Miyazono et al. 2016) via integration with arbitrary substrates. DNA origami breadboards enable the facile spatial manipulation of single molecules by enlarging their effective footprints to within the resolution limit of nanofabrication tools such as Electron-Beam Lithography (EBL). Presently, however, DOP is reliant on sophisticated infrastructure (EBL) and highly-trained personnel for its reproducible execution, oftentimes making it prohibitively expensive for researchers. These are the prominent factors that limit the potential applications of DOP in the fields of high-throughput biological physics, and single molecule array-based digital diagnostics. Several bottom-up, and hybrid techniques have been reported as substitutes for top-down fabrication (Hawker and Russell 2005, Mijatovic, Eijkel et al. 2005, Isa, Kumar et al. 2010, Colson, Henrist et al. 2013, Vogel, Retsch et al. 2015). A self-assembly technique such as Nanosphere Lithography (NSL), offers a variety of advantages – it is cheap, enables fast, parallel-processing, and numerous crystallization techniques exist for covering arbitrarily large surface topologies (Vogel, Weiss et al. 2012, Colson, Henrist et al. 2013, Vogel, Retsch et al. 2015).

In this work, we developed a novel method for bench-top, cleanroom-free, DNA origami placement in meso-to-macro-scale grids using tunable colloidal nanosphere masks (Deckman 1983, Ye and Qi 2011, Colson, Henrist et al. 2013, Wu, Zhang et al. 2013, Vogel, Retsch et al. 2015), and organosilane-based surface chemistry modification. Similar NSL-assisted passivation strategies have been reported previously for patterning multiple gold nanoparticles per spot and protein dot arrays (Li, Lusker et al. 2009, Taylor, Patel et al. 2009). However, as per our knowledge, a nanostructure as large as DNA origami — capable of providing a template for high-yield single molecule patterning — has not been patterned using a bottom-up technique. Bench-top DNA origami placement is therefore the first demonstration of its kind which facilitates precision placement of single molecules with high efficiency in any given diffraction-limited spot.

During the course of this work we have: (1) optimized a bottom-up, benchtop DNA origami nanoarray fabrication paradigm through the creation of long-range, hexagonally-close packed (HCP), self-assembled binding sites; (2) validated the biophysical relevance and robustness of the nanoarray platform via high-throughput experiments probing *ss*DNA counting and pattern resolution; (3) highlighted the potential of DNA origami nanoarrays as a diagnostic platform for low-cost, quantitative biomarker detection.

These studies help determine the suitability of DNA origami nanoarrays as an affordable, single molecule dynamics and quantitative detection platform.

1.4 Organization of the thesis

The work in this thesis has its roots in three broad questions with implications for the DNA nanotechnology, single molecule biophysics and diagnostic fields alike. The contents of this thesis are therefore divided into three chapters, tackling one question per chapter:

1.4.1 Technological challenge: Can we develop a fully bench-top protocol for DNA origami placement on a glass substrate without the use of top-down techniques and sophisticated equipment such as EBL to significantly lower the barrier for adoption?

Chapter 2 introduces the concept of bottom-up self-assembly of nanospheres and discusses their utility in creating a close-packed crystalline "mask" for the parallel fabrication of origami binding sites. I introduce a workflow for bench-top DNA origami immobilization and characterize the important parameters responsible for maximizing single-molecule occupancy. A comprehensive protocol and guide to troubleshooting the entire process for ease of reproducibility is also included in this chapter. I further demonstrate the efficiency of this method compared to the statistical limit imposed on traditional top-down loading methods. I draw comparisons between EBL-based DOP and NSL-assisted DOP and the advantages and shortcomings of each mode of DNA origami immobilization. Lastly, I introduce an automation step which enables the mitigation of manual errors propagating through the process flow and makes the protocol more robust.

1.4.2 Research challenge: Can we demonstrate the robustness of the platform and its utility in increasing the throughput and overcoming stochasticity in single-molecule experiments?

Chapter 3 discusses the robustness of the DNA nanoarray platform under various experimentally relevant conditions and introduces a new paradigm for performing single-molecule biophysics experiments at maximum throughput in the diffraction-limited setting. I first characterize the efficiency of single molecule binding on DNA origami nanostructures through conventional photobleaching experiments, and move on to more complex, super-resolution regime counting experiments based on DNA-PAINT technology. These experiments are a departure from the heretofore universal biotin-streptavidin conjugation strategies for biomolecule-to-surface attachment used in SMEs,

and we provide comparisons between classical experiments and nanoarray-based deterministic experiments as a measure of efficacy and throughput.

1.4.3 Real-world viability challenge: Can we provide a proof-of-concept for the technique's utility as a potentially portable, low-cost diagnostic platform for quantitative biomarker detection?

In Chapter 4, I discuss the differences between analog and digital assays, and provide evidence for the potential of the nanoarray platform as a portable detection device. The targeted application of this platform is in low-cost, enzyme-free amplification of biomarker, specifically *ss*DNA/RNA binding events and their consequent quantitation facilitated by the facile separation of each binding event by a distance greater than the diffraction limit of light. The DNA nanoarray chip itself is amenable to use in the low-resource settings, but I show preliminary data for its integration with a low-cost imaging setup for field-research. Results on the surface passivation strategies, assay sensitivity (Limit of Detection), and specificity against serum-spiked medium and ~200 random oligonucleotide sequences are also presented.

Chapter 5 outlines future directions for this project, and comprises discussions about (1) Preliminary data for iterative size reduction of binding sites to facilitate further simplification of the imaging apparatus, especially in low-resource settings, thus overcoming the current limitation of the technique imposed by origami size; (2) An extension of the current technology to the development of inexpensively fabricated Zero Mode Waveguides (ZMWs) for high-throughput SMEs at physiologically relevant ligand concentrations with unprecedented SNRs and temporal resolution; (3) Amplification-free paradigms for biomarker detection (DNA, RNA, protein, small molecules); and (4) The possible application of metalenses in the imaging system.

1.5 List of contributions

Manuscripts in preparation:

1. R.M. Shetty, S. Brady, E. Le, M. Kennedy, P.W.K. Rothemund, R.F. Hariadi, A. Gopinath, "A facile, cleanroom-free DNA origami nanoarray platform for non-Poisson digital assays"
2. R.M. Shetty, T. Sneh, S. Brady, A. Gopinath, R.F. Hariadi, "$1 DNA nanoarrays for point-of-care, digital biomarker detection"

Conference presentations:

1. R.M. Shetty, S. Brady, E. Le, K. McRae, A. McGirr, F. Djutanta, P.W.K. Rothemund, R.F. Hariadi, A. Gopinath, "DNA origami nanoarrays: A modular platform for quantitative biophysics," Biophest, University of Arizona, poster & oral presentation
2. A. Gopinath, R.M. Shetty, P.W.K. Rothemund, R.F. Hariadi, "Democratizing single molecule nanoarrays", Foundations of Nanoscience Conference, 2018, Utah, *invited talk*

Provisional patent:

A. Gopinath, P.W.K. Rothemund, R.F. Hariadi, R.M. Shetty, "Modular, self-assembled, single nucleic acid and protein arrays for sensitive and non-Poisson digital diagnostics", 2017.

CHAPTER 2* A CLEAN-ROOM FREE BENCH-TOP PARADIGM FOR SINGLE-MOLECULE NANOARRAY FABRICATION BEYOND THE POISSON LIMIT

Abstract

What if a molecule could act as a bridge between the bottom-up worlds of biology and chemistry, and the top-down world of nanofabrication? Single-molecule nanoarrays have been extremely difficult to fabricate owing to the lack of nanofabrication tools boasting single-molecule resolution. A molecule large enough for lithographic manipulation did not exist until a little over a decade ago. DNA origami, invented in 2006, presents a ~100-nm breadboard for the decoration of single molecules with 3-5 nm resolution. A tool such as electron-beam lithography (EBL) can subsequently enable the programmed localization of these origami nanostructures on an experimentally relevant substrate with an efficiency far greater than the Poisson limit for stochastic loading of single molecules. To make this placement technology more accessible, however, a more simplified approach needs to be introduced. We combine bottom-up self-assembly based Nanosphere Lithography (NSL) with selective surface passivation to create meso-to-macroscale grids of binding sites for single molecule placement on glass via origami immobilization. The approach is cleanroom-free, easily reproducible and scalable, with an efficiency ~2x the Poisson limit, and costs ~ $1 per chip.

*Extensive parts of this chapter appear in a manuscript in preparation:

Facile, cleanroom-free fabrication of single molecule nanoarrays

Rishabh M. Shetty, Sarah Brady, Eric Le, Maeve Kennedy, Paul W. K. Rothemund, Rizal F. Hariadi, Ashwin Gopinath

2.1 Introduction

In 1991, Whitesides et al. predicted self-assembly to be a cornerstone of the field of nanotechnology (George M. Whitesides 1991). Whitesides reiterated this belief in 2002 (Whitesides 2002) by stating that it was one of the only practical solutions for making ensembles of nanostructures, defining self-assembly as "the autonomous organization of components into patterns or structures without human intervention – processes common throughout nature and technology." He argued that autonomous-assembly based approaches had the unique potential to provide a framework for parallel fabrication of structures from components either too diminutive or innumerable to be handled robotically.

DNA origami was invented in 2006 (Rothemund 2006) as a method capable of matching the order and complexity of nanostructures routinely achieved by "top-down" lithography techniques – bridging the gap with the "bottom-up" world of chemistry and biology. 2-D and 3-D DNA origami nanotechnology is modular and spatially-programmable (Bui, Onodera et al. 2010, Pinheiro, Han et al. 2011, Bald and Keller 2014, Heucke, Baumann et al. 2014, Pibiri, Holzmeister et al. 2014, Basu 2017); an assembled origami unit being capable of carrying up to 200 individually addressable biological and non-biological molecules of interest (Pal, Deng et al. 2010, Ko, Du et al. 2013, Hariadi, Cale et al. 2014, Kuhler, Roller et al. 2014, Hariadi, Sommese et al. 2015). These breadboards facilitate the rational design, synthesis, and manipulation of integral nanoscale objects in the fields of biology, and biochemistry. In the last decade, origami nanostructures have been utilized for a myriad of applications ranging from electronic (Ding, Deng et al. 2010, Geng, Wei et al. 2014) and optical devices (Dutta, Varghese et al. 2011, Acuna, Möller et al. 2012, Kuzyk, Schreiber et al. 2012, Kuhler, Roller et al. 2014), to single-molecule biophysics (Dai, Jungmann et al. 2016, Jungmann, Avendano et al. 2016,

Shrestha, Emura et al. 2016, Schnitzbauer, Strauss et al. 2017, Heydarian, Schueder et al. 2018), biosensing (Voigt, Torring et al. 2010, Godonoga, Lin et al. 2016, Ochmann, Vietz et al. 2017), and nanofabrication (Kershner, Bozano et al. 2009, Gopinath and Rothemund 2014, Gopinath, Miyazono et al. 2016, Brassat, Ramakrishnan et al. 2018, Takabayashi, Kotani et al. 2018).

By virtue of being synthesized in solution, spatial stochasticity is intrinsically linked with DNA origami and the single molecules associated with them when deposited on a microscopically addressable substrate such as glass. Exerting positional control over origami on experimentally relevant surfaces is therefore an area of interest. In addition, the size of a DNA origami molecule makes it amenable to electron beam-lithography-based manipulation. Thus, a potentially lucrative, and as yet underexplored application of DNA origami nanotechnology is its ability to interface biochemically-relevant functional moieties with the outside world through large-scale integration on a variety of substrates. A precedent has already been set for the advantages of immobilizing DNA origami through electrostatic or covalent coupling to mica, glass, silicon, and various other substrates (Kershner, Bozano et al. 2009, Gopinath and Rothemund 2014). Gopinath et al. demonstrated the large-scale integration of functionalized DNA origami through placement on ~100-nm binding sites with >90% efficiency and positional accuracy up to ~20-nm for hybrid nanodevice fabrication (Gopinath, Miyazono et al. 2016). DNA origami placement (DOP) adds another dimension of scalability and positioning dexterity to the field of structural DNA nanotechnology. Such a composite nano-to-micro-manipulation technique enables experimenters to exert bi-level control — First, through the arbitrary decoration of hundreds of nanoscale components with a resolution of 3-5 nm on origami nanostructures, and second, by deterministically positioning these origami at lithographically-patterned sites on a desired substrate at the mesoscale. Such a top-down

strategy of fabrication, however, can be resource-intensive in the academic setting, costing upwards of $100 per chip.

A bottom-up technique, such as Nanosphere Lithography (NSL) (Deckman 1983, Colson, Henrist et al. 2013) is an attractive alternative to EBL. It may be possible to utilize individual colloidal particles as "nano-masks" to selectively passivate interstitial areas with an organosilane (Li, Lusker et al. 2009, Taylor, Patel et al. 2009) and develop a protocol for bench-top NSL-based DOP. Specifically, using NSL, we designed and optimized our workflow to match the binding site and origami geometry to maximize single bindings. Nanosphere diameter selection was informed by Atomic Force- and Scanning Electron-Microscopy- (AFM, SEM)-based characterization of associated binding site size. Finally, we introduced an automated washing process to minimize user-associated variability and its detrimental effects on fabrication quality.

In this work, we developed a method for bench-top, cleanroom-free, DNA origami placement in meso-to-macro-scale grids using tunable colloidal nanosphere masks (Deckman 1983, Ye and Qi 2011, Colson, Henrist et al. 2013, Wu, Zhang et al. 2013, Vogel, Retsch et al. 2015), and organosilane-based surface chemistry modification. Similar NSL-assisted passivation strategies have been reported previously for patterning multiple gold nanoparticles per spot and protein dot arrays (Li, Lusker et al. 2009, Taylor, Patel et al. 2009). However, as per our knowledge, a nanostructure as large as DNA origami — capable of providing a template for high-yield single molecule patterning — has not been patterned using a bottom-up technique. Bench-top DNA origami placement is therefore the first demonstration of its kind which facilitates precision placement of single molecules with high efficiency in any given diffraction-limited spot at a cost of $1/chip. This technique has the potential to democratize high-throughput single molecule experiments in laboratories worldwide.

2.2 Materials and Methods

2.2.1 DNA origami design, preparation and purification

Design. Circular origami were designed using caDNAno (http://cadnano.org/), and as detailed by Gopinath et al., 2018 (Gopinath, Thachuk et al. 2018) to position all staple ends on the same face of the origami so that single-stranded 20T extensions to 5' staple ends would all project from the same face of the origami.

Preparation. Staple strands (Integrated DNA Technologies, 640 nM each in water) and the scaffold strand (single-stranded p8064, 100 nM from Tilibit for circular origami) were mixed together to target concentrations of 100 nM (each staple) and 20 nM, respectively (a 5:1, staple:scaffold ratio) in 40mM Tris, 20mM Acetate and 1mM EDTA with a typical pH around 8.6, and 12.5 mM magnesium chloride (1xTAE/Mg^{2+}). 100 µL volumes of staple/scaffold mixture were heated to 90°C for 5 min and annealed from 90°C to 25°C at 0.1°C/min in a PCR machine. Once purified, the origami were stored in 0.5 mL DNA LoBind tubes (Eppendorf) to minimize loss of origami to the sides of the tube.

Purification. A high concentration of excess staples will prevent origami placement. Thus, origami were purified away from excess staples using 100 kDa molecular weight cut-off spin filters (Amicon Ultra-0.5 Centrifugal Filter Units with Ultracel-100 membranes, Millipore, UFC510024). By the protocol below, recovery is generally 40–50% and staples are no longer visible by agarose gel:

1. Prime the filter by adding 500 µL 1xTAE/Mg^{2+}.
2. Spin filter at 6000 rcf for 5 min at room temperature (RT), until the volume in the filter is ~80 µL. Discard the filtrate.
3. Add 100 µL of unpurified origami and 300 µL 1xTAE/Mg^{2+}. Spin at 6000 rcf for 5 min at RT.
4. Discard the filtrate. Add 420 µL 1xTAE/Mg^{2+} and spin at 6000 rcf for 5 min at RT.

5. Repeat step (4) two more times.
6. Invert the filter into a clean tube and spin at 6000 rcf for 5 min at RT to collect purified origami (~ 80µL).

NOTE: In case of origami annealed with an excess of fluorophores (for photobleaching) or DNA-PAINT, spin the filter at 2000 rcf or lower for 15 min, 5-7 times before inverting into a new tube to collect the purified product. This is to avoid fluorophores (and associated origami) from sticking to the sides of the filter and adversely affecting the purified origami yield or causing origami aggregation/deformation. Always check the purity of origami using agarose gel electrophoresis (100v, 1%, 1x TAE, 1-hr).

The total time required for this purification is roughly 30 minutes-2 hours. Post-purification, origami are quantified using a NanoDrop spectrophotometer (Thermo Scientific), estimating the molar extinction coefficient of the DNA origami as that of a fully double-stranded p8064 molecule (ε =164,568,055/M/cm; we do not correct for small single-stranded loops which are present on the edges of some designs). We typically work with stock solutions of 20–30 nM DNA origami (3–5 OD). The working concentration for origami during placement is 100-500 pM, which is too small to be measured with the NanoDrop, so serial dilutions must be performed. High quality placement is very sensitive to origami concentration. To maintain consistency for each series of experiments, a single high concentration stock solution (from a single purification) was maintained and diluted to a nominal concentration of 100-500 pM as needed. Origami concentration was optimized for best placement results for each new batch of origami annealed and purified.

2.2.2 Fabrication of binding sites and origami placement

Materials and equipment required:

1. 10x10 mm coverslips (Ted Pella, 260375-15).

2. Plasma cleaner (Harrick Basic Plasma Cleaner PDC-32G / PDC-32G-2), Hotplate and Stirrer (Denville), Desiccator (Hach, Product # 223830), Branson ultrasonic bath, AFM (Bruker FastScan).
3. Appropriately sized Polystyrene (PS) microspheres (3000 Series Nanosphere; Size Standards (4000 Series Monosized 1 μm particles 4009A; 700 nm [3700A]; 495 nm [3495A]; and 400 nm [3400A]), Thermo Fisher Scientific).
4. Passivation agent: HMDS (440191-100ML, Sigma).

A step-by-step protocol for binding site creation is outlined below:

1. Isopropanol (IPA) wash for 2 minutes, and N_2 blow dry glass chip.
2. 10-minute air plasma cleaning in Harrick plasma cleaner (~18 W, "High" setting).
3. In an eppendorf Tube: pour 10 drops (~360 μL) suspension of 1 μm/700 nm/500 nm/400 nm PS beads (bottle vortexed briefly before use).
4. Spin at 8,000-10,000 rpm for 5 minutes (faster/longer spinning for smaller bead sizes).
5. Remove supernatant and add 360 μL of ultrapure water to re-suspend pellet.
6. Spin at 8,000-10,000 rpm for 5 minutes.
7. Remove supernatant and resuspend pellet in 25% ethanol and 75% water (~3.5x more concentrated, i.e. 100 μL). Pipette/vortex aggressively to resuspend all particles (~ 6.5 e^{10} particles/mL for 1 μm beads at 1% w/w solids).
8. Drop-cast onto activated chip surface and let dry at ~45° angle at R.T (resting against a glass stirrer or similar object). Cover entire surface (generally requires 5-10 μL for a 10x10 mm chip). Once dried, you should be able to observe a diffraction pattern (crystalline structure) confirming the existence of a close-packed monolayer/multilayer of beads. If unsure, check under a microscope.
9. Heat at 60°C for 5 minutes to remove any moisture.

10. 2-minute “descum” plasma (air ~18 W) in Harrick cleaner.
11. In a desiccator, add a few (8-10) drops of HMDS (in a glass cuvette), and deposit under a vacuum seal for 20 minutes. This should work equally well in an enclosed petri dish.
12. Lift-off PS beads with water sonication in a Branson ultrasonic bath (30-60 seconds) to create origami binding sites. In the absence of an ultrasonic bath, continuous stirring in water for a longer period of time is adequate. The nanospheres visibly come off the surface,
13. Blow dry with N_2 gun.
14. Bake at 120°C, 5 minutes, to stabilize the HMDS on the surface.

NOTE: If you find "islands" of patterned origami/binding sites, you may need a higher concentration of beads (this is generally observed for 1 μm or 700 nm beads). A good sanity check is to label the origami with fluorophores, if possible, and observe under a fluorescence microscope for grids. AFM can tend to sample a very small area of a large chip surface and microscopy may be a quicker route to take. For <500 nm bead sizes, finding origami grids should not be a problem at all.

Origami placement materials required:

1. Thermal Cycler (Life Technologies) for origami annealing, 100k spin filter columns (Amicon) and a benchtop centrifuge (Denville, 6k g, 3-5, 5-min reps) for origami filtration.
2. Origami: Death Star (Gopinath, Thachuk et al. 2018), modified appropriately.
3. Tris-HCl buffer (Buffer 1: pH 8.35, 40 mM Mg^{++}, 40 mM Tris, and Buffer 2: pH 8.9, 35 mM Mg^{++}, 10 mM Tris) [Magnesium Chloride Hexahydrate | M9272-500G, Sigma; Tris, T-400-1 GoldBio].
4. 50%, 75%, and 85% Ethanol in ultrapure water (459836 Sigma Aldrich).

A step-by-step protocol for origami placement and washing steps is outlined below:

1. Incubate chips with ~100-200 pM origami (nominal concentration for 1 μm pitch, concentration inversely proportional to nanosphere size) in ~ 40 mM Mg, Tris-HCl (40 mM Tris) buffer (pH- 8.3) for 60 minutes.
2. Wash in ~ 40 mM Mg, Tris-HCl (40 mM Tris) buffer (pH- 8.3) for 5 minutes either manually or automatically (using a peristaltic pump) or shaker in a petri dish.
3. Transfer to ~40 mM Mg 1x TE (pH-8.3) + 0.07% Tween 20 and wash for 5 minutes.
4. Transfer to ~35 mM Mg, 10 mM Tris (pH-8.9) to hydrolyze HMDS and lift off origami non-specifically bound to the background and wash for 5 minutes.
5. For AFM characterization, transfer to ethanol drying series: 10 seconds in 50% ethanol, 20 seconds in 75% ethanol, 2 minutes in 85% ethanol.
6. Air-dry, followed with AFM/fluorescence verification of patterning.

Note: All of the work reported here was performed with spin-column purified origami, which is suitable for small amounts of origami. After purification and quantification, it is especially important to use DNA LoBind tubes (Eppendorf) for storage and dilution of low concentration DNA origami solutions. Low dilutions, *e.g.* 100 pM, must be made fresh from more concentrated solutions and used immediately— even overnight storage can result in total loss of origami to the sides of the tube. Addition of significant amounts of carrier DNA to prevent origami loss may prevent origami placement, just as excess staples do. We have not yet determined whether other blocking agents such as BSA might both prevent origami loss and preserve placement.

2.2.3 AFM characterization

All AFM images were acquired using a Dimension FastScan Bio (Bruker) using the “short and fat”, or “long and thin” ScanAsyst-IN AIR or ScanAsyst-FLUID+ cantilever from an

SNL probe ("sharp nitride lever", 2 nm tip radius, Bruker) in ScanAsyst Air or Fluid mode. All samples were ethanol dried prior to imaging. Single and multiple binding events for placed origami were hand-annotated for origami occupancy statistics and image averaging of arrays of binding sites (ImageJ) was used to determine nanosphere diameter vs. binding site size relationship. Origami occupancy was visually assessed for every nanosphere diameter and reported as zero, single, or multiple origami nanostructures per binding site. Each occupancy value was determined by performing origami placement experiments on three separate chips on three different days, and the number of binding sites assessed per nanosphere diameter was >600. All error bars denote standard deviation. Similarly, for estimation of binding site sizes as a function of nanosphere diameters, measurements were made by image averaging of at least one field-of-view obtained from three individual chips post nanosphere lift-off on three different days. The number of binding sites averaged per data point was >400, and the error bars denote standard deviation.

2.2.3 SEM characterization

In this work, images of close-packed nanosphere crystals, as well as individual nanosphere cross-sections were obtained using a Hitachi S-4700 Field Emission Scanning Electron Microscope (ASU Nanofab, Center for Solid State Electronics Research, Tempe, AZ) at 1-5 keV and the stage (or electron beam) was manipulated as required. In order to prevent charging effects and distortion of the image collected, a sputter coater (Denton Vacuum Desk II, New Jersey) was used to coat the specimen (glass with nanospheres) with Gold-Palladium (Au-Pd), and carbon tape was used to provide a conduction path from the glass surface to the SEM stub (ground). For the cross-sectional images specifically, the glass coverslip was broken in half post sputter-coating and wedged inside a standard cross-sectional SEM sample holder such that the electron beam path was perpendicular to the flat edge of the glass coverslip. Measurements from high-resolution images were made

manually using ImageJ. Similar to AFM estimation of binding site sizes, SEM measurements were reported by visually assessing at least one field-of-view obtained from at least two individual chips with the same nanosphere diameters, prepared and imaged on the same day in the interest of resource- and cost-effectiveness. The number of nanospheres assessed per data point was >10, and the error bars denote standard deviation.

2.3 Results and Discussion

2.3.1 Nanosphere lithography-based "masks" for origami immobilization

We sought to develop a device platform which would enable single-molecule experiments to be performed at the highest packing density while significantly simplifying the fabrication process. This meant positioning DNA origami at distinct sites separated by a pitch slightly larger than the diffraction limit of visible light: $\lambda/2NA$; where λ is the wavelength of light used, and NA is the numerical aperture of the microscope objective lens. This overcomes the need to use super-resolution microscopy for resolving individual signaling events occurring on the DNA origami substrate or its payload of functional moieties (Figure 2.a). Drying of polystyrene nanospheres in a solvent-based aqueous solution on a slightly tilted hydrophilic glass surface yields a close-packed monocrystalline layer. Cross-sectional Scanning Electron Microscopy (SEM) reveals contact areas between individual nanospheres and the glass substrate that can be conveniently utilized as "masks" for bulk-passivation with an organo-silane such as hexamethyldisilazane (HMDS). Subsequent nanosphere "lift-off" results in the creation of nanosphere diameter-dependent binding sites in these masked areas. The binding sites contain silanol groups which serve as Mg^{2+} sequestering locations at an ionizing pH of ~8.3 (Gopinath and Rothemund 2014) (Figure 3). These Mg^{2+} bridges (40 mM) immobilize DNA origami on

the binding sites in the hundreds of picomolar concentration regime (schematic and experimental results in Figure 2.b, c respectively). Placement yield and quality are a function of various parameters such as pH, Mg^{2+} concentration, origami concentration, and incubation time, as previously described (Gopinath and Rothemund 2014).

2.3.2 Characterization and correlation of mask size to origami geometry

We performed SEM and Atomic Force Microscopy (AFM) to characterize the binding site size as a function of nanosphere diameters ranging from 1 μm down to 200 nm (Figure 4, Figure 5). Origami align themselves on binding sites (to maximize the number of silanol - Mg^{2+} - origami bridges) by a process of 2-D diffusion once they land on the surface. Numerically matching the binding site geometry with origami geometry (~100-nm in diameter) is therefore paramount to maximizing single bindings. The aim of this characterization process was to rationally inform the selection of nanosphere diameters most suited to high-density data collection while enabling quantitative counting, and visual observation with diffraction-limited optics. As expected, we observe an almost linear correlation between nanosphere diameter and binding site size for both, optical (SEM)- (R^2=98%), and contact (AFM)- (R^2=94%) modes of imaging. This relationship can be given by $x = kD$, where D is the binding site diameter, x is the nanosphere diameter, and k is the scaling co-efficient, i.e. the ratio of nanosphere footprint to its diameter (Figure 6). Over the range of nanosphere diameters tested, we find a global discrepancy of ~11% between the linear fits, with SEM (k=0.38) providing consistently larger estimates than AFM (k=0.27). We first note that each of the SEM mean and SD values are gleaned from ≥10 nanospheres, whereas corresponding AFM values are determined using weighted means and SDs from averaged images of >400 binding sites (superimposed images of seven HCP binding sites) per any given nanosphere diameter. We offer two

possible explanations for this phenomenon: (i) HMDS is a miniscule molecule (~ 1-nm, smaller than the resolution limit of an SEM) which can lead to larger coverage of interstitial spaces between nanospheres than can be accurately measured using an indirect visualization technique such as SEM, pre-passivation. We speculate that this may result in overestimation of masking areas when examining electron micrographs. All electron micrographs were collected by sputter coating sample cross-sections with a ~10-nm Gold-Palladium (AuPd) layer (for conductivity) which may additionally contribute to higher estimated values.

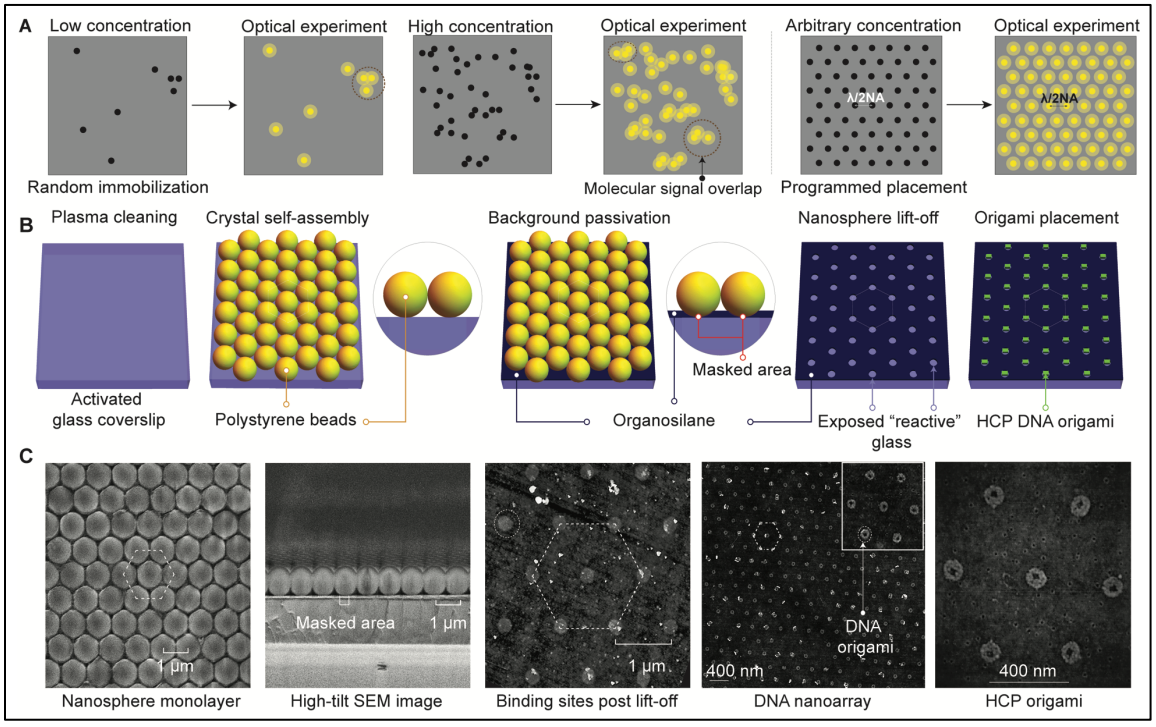

Figure 2: Bench-top DNA origami nanoarray fabrication. (A) A comparison between the ease of counting individual fluorescent events when using randomized immobilization of origami (and other) single molecules versus their programmed placement at the diffraction-limit. Diffraction-limited binding of multiple origami molecules is circled in the random immobilization case. (B) Schematic illustration of the DNA origami nanoarray patterning process which proceeds through 2D nanosphere close-packing, selective passivation, lift-off, and finally, Mg^{2+}-mediated programmed origami placement. (C) Scanning electron micrographs of nanosphere close-packing (top view, and cross-section), and Atomic force micrographs of binding sites, and micro-scale origami placement analogous to schematic depiction (B) of process steps.

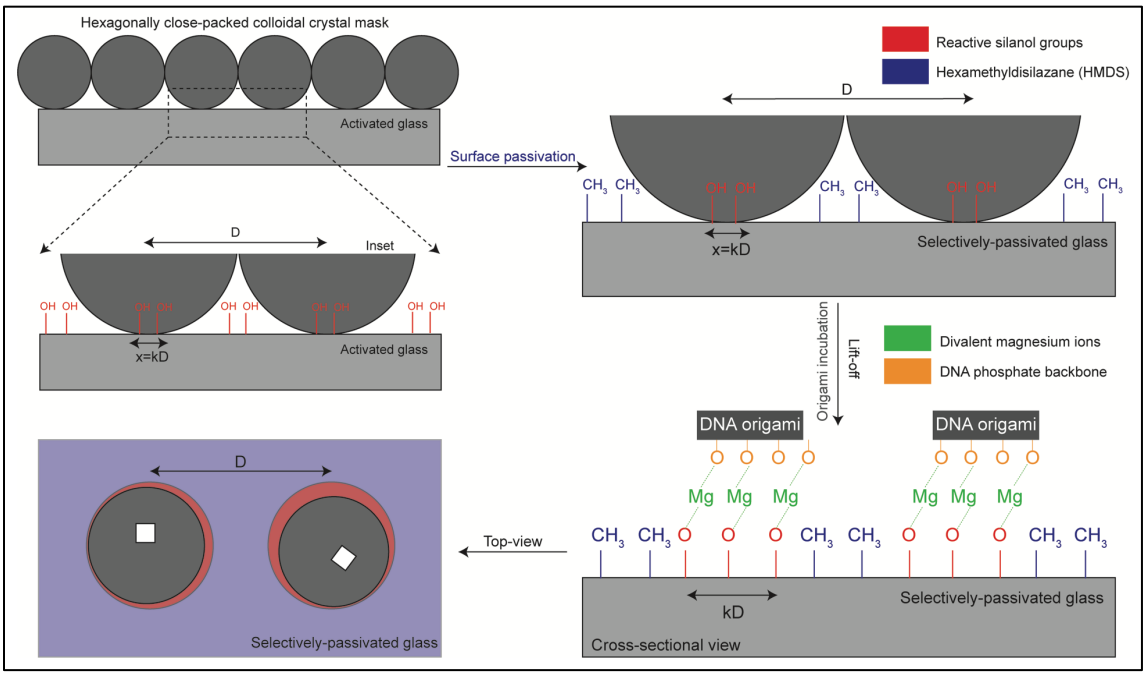

Figure 3: Schema of reactive silanol groups being protected by a close-packed colloidal crystal mask (CCM) of appropriately-sized nanospheres with the nanosphere footprint intrinsically linked to its diameter "D" by the relation: x=kD. A surface passivation step (HMDS) results in the selective passivation of the entire chip surface with neutral methyl groups. Upon lift-off of nanospheres, magnesium-mediated placement of negatively charged DNA origami to the reactive silanol groups proceeds through a process of diffusion, and alignment prior to immobilization. The important parameters that determine quality of nanoarray formation are Mg^{++} concentration, buffer pH, time of incubation, origami concentration, and quality of washing.

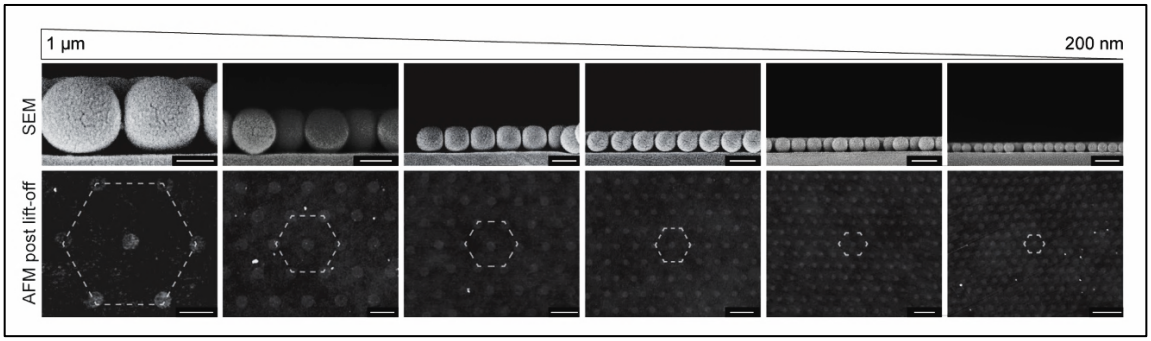

Figure 4: Nanosphere diameter-dependent binding site sizes: Cross-sectional electron micrographs of various nanosphere sizes (1 µm, 700 nm, 500 nm, 400 nm, 300 nm, 200 nm) and their corresponding contact (masking) areas with the glass surface (top row), and atomic force micrographs of origami binding sites observed post lift-off of nanospheres. Scale bars are 500 nm.

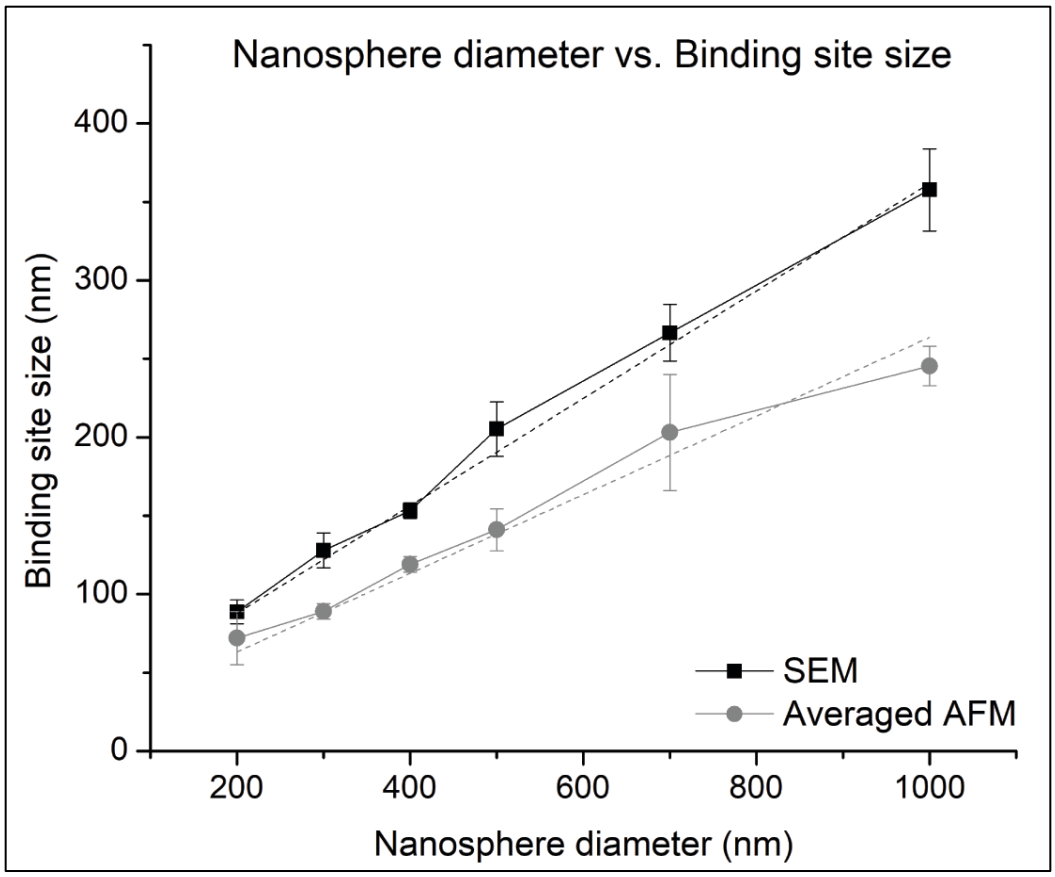

Figure 5: Nanosphere diameter-dependent binding site size indicating a x = kD relationship for scanning electron and atomic force micrographs, where x is the diameter of the binding site, D is the diameter of the nanosphere, and k is the scaling co-efficient; k is 0.27 for SEM ($n \geq 10$), and 0.38 for AFM ($n \geq 400$).

AFM, however, provides a direct mode of measurement post-passivation with HMDS, and is inarguably more representative of the "footprint" of each individual nanosphere in a hexagonally-close packed monocrystalline layer. AFM-based measurements could therefore be considered more reliable than those from SEM as a means of estimating binding site size. (ii) On closer observation of electron micrographs, we found an apparent distortion of nanosphere geometry along the XY-axes (Figure 4). This alteration in morphology is dependent on the position of each nanosphere with respect to the substrate edge (variable, depending on quality of razor "cut" for cross-sectional SEM), and its relative position to other, adjacent nanospheres. It is plausible that

attractive forces during the solvent evaporation process contribute to the departure from a spherical shape to a more flattened, circular shape upon interaction with neighboring colloidal particles. We note that for an 8% distortion along the vertical axis of a nanosphere (80 nm for a 1 μm diameter), the predicted binding site size follows the experimental SEM values closely (Figure 6), which may help explain the discrepancy between the observed SEM and AFM values. 2.3.3 Single origami binding statistics and an autonomous washing process

Circular, 2-D origami (Gopinath, Thachuk et al. 2018), approximately 100-nm across were synthesized to best match the binding site geometry and enable statistical assessment of origami placement from atomic force micrographs. We do not report occupancy statistics for nanosphere diameters up to 1 μm since we reach the Poisson limit of single molecule occupancy (37%) at 500 nm (Figure 7, Figure 8). Increasing the binding site size any further results in an unfavorable, sub-Poisson limit performance. We expect the highest single origami occupancy values to be around the 300-400 nm nanosphere diameter range owing to the origami and binding site geometries being almost identical to each other. We further expect close to 100% occupancy of all binding sites under optimal incubation conditions, and a consistent reduction in multiple origami bindings per site with a reduction in nanosphere diameter (<1:1 ratio). Our experimental observations are consistent with the predicted result and a maximal, $72.4 \pm 2.13\%$ single origami occupancy is observed when the origami are 350-nm apart from each other – a pitch that is at the limit of diffraction for a standard microscope. While the efficiency of single molecule occupancy is lower than the >95% previously reported using Electron-Beam Lithography (EBL) at optimized placement conditions, we argue that this drawback is offset by the technique's simplicity and cost-efficiency (Table 1).

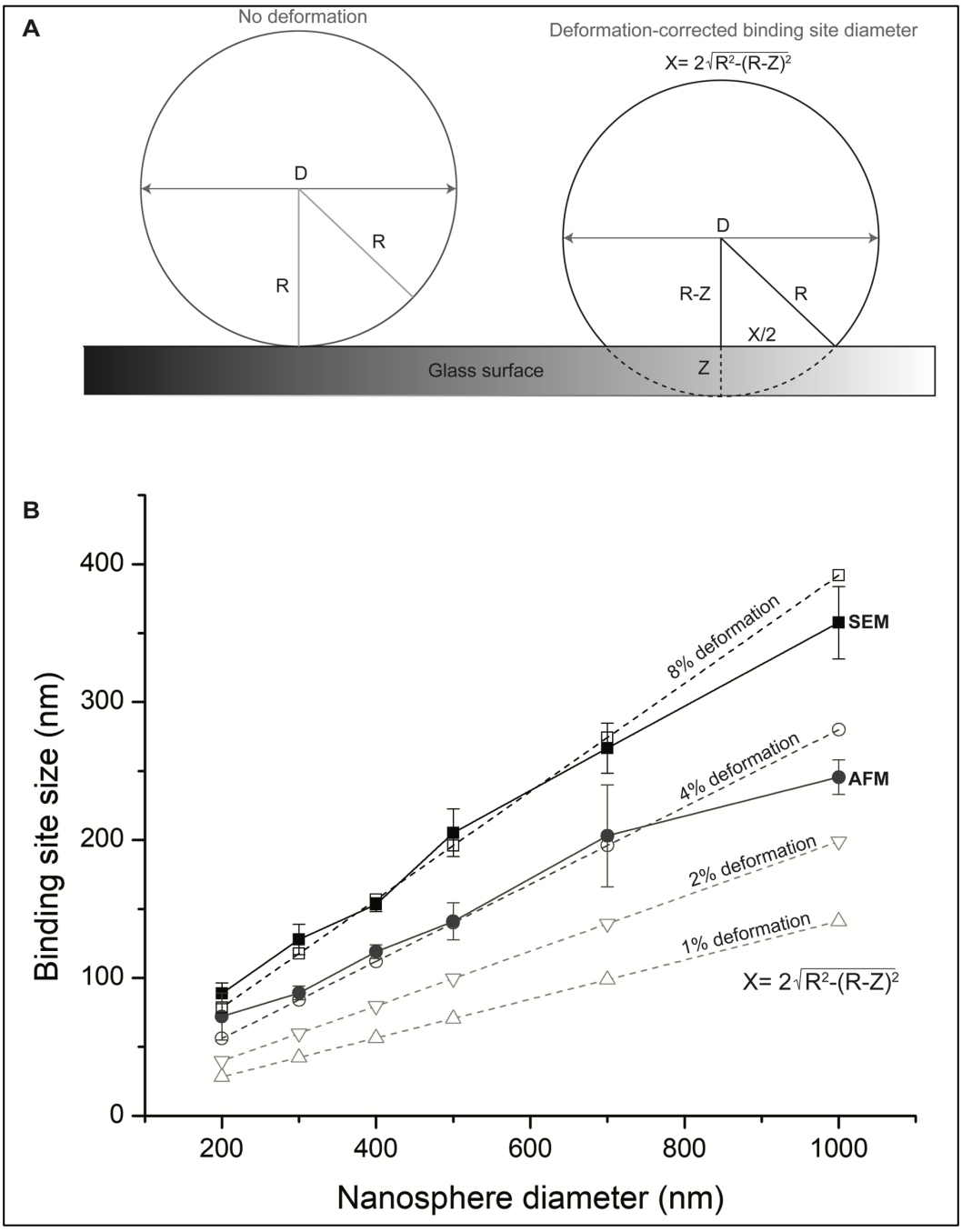

Figure 6: Schematic showing deformation-corrected binding site estimates of nanospheres resting on the surface. Panel (A) depicts the deformation-free case, and the distortion of nanosphere geometry owing to deformation; where "X" denotes the predicted binding site diameter owing to the deformation. Panel (B) plots the deformation (1%, 2%, 4%, and 8%) and their corresponding (predicted) binding site sizes in comparison with binding sites measured via SEM and AFM (Figure 5). A deformation of 8% closely follows the values obtained using SEM measurements and could likely explain the discrepancy seen between the measured SEM and AFM values.

Materials	Estimated cost/chip ($)
DNA origami	$0.1
Nanospheres	$0.5 – 1
Glass coverslip (10 mm x 10 mm)	$0.5
Passivation layer (HMDS)	$0.1
Total	$1.2 – 1.7

Table 1: Conservative estimate of the cost of fabricating the DNA nanoarray platform.

Similar to a previous study (Gopinath and Rothemund 2014), our measurement statistics likely underestimate the number of single and multiple bindings of origami on the binding sites and are, in fact, a more comprehensive reflection of the fabrication process quality. All of the atomic force micrographs presented here were obtained via imaging on an (ethanol-) dehydrated substrate. Comparable to the previous study, we observed only a fractional drop in single binding efficiency in slightly undersized sites (~70-80% of origami diameter) as a result of using 200 nm nanospheres. However, while more densely packed, origami were well below the diffraction limit, and this particular spacing was not utilized for experiments. Incubation conditions such as time, and origami concentration were altered based on nanosphere diameter used; smaller diameters required higher values for both these parameters. The pH (8.3-8.4), and Mg^{2+} concentration (40 mM) remained constant for all experimental results reported herein. Variability associated with placement results can be attributed, in part, to three manual washing steps prior to drying and AFM characterization. We automated this washing process and demonstrate ~66% single origami occupancy with this method. The setup comprises a peristaltic pump and 3-D printed tube holder (Figure 9.a) for positional alignment between runs without manual intervention (Figure 9.b).

Finally, we show a comparison between EBL-based DOP, and NSL-assisted DOP to highlight the key differences between these paradigm shifts in single-molecule

placement technology (Table 2). Chapter 3 and 4 will discuss in further detail some of the application-oriented points of comparison.

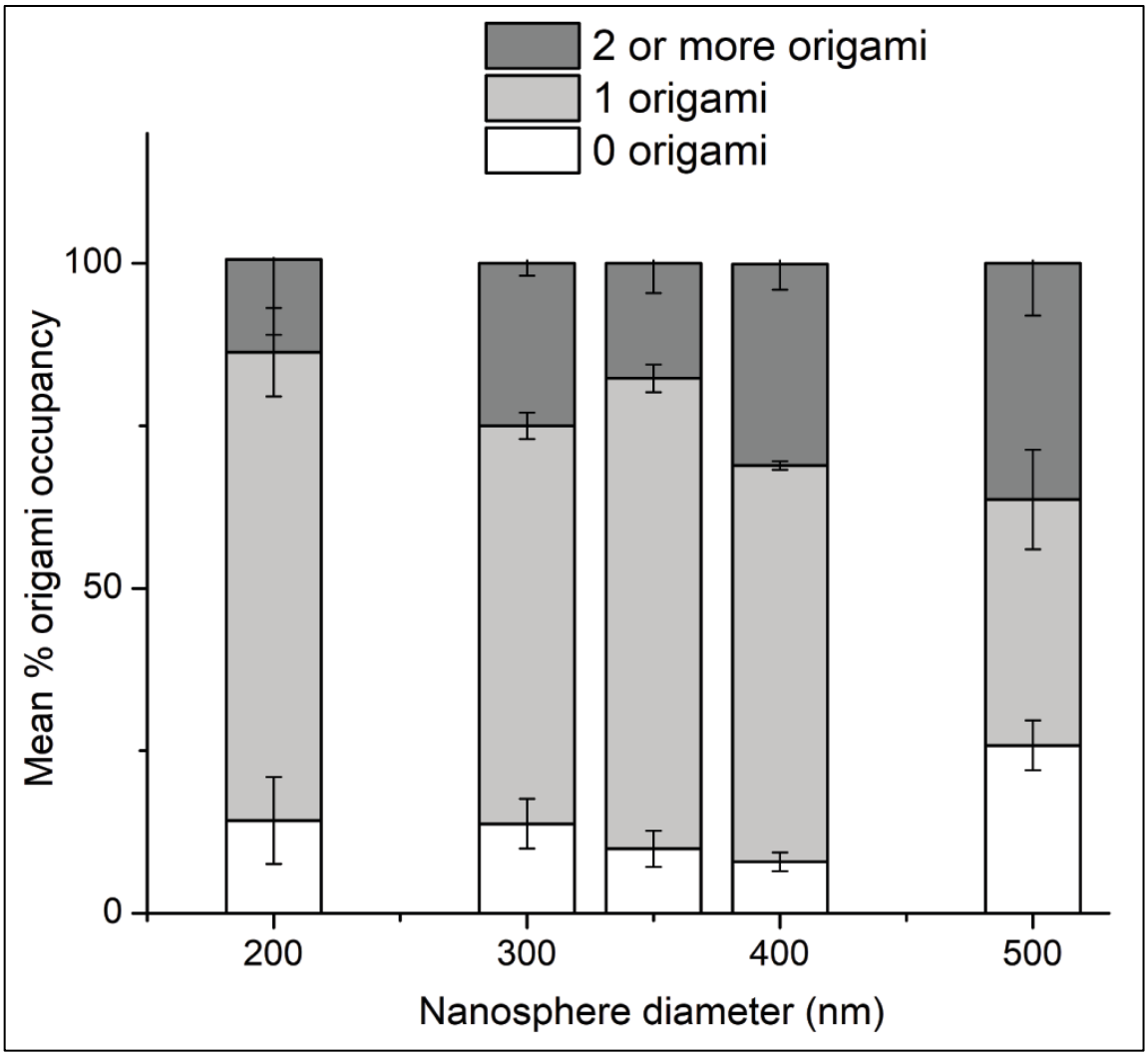

Figure 7: Mean percentage binding of zero, exactly one, and two or more origami as a function of nanosphere diameter ($n \geq 600$) demonstrating non-Poisson statistics for single molecule binding, with maximal $72.4 \pm 2.14\%$, and $72 \pm 6.84\%$ single origami binding for 350 nm, and 200 nm nanospheres.

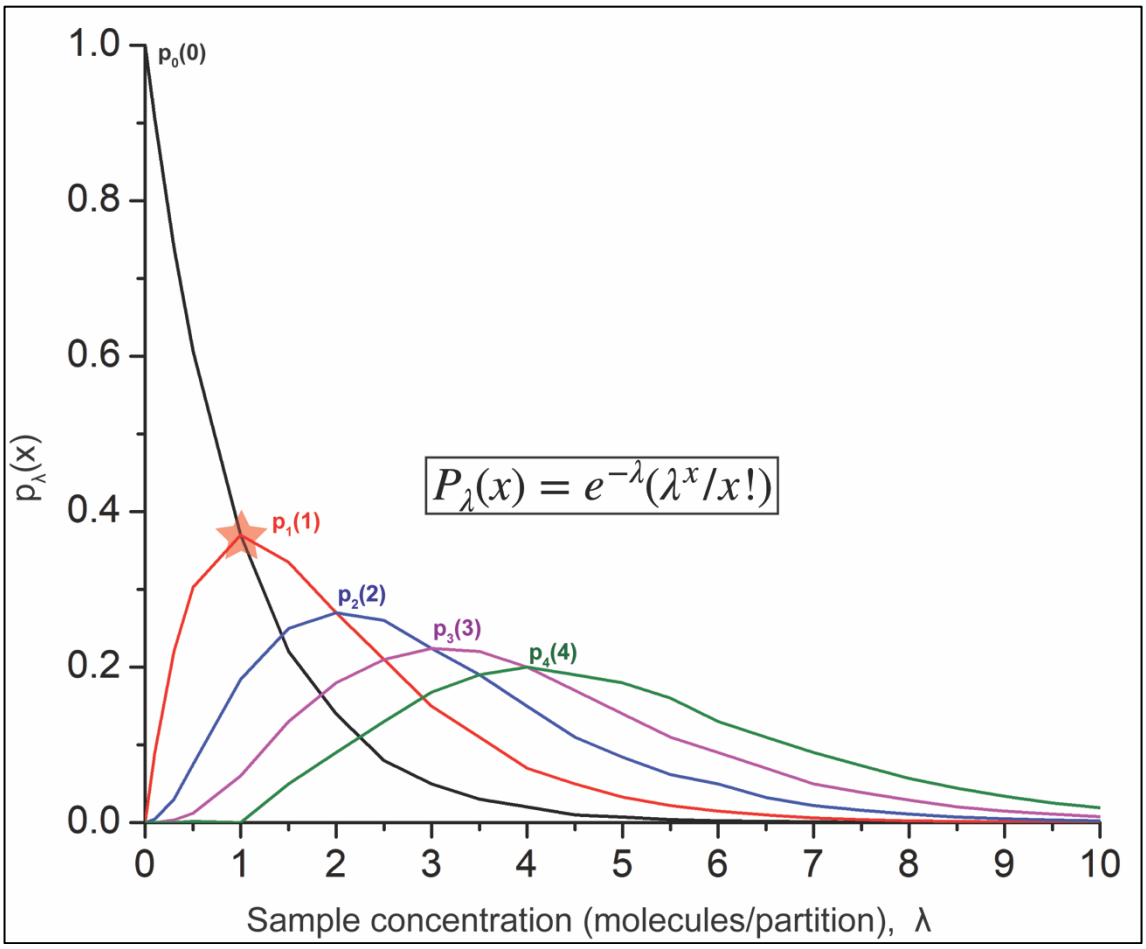

Figure 8: The Poisson distribution which poses a statistical limitation on the probability of a single molecule occupying a single partition/well on a substrate. The highest single molecule occupancy occurs in the case where the ratio of molecules to wells is one and is 37% (red star). This is the case for every stochastic top-down loading process unless a steric hindrance approach in the form of a DNA origami macromolecule (DOP (Gopinath and Rothemund 2014, Pibiri, Holzmeister et al. 2014)) is used to prevent multiple molecules from binding to the same spot, consequently driving the single molecule occupancy beyond the Poisson limit.

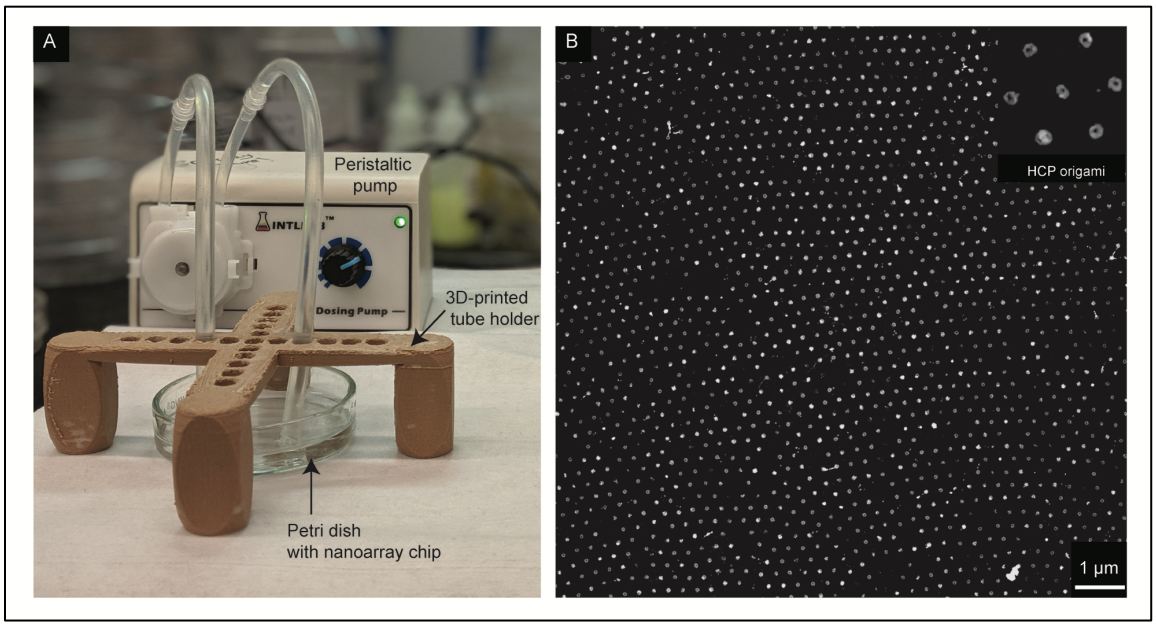

Figure 9: Automated washing using a peristaltic pump. (A) A peristaltic dosing pump utilized to automate the three, five-minute washing steps for optimized cleaning of nanoarray chips, with a 3D-printed tubing holder maintaining a constant position for consistency in quality. The dosing pump primarily mitigates user-variability introduced during the washing steps. (B) Atomic force micrograph of patterning at 66% single molecule efficiency facilitated by a peristaltic pump in lieu of high error rate manual washing steps.

Parameters	Top-down DOP	Bench-top DOP
Processing	Serial (slow)	Parallel (fast)
Single molecule yield	>90%	~75%
Cost/chip	>$100	<$1
Fabrication complexity	High	Low
Training required	Intensive	Minimal
Feature flexibility	Arbitrary	Spherical/circular
Assay format	Digital/quantitative	Digital/quantitative
SME relevance	High-throughput	High-throughput
Diagnostic relevance	Surface diffusion-limited	Surface diffusion-limited
Substrate compatibility	Mica, glass, ITO, silicon, etc.	Glass (so far)
Scalability	Chip (meso-to-macro)	Chip (meso-to-macro)
Years in development	~10	~1.5
Expected area of easy adoption	Industrial	Academia, and industry

Table 2: A comparison between the advantages and disadvantages of top-down (EBL-)-based DNA origami placement and bottom-up self-assembly (NSL-)-based nanoarray fabrication.

2.4 Conclusions

In summary, we have developed a novel, cleanroom-free, self-assembly-based benchtop DNA nanoarray patterning technique which is not limited by Poisson statistics for single molecule occupancy due to its bottom-up architecture. The technique circumvents the need for sophisticated equipment and training previously required for fabricating single-molecule nanoarrays on the micro-to-macro-scale; all at a fraction of the cost (<$1 per chip). We characterized binding site sizes concomitant with various nanosphere diameters via atomic force and electron microscopy. This provides a framework for the design of appropriately sized 2D or 3D DNA nanostructures for various single-molecule applications, with larger origami dimers enabling the use of simpler optics for resolving individual kinetic events. We report that a nanosphere diameter of ~350-400 nm is essential to optimize the binding, and diffraction-limited imaging of single, circular DNA origami nanostructures (~75%) and their associated payloads on high-density grids.

CHAPTER 3* DEMOCRATIZING HIGH-THROUGHPUT, DETERMINISTIC, SINGLE-MOLECULE EXPERIMENTS ON THE NANOARRAY PLATFORM

Abstract

Traditionally, single-molecule experiments (SME) have relied on stochastic immobilization of molecules-of-interest through biotin-avidin or similar chemistries. This presents a "concentration vs. throughput" conundrum, i.e. higher throughput would mean a higher probability of multiple molecules randomly overlapping each other in the same diffraction-limited spot. Unless super-resolution techniques are employed, this would confound data interpretation owing to poor localization of signals from fluorescence events corresponding to individual molecules. On a conventional, diffraction-limited microscope, sophisticated data analysis strategies, and oftentimes, multiple experiments need to be performed in order for useful information to be gleaned. Conjugating molecules-of-interest to DNA origami deterministically placed at a predetermined pitch in a meso-to-macroscale array represents an elegant method to maximize the throughput of any single-molecule experiment. Furthermore, the underlying grid-based pattern can enable straightforward rejection of noise and make analysis paradigms simpler for potentially digital assays.

*Some parts of this chapter appear in a manuscript in preparation:

Facile, cleanroom-free fabrication of single molecule nanoarrays

Rishabh M. Shetty, Sarah Brady, Eric Le, Maeve Kennedy, Paul W. K. Rothemund, Rizal F. Hariadi, Ashwin Gopinath

3.1 Introduction

The first question to ask ourselves is: Why bother with single molecules? Surely macroscopic analytical tools are better suited to studying larger systems such as cells and tissues, and it would allow the sampling of a higher number/range of molecules at once, would it not? The simple answer is that for all single-molecule methods and by extension, novel physical methods and analyses to exist is the fact that at the molecular level there is a prevalence of *heterogeneity*. This makes it impossible to sample all at once the multiple different states and conformations single molecules can take up to perform different functions at different times in a cellular system, yielding, at best, average measurements that may ultimately be inaccurate for making overarching conclusions. The real strength of single-molecule biophysics experiments is therefore that subpopulations of molecular states can be investigated, without having to painstakingly introduce highly improbable and physiologically disruptive synchronicity in bulk systems. One of the important limitations with single-molecule studies, however, is their low-throughput nature (Leake 2012).

To understand the functional significance of molecular processes in the cell such as transport of cargo, transcription, translation, protein folding, etc. it is important to study their spatial and temporal organization at the molecular level (Dulin, Lipfert et al. 2013). The interest in gaining quantitative and mechanistic insight into the coordinated actions of purified systems in the context of the living cell has guaranteed the rapid advancement of the fields of molecular biology and biochemistry and their sub-disciplines such as biophysics, bioinformatics, and nanotechnology. The analytical tools required to probe these processes have seen a similar inflection in development with the ability to observe events at the nanometer-scale spatial and millisecond-scale temporal resolution.

Since the introduction of fluorescence microscopy, and especially Total Internal Reflection Fluorescence Microscopy (TIRFM) (Axelrod, Burghardt et al. 1984, Axelrod 2001) and super-resolution microscopy (Huang, Bates et al. 2009), single-molecule experiments studying kinetics of protein and nucleic acid conformational fluctuations, folding mechanisms, etc. have become commonplace in a host of biophysics laboratories (Ha 2001, Roy, Hohng et al. 2008). These experiments for studying dynamic events are generally performed at low salt concentrations to avoid aggregation of proteins, and other single molecule components in addition to yielding faster dynamics.

Classical single-molecule experiments are stochastic in nature (Ha 2001, Roy, Hohng et al. 2008, Dai, Jungmann et al. 2016, Jungmann, Avendano et al. 2016, Schnitzbauer, Strauss et al. 2017, Strauss, Schueder et al. 2018, Stehr, Stein et al. 2019), i.e. biophysicists lack the ability to control where individual molecules bind on a glass surface. This leads to the possibility that two or more molecules may occupy the same diffraction-limited spot, confounding data interpretation. Reducing the concentration of molecules observed is a possible solution but ultimately has the caveat of lowering experimental throughput. This is the underlying limitation of most current single-molecule experiments. Maximizing throughput while programmatically positioning molecules-of-interest on an experimentally relevant substrate requires the close-packing of individual molecules at the diffraction limit of light, a non-trivial problem, to say the least. DNA origami, touted as the bridge from bottom-to-top (Xu, Harb et al. 2017), has the potential to facilitate these high-throughput, deterministic, single-molecule experiments (SME) on a basic laboratory benchtop through the nanoarray platform.

Traditionally, *in vitro* single-molecule studies have employed the classical biotin-avidin based immobilization of the molecules-of-interest. While being extremely attractive, one of the primary limitations of this chemistry is the non-specific binding

(stochasticity) associated with it. It is routinely in the final phase of analysis that an experiment can be categorized as reliable or unreliable. Predefined placement of single molecules on a hexagonally-close packed (HCP) grid not only circumvents the unwanted immobilization of multiple molecules to the same spot but also lends an unmistakable "blueprint" to each experiment. This enables the straightforward rejection of regions without grid-like areas or of data points not part of a grid as those associated with background noise (e.g. signal associated with non-specifically bound origami on the passivated surface). While the patterning does not eliminate non-specific binding completely, it presents an attractive solution for noise filtering during downstream analysis. Another significant advantage of the nanoarray platform is the ability to pre-or post-label the DNA origami with fluorophores (e.g. Cy-5) spectrally-separated from experimentally relevant fluorescence (e.g. Cy-3, Cy-3b). This provides an additional layer of signal integrity verification by correlating two fluorophore channels and ensuring specificity of signaling events on the underlying grid of origami.

In this work, we first explored the robustness of the nanoarray platform to test its relevance for biophysical experiments conducted at low salt concentrations. The stability of origami nanostructures themselves under varied conditions is well characterized (Kim, Surwade et al. 2014, Gerling, Kube et al. 2018). Furthermore, we argue that while facilitating high-throughput experiments, predefined placement of single molecules on an HCP grid lends a recognizable pattern to each experiment. Such *a priori* information on the spatial location of molecules not only aids experimental troubleshooting but also noise filtering during downstream analysis. Finally, we demonstrate a high-throughput version of a classical SME: DNA-Points Accumulation for Imaging in Nanoscale Topography (PAINT) (Jungmann, Avendano et al. 2016, Schnitzbauer, Strauss et al. 2017, Strauss, Schueder et al. 2018) on the nanoarray platform, and report on the differences observed

in deterministic vs. stochastic experiments. We foresee the wide application of this nanoarray technique in the same vein as other high-throughput methods predominantly based on chip-based microfluidics (Greene, Wind et al. 2010, Ullman, Wallden et al. 2013).

3.2 Materials and Methods

Origami design, preparation, and purification were performed as detailed in Chapter 2. For annealing DNA-PAINT origami, and any other origami annealed overnight (photobleaching), a ramp of 0.004°C/min was used in the critical "folding" range of 60°C-50°C, a 0.005°C/min ramp was used between 70°C-60°C and 50°C-40°C, and a 0.1°C/min ramp was used between the 90°C-70°C and 40°C-25°C temperature ranges. Docking strand staples were introduced at 75-100x excess to the annealing mix as suggested by Jungmann et al. (Jungmann, Avendano et al. 2016). Instead of spinning at 6000g as with unmodified origami, DNA-PAINT, and photobleaching origami (especially when annealing with fluorophores) were spun at 1500g-2000g, for 15-30 mins, 5-8 times before collecting the purified product and running a gel for validation of purity.

Control experiments were performed by preparing fresh dilutions of origami and utilizing Mg^{++}-mediated immobilization to activated glass substrates. All TIRF experiments were conducted on a benchtop super-resolution, Oxford Nanoimager (Oxford, UK). For control DNA-PAINT experiments, a glass chip was activated for 10 minutes, followed by the creation of a "flow chamber" (using double sticky Kapton tape, ULINE, WI) and 30-minute incubation of 100-500 pM DNA origami at 40 mM Mg^{2+}. Non-specifically bound DNA origami was washed off using several rounds of wicking the incubation buffer through the chamber. Next, a 0.05% Tween-20 (Cat # P1379, Sigma Aldrich) v/v in 40 mM Mg^{2+} placement buffer was flown through several times before incubating the solution for 5 minutes. This prevents non-specific *ss*DNA binding during the experiment. Subsequent washing in Tween-buffer, and placement buffer was followed

by the introduction of up to 5 nM P1-imager solution in placement-Tween buffer, 10x dilution of 40-nm Gold nanoparticles (fiducials for drift correction, Cat # 741981, Sigma Aldrich), and an oxygen scavenging system (2x, 3x, 5x concentrations of PCA, PCD, and Trolox-Quinone respectively). To ensure the gold nanoparticles settle on the bottom chip, it was taped to a 96-well plate holder in a centrifuge and spun at 150g for 5 minutes. Experiments with patterned chips were conducted by sticking the 10 mm x 10 mm coverslip onto a double-sided sticky Kapton tape and repeating the procedure as outline above starting with incubation with 0.05% Tween-20 in placement buffer. Buffer components are detailed in Table 3.

DNA-PAINT data were analyzed using Picasso (Schnitzbauer, Strauss et al. 2017). Briefly, a dataset less than 4 Gb was prepared for analysis on Picasso *Localize*. A min. net gradient of 5000 was chosen to avoid non-specific signals from being analyzed. After the fits were found, the .hdf5 file was loaded in the *Filter* module of Picasso. This module allows localization precision filtering, as well as the filtering of "double" localizations by manually selecting a Gaussian profile of localization photons. The filtered localizations dataset is then loaded into Picasso *Render* where multiple cross-correlation-based drift corrections and multiple corrections based on picking fiducial markers on the sample (Gold nanoparticles and/or origami themselves ["pick similar"]) were used to perform more precise nm-scale drift correction. The threshold was adjusted prior to automatic or manual picking of structures to be averaged. The picked localizations were then registered into Picasso *Average* where they were aligned using center of mass followed by multiple iterations of rotational and refined translational alignment to form the final "summed" image. A nominal oversampling value of 200 was used to represent the structures prior to measuring the PSFs in ImageJ using an ROI drawn around each vertex and finding its full width at half maximum (FWHM).

Note:

1. A concentration beyond 0.1% Tween-20 may result in displacement of origami from the binding sites.
2. All datasets analyzed had duty cycles of 1:10-1:50 (10,000-12,000 frames) and were screened based on amount of photobleaching as a quality control measure.

Buffer components	Volume (µL)
Imager "P1" in 40 mM Mg^{++} + 0.05% Tween-20 (10 nM, stock)	30
40 mM Mg^{++} + 0.05% Tween-20	16.7
40 nm gold nanoparticles	6
PCA (50x, stock)	2.5
PCD (100x, stock)	1.8
Trolox-Quinone (100x, stock)	3
Total	60

Table 3: DNA-PAINT buffer components for optimized PAINT experiments on the nanoarray platform.

Photobleaching experiments were performed immediately after grid formation in imaging buffer (1x TAE. Mg^{2+} at 12.5 mM, and oxygen scavenging [PCA, PCD, Trolox-Quinone] similar to PAINT). Control experiments of randomly immobilized origami (in 40 mM Mg^{++} on an activated coverslip) were also performed. In both cases, fluorophore-labeled strands were added at a concentration between 10 nM-100 nM (i.e. >10x-100x excess). Laser intensity was adjusted in order to have a slow gradient of fluorophore intensity bleaching to make step-counting easier. Steps were quantified using two methods: ImageJ, and iSMS (http://inano.au.dk/about/research-groups/single-molecule-biophotonics-group-victoria-birkedal/software/). For the latter, the field-of-

view was cropped, and the two ROIs were aligned to count the number of steps distinctly. The following were the conditions when analyzing photobleaching data:

- Must bleach completely
- Must look like a single molecule and not aggregates
- Must show <= 6 steps
- Must have a consistent step size (quanta) to be counted as a bleaching event

3.3 Results and Discussion

3.3.1 Evaluation of nanoarray robustness in low salt concentrations, and shelf-life

We explored the robustness of the nanoarray platform presented here to test its relevance for biophysical experiments conducted at low salt concentrations. We first performed control experiments on multiple glass substrates to test the quality of random immobilization of circular origami (250 pM, 30-minute incubation) suspended in varying Mg^{2+} concentrations (1 mM - 40 mM) and observed (post-dehydration) that a minimum of 5 mM Mg^{2+} was required to stabilize origami on an activated glass surface (Figure 10, top row). Beyond 20 mM Mg^{2+} (data not shown) there was no noticeable change in the number of origami immobilized in any given scanned area. Next, we randomly immobilized origami suspended in placement buffer (40 mM Mg^{2+}, pH 8.3), (ethanol-) dehydrated the surface for AFM characterization, rehydrated the origami in low salt concentrations for two hours (1 mM- 40 mM Mg^{2+}), dehydrated once more, and observed no apparent change in the quality of origami immobilization under AFM (Figure 10.b, middle row). Finally, to confirm that this process translated effectively to programmatic placement, we patterned origami on a 700-nm “grid” (40 mM Mg^{2+}, pH 8.3, 300 pM), dehydrated the surface, rehydrated for two hours in 1 mM-40 mM Mg^{2+} concentrations, and dehydrated again to observe high-quality grids via fluorescence micrographs as assessed by their 2D-Fourier Transforms (Figure 10.c, bottom row). These results help

demonstrate the robustness of this platform at low salt concentrations and validate its use for relevant single-molecule biophysics experiments. Prior to each dehydration step, the substrate was washed for one minute in 1x TAE (12.5 mM Mg^{2+}) buffer to remove any non-specifically bound origami. We suspect that the drying process sequesters and stabilizes Mg^{2+} bridges between the origami and the silanol groups on the binding sites such that origami are conserved in an entropically-favorable energy state, preventing dissociation or structural disintegration upon rehydration. Subsequent resuspension in lower divalent salt concentrations has no adverse effects on these immobilized/placed origami, unless they are resuspended in a buffer containing monovalent cations such as Na^{+}. This is presumably because the Na^{+} ions displace the sequestered Mg^{2+} ions but are unable to bind the origami strongly enough to keep them immobilized. Perhaps increasing the monovalent salt concentration (100x Mg^{2+}) might be required to maintain the immobilized state of origami molecules. Further proof of platform robustness is demonstrated through its long shelf life of several months without the need for sophisticated storage (Figure 11).

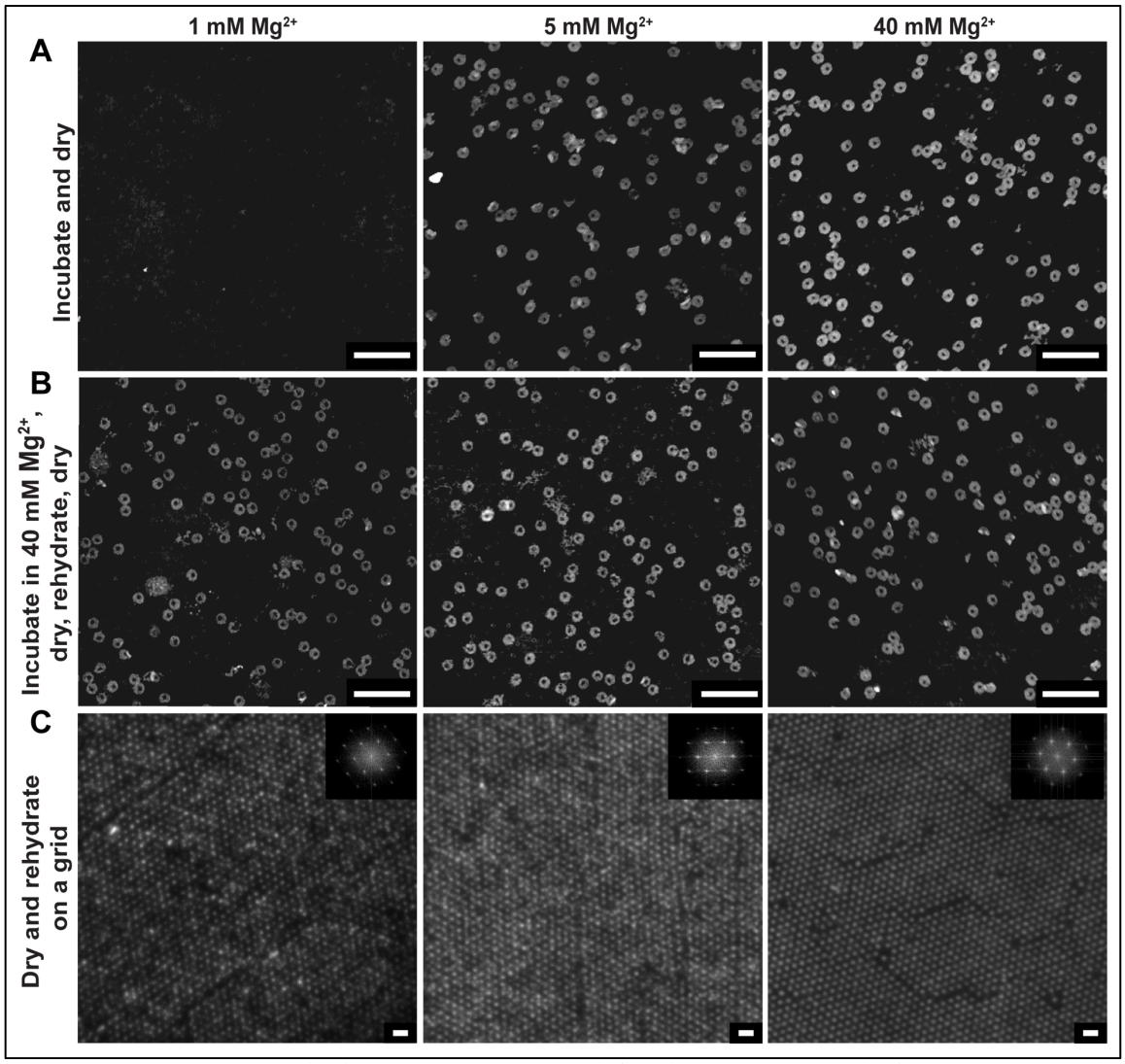

Figure 10: Nanoarray platform robustness and flexibility. A) Atomic force micrographs demonstrating robustness of origami immobilization post-ethanol drying and rehydration on an activated glass substrate through direct incubation in 1 mM, 5 mM, and 40 mM Mg buffer (controls, top row); (B) Incubation in 40 mM Mg followed by ethanol drying and 2-hr rehydration in different salt concentrations of 1 mM, 5mM, and 40 mM Mg, and consequent drying (middle row); and finally, (C) Fluorescence micrographs of Mg-mediated immobilization on the nanoarray platform at 40 mM Mg followed by 2-hr rehydration in the respective 1mM, 5 mM, and 40 mM Mg buffers. Scale bars are 1 μm.

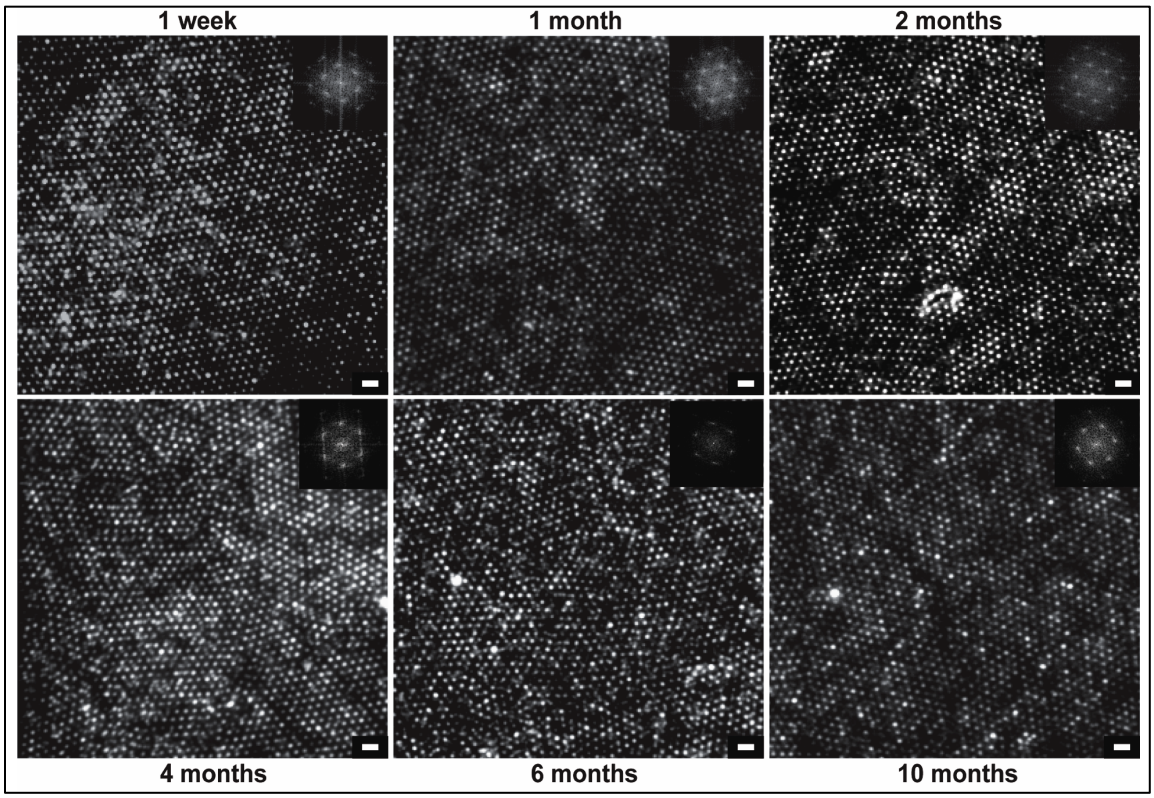

Figure 11: DNA nanoarray shelf-life was validated using two chips: labeled with fluorophores, and unlabeled. At each time point, both chips were visualized, with the second being labeled immediately prior to observation. Post 2-months, already labeled chips were the only ones visualized every month for quality assessment. Scale bars are 1 μm.

3.3.2 Platform versatility: high-throughput, deterministic biophysics

As a final demonstration of the platform's utility, we performed several experiments aimed at highlighting its application-oriented advantages. We began by attaching six fluorophore-labeled strands to each circular origami and characterizing the number of fluorophores unequivocally tethered onto each origami baseplate (Figure 12). Owing to its targeted single-molecule applications, it is essential to understand the efficiency of hybridization prior to performing these experiments. While we observed an average of ~50-60% conjugation efficiency using two characterization metrics (photobleaching, and DNA-PAINT), location-dependent yields of 84% have been previously reported (Strauss,

Schueder et al. 2018). We hypothesized that this could possibly be due to poor strand accessibility or low conjugation efficiency. It is important to note that the circular origami have been empirically shown to break up-down symmetry using staples modified with 20T extensions that act as entropic brushes, with 95.6% origami facing right-side up (Gopinath, Thachuk et al. 2018). We first tested whether the dehydration step may be causing a fraction of the six "handle" strands to collapse onto the surface in a manner that precluded access to them during experiments. However, circumventing the dehydration step (to rule out the accessibility problem) and additionally, directly annealing the fluorophore-labeled complementary strands with the handle strands (to probe the conjugation conundrum) did not lead to any significant changes in incorporation efficiency. The reasons for sub-par conjugation efficiency may therefore be sequence-, strand concentration-, strand purity-, strand position on origami-, or origami purification strategy-dependent. This, while concerning, is a broader question for the field of structural DNA nanotechnology itself and a comprehensive examination is therefore beyond the scope of this work.

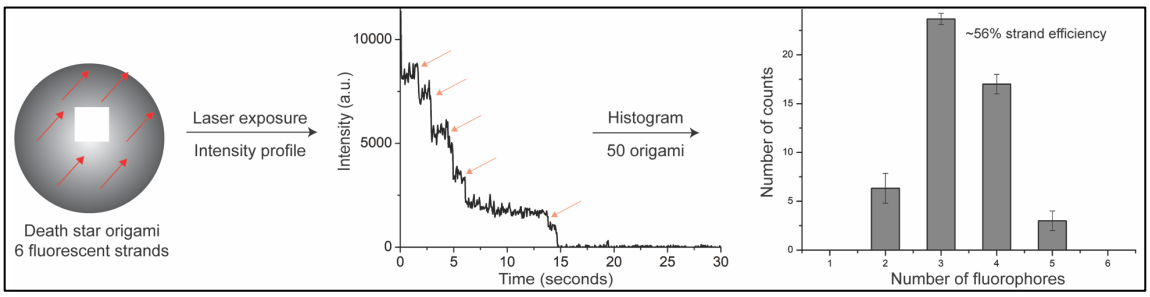

Figure 12: Schema of the hexagonal arrangement of single, fluorophore-labeled DNA strands on individual origami. Intensity profiles of each photobleaching event enables step counting and a histogram of conjugation efficiency is presented; which is ~56%, i.e. 3.36 strands of a possible 6.

Counting of photobleaching events for characterization of single-molecule conjugation efficiency appears to be a relatively straightforward process. However, it has been reported to be experimentally and analytically cumbersome (Jungmann, Avendano

et al. 2016, Tsekouras, Custer et al. 2016) owing, in part, to the complex photophysics of dye molecules. Super-resolution DNA-PAINT (Dai, Jungmann et al. 2016, Jungmann, Avendano et al. 2016, Schnitzbauer, Strauss et al. 2017, Heydarian, Schueder et al. 2018, Strauss, Schueder et al. 2018) has proven to be an effective alternate strategy of quantification for up to 150 distinct *ss*DNA and (potentially) other conjugated moieties on DNA origami substrates (Jungmann, Avendano et al. 2016). However, DNA-PAINT experiments, like other single molecule experiments, can be stifled by the concentration of DNA origami immobilized on the surface via biotin-avidin chemistry. Utilizing the nanoarray platform for high-throughput PAINT experiments on a grid presents an attractive extension to this technology.

To provide a real-world example of the "concentration vs. throughput conundrum," as schematically represented (Figure 2.a), we performed DNA-PAINT experiments on randomly immobilized origami nanostructures as well as patterned origami nanostructures. We first provide atomic force micrographs as evidence that even at low concentrations of origami or other single molecules (Figure 13, left panel) it is more than likely that two or more structures could randomly immobilize in a diffraction-limited spot and confound interpretation of data. An increase in concentration to improve throughput only results in a higher fraction of structures overlapping each other (Figure 13, middle panel). However, when patterned on a glass substrate by a distance slightly greater than the diffraction-limit, up to 75% of origami molecules singly occupy individual binding sites (Figure 13, right panel). The nanoarray platform therefore presents the optimal solution to the conundrum most biophysicists are faced with.

We arranged three "docking" strands per vertex of a hexagon as schematically depicted (Figure 17, top row, second column) to transiently bind fluorescently labeled "imager" strands in solution. The rationale behind using three strands per vertex was to

counteract the low conjugation efficiency observed through photobleaching experiments and increase the probability of at least one of them binding imager strands. Control experiments with randomly dispersed origami were first performed to justify conducting PAINT on origami immobilized through Mg^{2+}-bridges on activated, and/or dehydrated glass coverslips. There seemed to be no qualitative difference between our experiments when compared to traditional, biotin-avidin based immobilization of DNA origami. In addition to the HMDS layer, which is intrinsically part of the nanoarray fabrication process, we passivated the glass surface against non-specific interactions of fluorescent, *ss*DNA via a 0.05% (v/v) Tween-20 detergent in the 40 mM Mg^{2+}, Tris-HCl "placement" buffer (pH 8.3). This passivation aided in improving the Signal-to-Noise ratio (SNR), making it comparable to those routinely reported with PAINT studies using standard imaging and data processing protocols(Schnitzbauer, Strauss et al. 2017). High-density PAINT experiments were then performed on patterned substrates with inter-origami pitches of 350-nm to provide mostly single origami per binding site and maintain diffraction-limited resolvability of grids. Fluorescence micrographs of the respective datasets (100 pM; 500 pM; 350-nm, 350 pM patterned) are also presented (Figure 13.b).

Our results indicate that when individual structures are averaged using the standard processing software, Picasso (Schnitzbauer, Strauss et al. 2017), and their full width at half maximum (FWHM) measured as a means to characterize the point spread function (PSFs) for the "sum" image, the corresponding hexagons reveal interesting details about the effect of patterning. Our analysis pipeline involved PSF comparisons (Figure 15) between the low (100 pM), and high concentrations (500 pM) of randomly immobilized origami with patterned origami (400 pM) for automatically-picked structures versus manually-picked structures (Figure 14).

We note that all origami used for these experiments broke up-down symmetry (20-T staple strands) and were therefore expected to have specific interactions with the imager strands. Based on an initial input of 5-10 manually-picked structures, Picasso automatically picks "similar" structures which can be saved and averaged by first aligning using their center of mass and finally through translational and rotational alignment over multiple iterations. This reveals the final averaged structure (Figure 14). We picked 200 structures (at least four out of six vertices present) manually for each dataset (Figure 14.b), whereas the software picked ~1800, 8000, and 5200 structures for the low, high, and patterned cases, respectively (Figure 14.a). This points to a ~3x increase in throughput from the low concentration experiment (standard) to the patterned experiment for automated picking. The theoretical number of structures available for the patterned dataset, however, was ~18000 structures (350-nm pitch), i.e. a theoretical improvement of almost an order of magnitude in throughput. While the manually-picked structures from the randomly immobilized origami had a comparable average PSF (with standard error of mean) of 22.19 ± 1.57 nm (low), and 23.02 ± 1.63 nm (high), the patterned data exhibited a lower average value of 19.57 ± 1.38 nm (Figure 15). As we expected, the automatically-picked structures showed a higher average PSF for the high concentration experiment (28.88 ± 0.32 nm) in comparison with the low concentration (23.66 ± 0.55 nm) and patterned (23.93 ± 0.33 nm) PSFs. This could indicate that the multiple overlapping structures in the high concentration case as evidenced through AFM images (Figure 13.a, middle panel) result in the software poorly localizing individual origami structures and a consequent (~20%) loss in image resolution. This is also visibly evidenced through the "smearing" of individual vertices in the averaged image (Figure 13.a, middle panel).

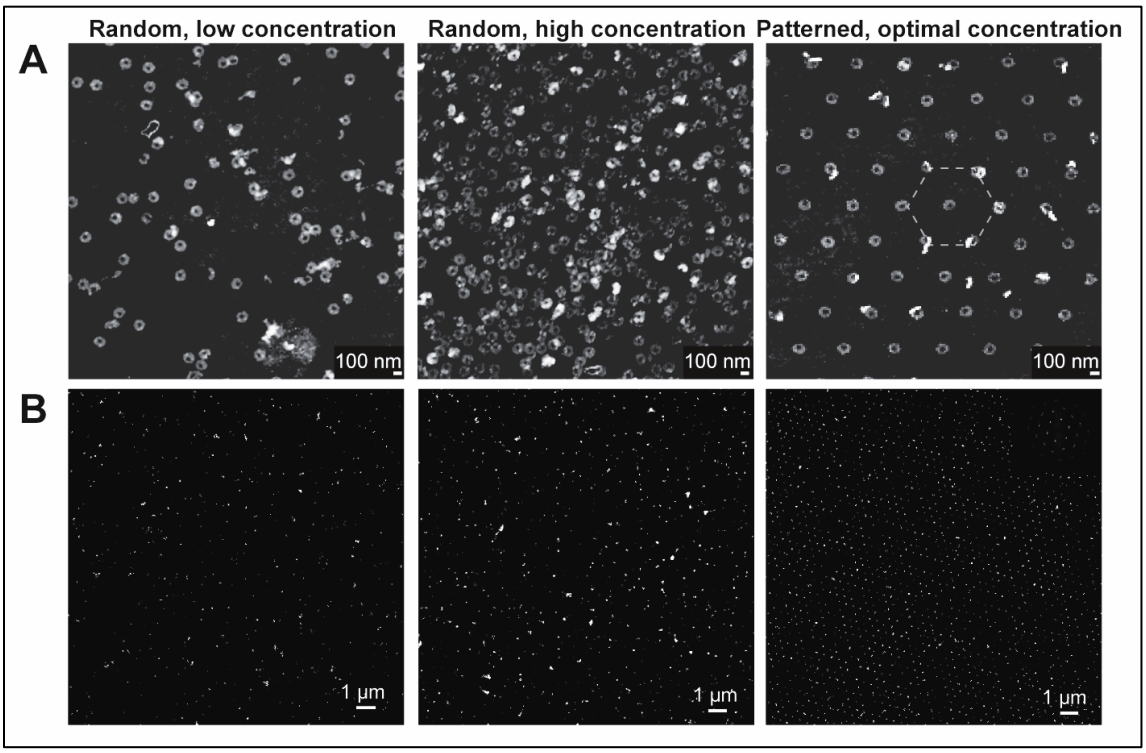

Figure 13: A platform for high-throughput, deterministic single-molecule studies. (A) Atomic force micrographs contrasting stochastic single-molecule immobilization for low (100 pM), and high (500 pM) origami concentrations with origami deterministically patterned at the diffraction limit. (B) Fluorescence micrographs of the same data as in (A) in Picasso Render.

We speculate that the bright points distinctly visible in both, automatically- as well as manually-picked structures could be a combination of two factors — location/sequence-dependent strand conjugation efficiency, as well as random noise. We expect random noise to be a factor especially in the case of automatically-picked structures with its source being non-specific interactions with- the surface, deformed origami, multiple overlapping origami, or gold nanoparticles used as fiducial markers for drift correction. For the manually-picked structures, we expect that the symmetry of the pattern (hexagon) contributes to the software localizing certain vertices more brightly than others, based on uncontrollable parameters (scoring function, alignment precision, etc.) in the analysis pipeline, in addition to the number of structures containing all six vertices. As a quality

control check to ascertain that the bright vertices were not solely a random function of the software analysis and might indicate a probability of certain strands being conjugated/accessible more than others, we performed experiments where we excluded the "docking" strands for one vertex and another where we excluded two vertices (Figure 16, third and fourth columns). We observed that there was a low occurrence of at least one of the locations along the horizontal axis of the origami in the case of four expected vertices, whereas the fifth vertex in the third column did not have as many occurrences as the others. Another possible reason for this (four vertices case) could be the rotational symmetry along the vertical axis biasing the software rotational alignment to make one vertex brighter than the other. In any case, it is evident that the nanoarray platform demonstrably provides an elegant solution to maximizing the throughput and quality of data. Further, due to its intrinsically deterministic nature, it is amenable to software automation for simpler data analysis paradigms. We also show a fluorescence micrograph

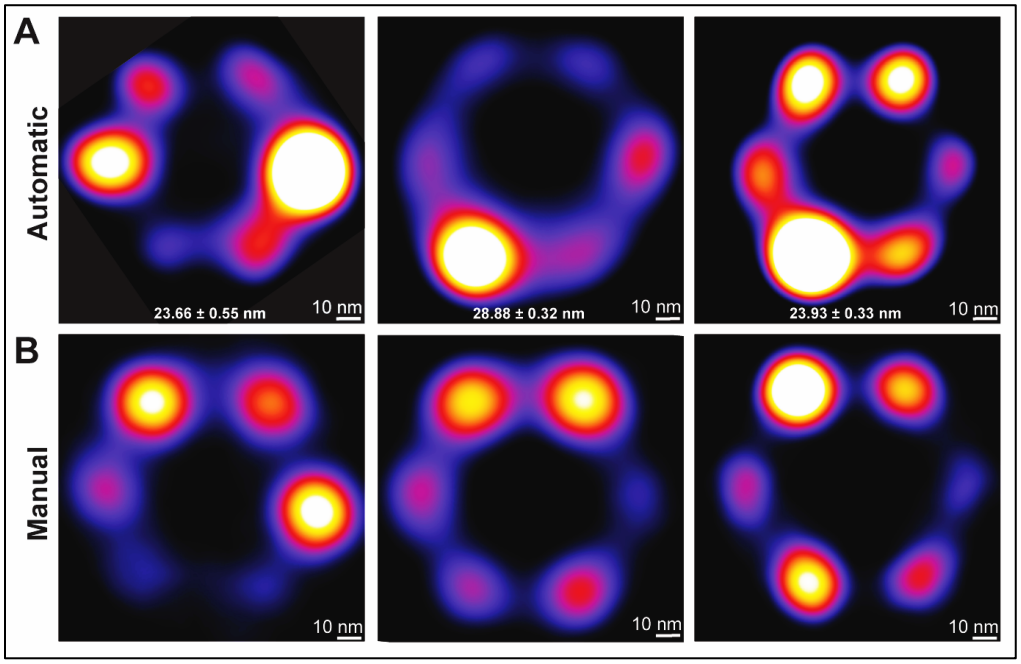

Figure 14: (A) An averaged image of automatically-picked structures corresponding to the low, high, and patterned experimental designs (N = ~1800, 8000, and 5000, respectively). (B) An averaged image of manually-picked structures corresponding to the low, high, and patterned experimental designs (N = 200, all cases).

of an exemplarily patterned PAINT-dataset of 11,000 frames (350-nm) collapsed along the Z-axis prior to analysis (Figure 17), in addition to the tunability of pitch on the nanoarrays (fluorescence micrographs for 1000-, 700-, and 400-nm, Figure 18). Appendix B provides a comprehensive list of strands used for DNA-PAINT, and photobleaching experiments as well as HCR experiments described in Chapter 4.

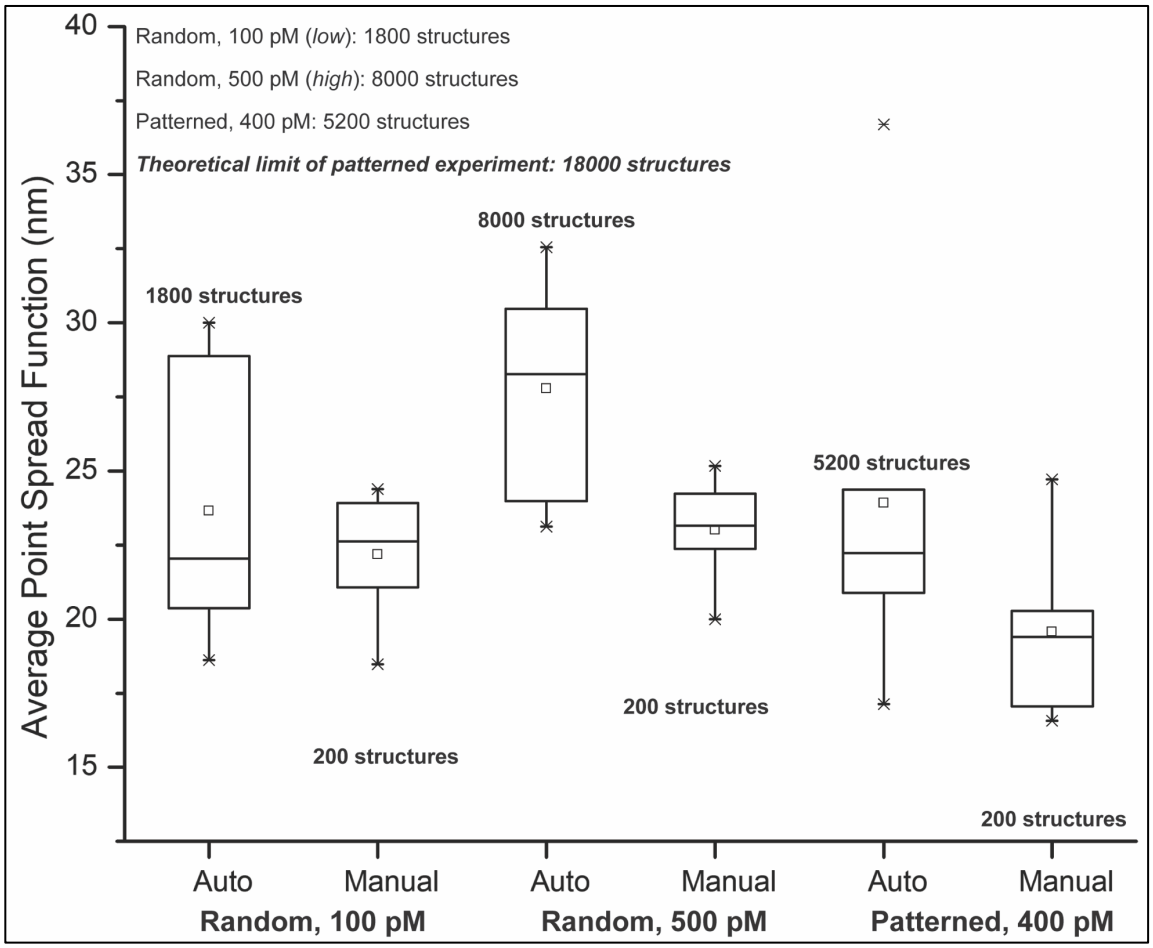

Figure 15: A box-plot of the Point Spread Function (PSF) of each hexagon and its individual (6) data points for the automatically-picked, and manually-picked averaged images in (B) and (C). The average PSFs are 22.19 ± 1.57 nm (auto) and 23.66 ± 0.55 nm (manual) for the low concentration dataset, 23.02 ± 1.63 nm (auto) and 28.88 ± 0.32 nm (manual) for the high concentration dataset, and 19.57 ± 1.38 nm (auto) and 23.93 ± 0.33 nm (manual) for the patterned dataset.

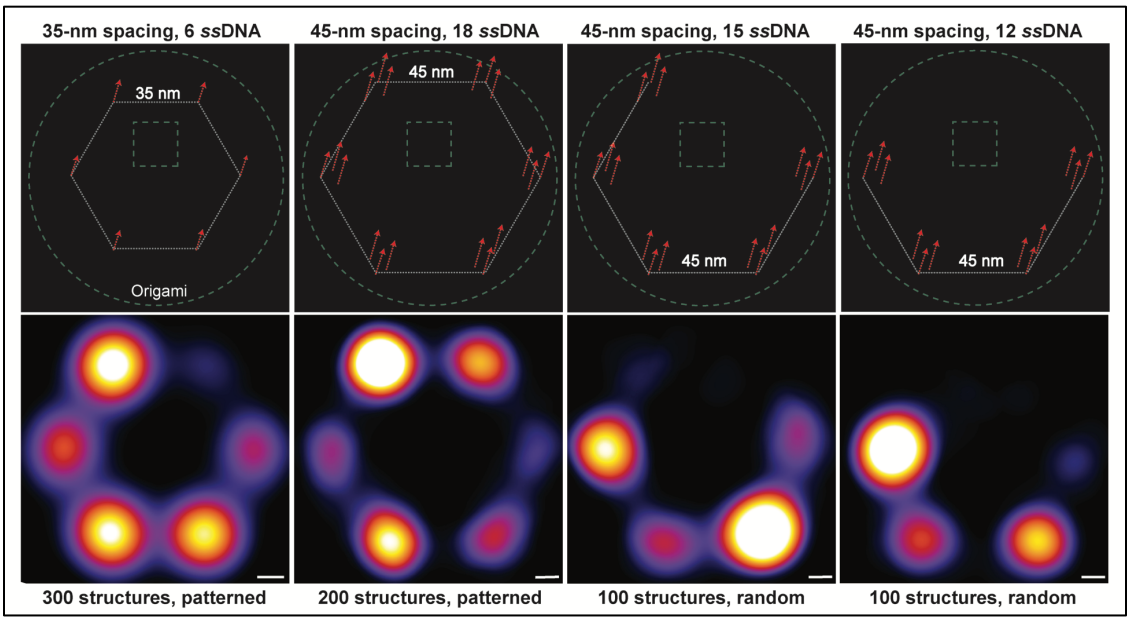

Figure 16: Three configurations of DNA-PAINT experiments with modified spacing (45-nm, and 35-nm) as well as number of "docking" strands (6, 18, 15, 12) and their corresponding averaged images formed using 10 iterations at an oversampling of 200. From left-to-right: manually picked structures in Picasso from a Patterned sample (N=300); Random control sample (N=200); Random control sample (N=100); and Random control sample (N=100). Each structure consists of at least 4 out of 6 vertices for the 6, and 18-vertices samples, at least 3 out of 5 vertices for the 15 vertices sample, and at least 3 out of 4 vertices for the 12 vertices sample. All scale bars are 10-nm.

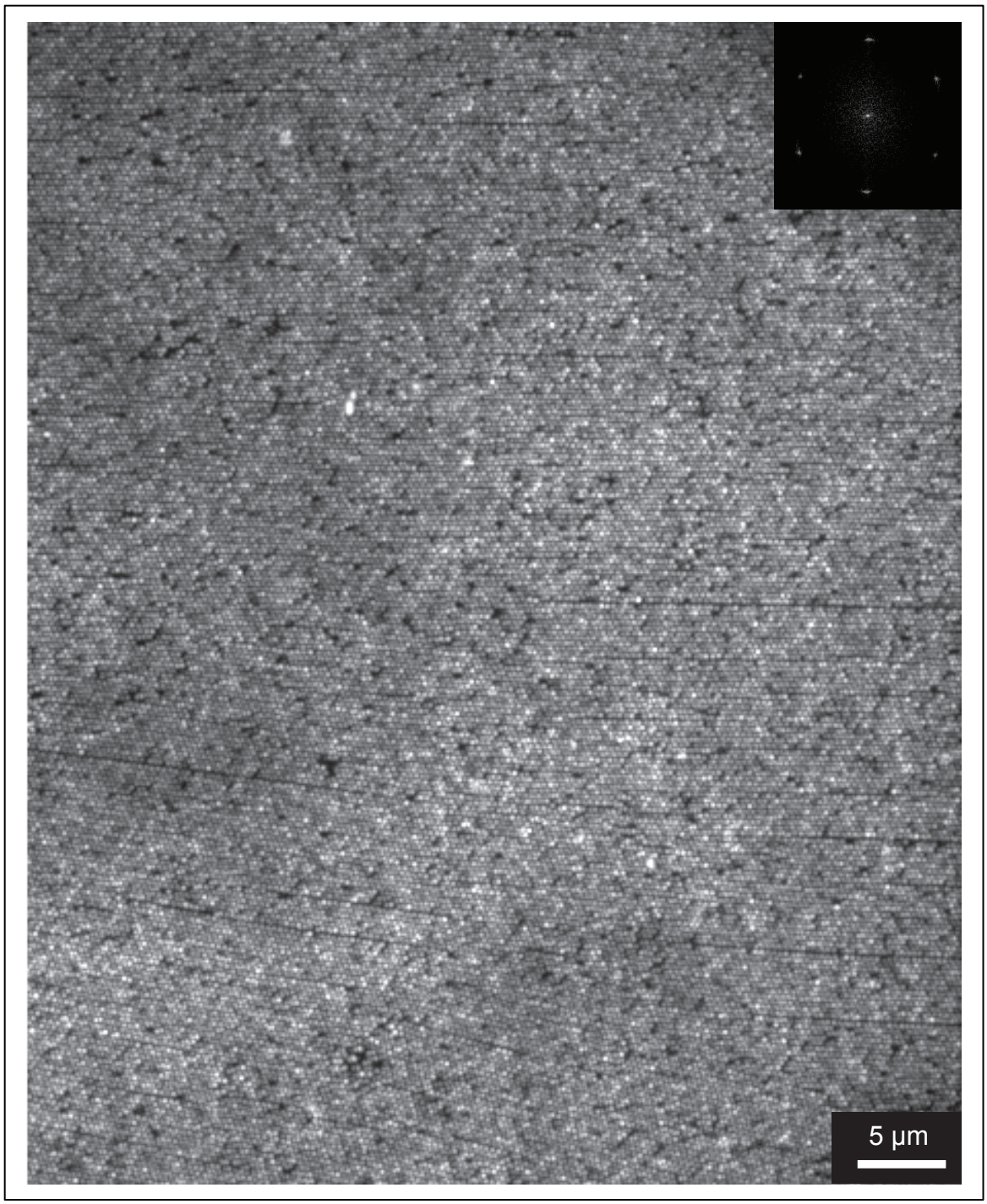

Figure 17: An exemplary, full field-of-view fluorescence image of 11,000 frames collapsed along the Z-axis of a patterned PAINT dataset (with an FFT inset) prior to data analysis on Picasso. The distance between origami was 350-nm.

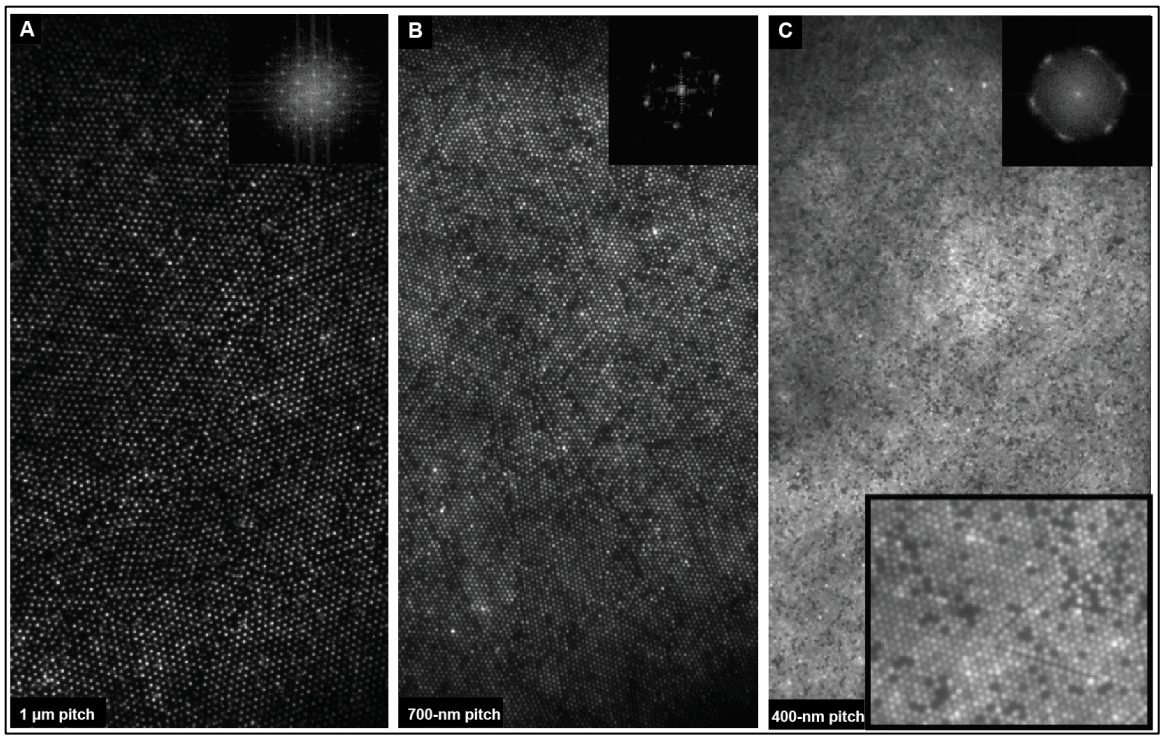

Figure 18: Tunability of nanoarray platform. (A), (B), and (C) represent 50 µm x 80 µm fields-of-view for 1 µm, 700-nm, and 400-nm grids of origami labeled with ~200, Poly-A Cy3b per origami. The single origami occupancy drops below the Poisson barrier with nanosphere diameters larger than 500-nm.

3.4 Conclusions

We validated the utility of the benchtop nanoarray platform for *in vitro* single-molecule experiments under low (1-5 mM) divalent salt concentrations and highlight its advantages of facile preparation, versatility, and high-density data (up to 10x) collection over the classical, biotin-avidin based surface immobilization chemistry. We report on the long shelf-life of the platform (up to 10 months), both qualitatively and with respect to its functionality. We demonstrate the high-throughput, and deterministic nature of the platform for single-molecule experiments such as super-resolution, traditionally stochastic, DNA-PAINT. We provide quantitative information on the advantages of this deterministic approach in comparison to stochastic single molecule experiments. We expect that a multitude of single molecule experiments can be performed on the nanoarray platform by attaching the molecules-of-interest to DNA origami baseplates in predetermined positions. We predict that the platform will be of great utility to biophysicists owing to its ability to democratize maximum throughput single-molecule experiments with benchtop fabrication in any laboratory setting worldwide.

CHAPTER 4* LOW-COST PLATFORM FOR DIGITAL DETECTION OF SYNTHETIC NUCLEIC ACID BIOMARKERS

Abstract

Analog biosensing assays preclude the study of molecular heterogeneity by performing ensemble measurements, whereas digital assays probe individual biomolecules as early predictors of disease while drastically improve processing times and throughput. DNA origami nanostructures present a unique opportunity to exert nanometer-precision control over the position, and density of detection molecules such as *ss*DNA, aptamers, and antibodies on a 100-nm breadboard. Conventional DNA origami-based biosensors, however, rely heavily on cumbersome and low-throughput detection equipment such as atomic force-, transmission electron-, and single molecule-microscopes to detect conformational changes and single molecule emission events in response to probe-target interactions. Bench-top DNA origami placement technology facilitates the facile organization of probe molecules in a digital fashion on meso-to-macroscale glass substrates. We present here, an enzyme-free, *in situ* amplification paradigm for the detection of synthetic *ss*DNA on a $1 chip decorated with DNA nanostructures and their associated *ss*DNA probes. A conventional, and potentially portable fluorescence microscopy setup can be used to count bound targets with a digital sensitivity of ~25 pM in 2-4 hours. The chip is robust over several months, consumes low reagent and sample volumes, and has the potential for multiplexing and microfluidic integration. We envision that this digital assay could cost <$10 and have utility at the point-of-care for the detection of all molecular classes of biomarkers.

*Extensive parts of this chapter appear in a manuscript in preparation:

$1 DNA nanoarrays for digital diagnostic applications in low-resource settings

Rishabh M. Shetty, Tal Sneh, Sarah Brady, Ashwin Gopinath, Rizal F. Hariadi

4.1 Introduction

Biosensing is critically important in fields ranging from healthcare to food science, and defense. A biosensor is loosely defined as an analytical device comprising a recognition element capable of specific interaction with a target-of-interest, and a transducer with the ability to produce a detectable signal concomitant with the target binding event. The recognition element could be naturally occurring, biologically derived, or a "biomimic," whereas the transducer is generally optical, piezoelectric, micromechanical, magnetic, or electrochemical in nature (Caliendo, Gilbert et al. 2013). The highest resolution measurement one can make in analytical chemistry is a single molecule counting event. Analog assays perform ensemble measurements of populations and tend to grossly underestimate molecular heterogeneity as a result (Leake 2012). The digital capture and analyses of biomolecules is not only higher throughput but capable of uncovering their inherent heterogeneity, thereby enabling better disease prediction. Counting molecules is simpler than integrating signal intensities and it is probable that the future of analytical measurements will be digital (Walt 2013).

Miniaturization of analytical tools is of great interest owing to the intrinsic size-compatibility between the measurement tool and the target-of-interest. Therefore, chip-based devices facilitating high throughput processing of samples are perfectly suited to the analysis of single-cell (micrometers) and single-molecule (nanometers) targets (Walt 2013, Walt 2014, Cohen, Hartman et al. 2017, Cohen and Walt 2017). Both serological and molecular diagnostic approaches have been used for the molecular identification of various pathogens, but some combination of the two techniques generally provides the most accurate diagnosis (Tang, Procop et al. 1997, Breitschwerdt 2011). Digital assays for the detection of nucleic acid targets through PCR amplification or protein targets through enzymatic amplification with fluorogenic substrates are both key techniques for sampling

biological heterogeneity and are early indicators of diseases (Basu 2017). Nucleic acid-based testing, however, significantly reduces the time-to-detection (Cloherty, Talal et al. 2016), and improves the sensitivity (Kozel and A.R.Burnham-Marusich 2017), which can be extremely important in the case of infectious disease outbreaks. Affordability, sensitivity, specificity, a user-friendly workflow, robustness and rapidity, simple and inexpensive (detection) equipment, and delivery to end users (i.e. ASSURED guidelines) are the characteristic requirements for a device deployed in low-resource, point-of-care (POC) settings (Puren, Gerlach et al. 2010, John and Price 2014, Nayak, Blumenfeld et al. 2017, Primiceri, Chiriaco et al. 2018). Despite their unmatched sensitivity, droplet digital ddPCR systems can employ complex microfluidics and have an instrument cost of greater than $100,000, which may be prohibitive in such settings (Basu 2017). As potential alternatives to qPCR and ddPCR, cost-effective, isothermal technologies such as Loop-mediated isothermal amplification (Notomi, H.Okayama et al. 2000), Hybridization Chain Reaction (Dirks and Pierce 2004, Choi, Beck et al. 2014) and Rolling Circle Amplification (Lizardi, Huang et al. 1998) have previously been used for amplification on diagnostic devices (Chang, Chen et al. 2012). Exponential growth kinetics have been reported for both, HCR and RCA (Xuan and Hsing 2014, Bi, Chen et al. 2015, Xu, Xue et al. 2017) for rapid product amplification and detection. The most challenging limitations for the digital detection of biomolecules in chip-based assays have been found to be non-specific binding (NSB), surface-diffusion, target concentration, and multiplexing (Walt 2013).

DNA origami nanostructures (Rothemund 2006), through their well characterized Watson-Crick base-pairing architecture are uniquely placed for biosensing applications. The nanometer-precision addressability of DNA nanostructures enables programmable decoration of detection molecules (Bald and Keller 2014) in various configurations in 2D

and 3D (Seeman 2010, Zadegan and Norton 2012) while their self-assembly based, one-pot synthesis provides a straightforward and reliable pathway towards large-scale, cost-efficient production. Incorporating several sensing elements onto a single DNA origami substrate adds multiplexing capabilities to origami-based assays. A variety of biomolecules including nucleic acid, small molecules, and protein biomarkers have been detected using DNA origami biosensors through their functional payload of detection elements such as aptamers, *ss*DNA, biotin, etc. (Wang, Meyer et al. 2017). Simply put, any probe molecule or ligand that can be attached to ssDNA can be incorporated onto a DNA origami molecular breadboard for the purpose of biosensing. Most origami-based biosensors rely on the detection of conformational changes using an atomic force microscope (AFM) in response to single biomarker detection events (Ke, Lindsay et al. 2008, Kuzuya, Sakai et al. 2011, Pei, Zuo et al. 2013) or use transmission electron (TEM)- or single molecule-microscopy (Nickels, Hoiberg et al. 2016, Nickels, Wunsch et al. 2016). This, despite theoretically having single molecule sensitivity, requires specialized and expensive equipment for the purpose of visual assessment. Fluorescence-based techniques for detection have been reported (Ge, Lin et al. 2014, Daems, Pfeifer et al. 2018, Selnihhin, Sparvath et al. 2018), but they can be limited by multiple origami binding in the same diffraction limited spot *in vitro*, and some suffer from low sensitivity. The advent of DNA origami placement (DOP) has enabled the programmed placement of these nanostructures on relevant surfaces such as silicon, and glass (Kershner, Bozano et al. 2009, Gopinath and Rothemund 2014, Gopinath, Miyazono et al. 2016, Xu, Harb et al. 2017, Gopinath, Thachuk et al. 2018), thereby allowing diffraction-limited imaging and digital observation of single-molecule emitters on a conventional fluorescence microscope. The creation of single-molecule arrays on the meso-to-macroscale through DOP could be a breakthrough for the field of DNA nanotechnology, significantly

broadening its potential impact in biosensing applications for the detection of all molecular classes.

Disease diagnosis in POC settings is further aided by the development of easily accessible and portable imaging setups similar to previously reported ones (Cybulski, Clements et al. 2014, Skandarajah, Reber et al. 2014, Sun and Hu 2018) for visualization of amplification reactions. Depending on the area of application — clinical or POC — various factors need to be considered, i.e. setup cost, time to detection, robustness, manual intervention, sensitivity, and specificity (Zhang, Ding et al. 2017). We present here, a digital assay for the enzyme-free, *in situ* isothermal hybridization chain reaction (HCR) amplification-based detection of a synthetic *ss*DNA target. This is, to our knowledge, the first demonstration of a digital detection technique using DNA origami-bound probe molecules programmatically decorated on a meso-to-macroscale chip. We report on the background passivation, sensitivity, and robustness (in biofluids) of this assay. The significant advantages of this method are its simplicity, minimal user-engagement, absolute quantification-based detection scheme, enzyme-free amplification, robustness, ~25 pM limit of detection, low reagent consumption, turnaround time, and low chip ($1)/assay ($10) cost. Furthermore, the platform is capable of multiplexing, and has microfluidic compatibility. We foresee its applications mainly in point-of-care testing (POCT) for detection of all classes of biomolecules, i.e. DNA, RNA, small molecules, proteins by integration with a low-cost, fluorescence microscopy platform.

4.2 Materials and Methods

4.2.1 Bulk, agarose-gel analysis of Hybridization Chain Reaction assay

Similar to previously reported studies (Dirks and Pierce 2004, Choi, Beck et al. 2014, Choi, Schwarzkopf et al. 2018), bulk, agarose-gel based electrophoresis was conducted on

hairpin strands (B4-HCR amplifier, Molecular Instruments, Los Angeles) in the presence and absence of initiator strands. Initiator strands (IDT DNA, IA) were prepared at a stock solution of 10 μM, and hairpins (3 μM stock, each) were first heated separately at 90 °C for 90 seconds, prior to flash freezing in liquid nitrogen for 30 minutes. A 1% gel was prepared, and each lane was loaded with a 10 μL solution of progressively reducing initiator concentration (1 μM, 100 nM, 50 nM), and 200 nM of H_1 and H_2 hairpins as well as a control lane (only hairpins), and a ladder. All dilutions were performed using 1x TAE, 12.5 mM Mg^{++}. The gel was run for 2 hours at 80 V on ice, post staining with SYBR Gold (1x), and 1x loading dye.

For origami-based HCR bulk experiments, the origami were first annealed at a 1 °C/min ramp from 95 °C to room temperature. This process took approximately 2.5 hours. The initiator binding complementary sequence extended out of a single staple strand on the origami (A12, Plate I). The initiator strands were first added at a 1 μM, 100 nM, and 50 nM concentration to 10 nM origami solution for 30 minutes. Hairpins were then added to the solution at 200 nM for a final volume of 10 μL. Similar to the purely strand-based reaction, a 1% gel was loaded with the appropriate negative control (origami + hairpins without initiator, origami alone) and the gel was run at 80 V for 2 hours after staining with 1x SYBR Gold, ad 1x loading dye.

4.2.2 Surface passivation experiments

Surface passivation experiments were performed on 24x50 mm (Ted Pella) chips decorated with DNA nanoarrays as detailed in Chapter 2. To run multiple experiments, an 8-well chamber was cut with double-sided Kapton tape and cut precisely into 8 mm x 8 mm wells using a Graphtec cutter (CE 6000-40, Graphtec America, CA), and these wells were fluidically isolated from each other. Leak tests were run using food color to ensure a

good seal with the tape. Wells were pre-incubated with 50 μL of passivating agent (10 μM PolyT, 1 μM H2, or 1 mg/mL BSA) in 10 mM $MgCl_2$ + 0.05% v/v Tween-20 in 1xTAE buffer for 60 minutes. They were then washed once with the same buffer and subsequently incubated with 50 μL of 10 nM hairpins in the appropriate buffer + Tween conditions for 1.5 hrs. Samples were washed with 50 μL of the corresponding buffer and imaged with approximately 25 μL of buffer present in wells. 10-frame images were taken with a TIRF super-resolution microscope (ONI, Oxford, UK) of areas with coordinates recorded for ease of quality control. Following data collection, the chips were incubated with 50 μL of 10 nM 20-A-Atto-647 to label all origami present (each origami has 20-T overhangs from every staple), after which the same coordinates were imaged to confirm presence of a complete grid. Images with a confirmed grid in their area (>90% coverage) were analyzed to obtain counts of non-specific binding of fluorescent hairpin strands. All surface-passivation experiments were conducted using hairpins labeled with Cy3b dye and end-point images were taken using 532-nm laser excitation. All experiments were performed in triplicates.

4.2.3 Fluorescence-based single-molecule HCR assay

DNA origami nanoarrays were prepared and dried on a 24x50 mm piece of glass as described earlier. These chips were placed in a humidity chamber before proceeding (an empty pipette tip box filled with water is sufficient). An 8-well chamber was cut out of 1 mil Kapton tape with chamber size 8 x 8 mm using a Graphtec cutter and was adhered to the DNA nanoarray chip. At this stage it is crucial to spend significant care in attaching the Kapton tape design to prevent leaks from one chamber to the next. 50 μL of sample (with appropriate initiator/target concentration) in 10 mM $MgCl_2$ + 0.05% v/v Tween-20 in 1xTAE buffer was slowly pipetted into a chamber, taking care to attempt to cover the

majority of the chamber surface. The sample was allowed to incubate in the humidity chamber for 120 minutes. After incubation, a sequential wash of sample removal, 75 µL of 10 mM $MgCl_2$ TAE buffer, 75 µL of 10 mM $MgCl_2$ + 0.05% v/v Tween-20 TAE buffer, and finally 75 µL more of the 10 mM $MgCl_2$ TAE buffer was performed. A hairpin mixture at 10 nM of each hairpin in 10 mM $MgCl_2$, 0.05% v/v Tween-20 in 1xTAE was added to each chamber and allowed to incubate for 90 minutes. Following this, a wash as described post the initiator hybridization step was performed. The samples were then imaged on a TIRF microscope with ~40 µL of buffer on top or dried with an ethanol drying series for viewing on our low-cost microscope set-up. An ethanol drying series consisted of drying for 10 s in 50% ethanol v/v, 20 s in 75% ethanol, and 120 s in 85% ethanol, then being left out to air dry completely. For troubleshooting purposes, it is imperative to incubate an area with a fluorophore bound to a strand complementary to the staples (20A-Atto647-20T) on the origami array after imaging. This is useful as these strands will label every origami present on the surface and make it easy to determine whether an experiment failed simply because of poor patterning of the DNA origami array to begin with. A 30-minute incubation at 10-100 nM 20-A-Atto647 provides sufficient time for hybridization in this case. All LoD and specificity validation experiments were conducted using hairpins labeled with Alexa-546 dye and end-point images were taken using 532-nm laser excitation. Single-molecule assay sensitivity and specificity experiments were performed in triplicates.

4.2.4 Low-cost detection platform for POCT

A low-cost fluorescence detection setup acquired from Manu Prakash's lab at Stanford enabled HCR signal detection on the nanoarray platform at larger spacing of 700-nm between adjacent origami molecules. This microscope uses a low-power laser light source, and a large camera sensor (used in security, low-light cameras). A parts list is detailed in

Appendix C (information courtesy: Hongquan Li). A more recent iteration of this platform has been recently detailed (Li, Soto-Montoya et al. 2019).

4.2.5 Data analysis

For surface passivation experiments, frames were first concatenated based on average intensity, with the intention that noise fluctuations would cancel out relative to real fluorescence signals. Using a positive control (10 nM initiator, 10 nM H_1 and H_2), it was determined that hairpin signals occur reliably at 8 standard deviations away from the mean of image background noise for 400-nm grids. A threshold was applied at this value, and then their maxima were counted using ImageJ. Three samples with maximum four areas per sample were taken, with images containing underlying grids used for preparation of graphs and data analysis.

For molecule counts in real experiments, a similar threshold to the one used in surface passivation experiments was applied to all acquired image stacks at every initiator concentration. The single-, and double-molecule occupancy on a 400-nm nanoarray (63%, and 3%) were accounted for in the final count of target binding events. Four arbitrary fields-of-view were analyzed, and this could be extrapolated to the entire chip surface area. Counts were reported per field of view, and a comparison was drawn to the number of molecules expected in an ideal (theoretical) setting. Only areas with underlying grids as determined by post-labeling were used for data analysis and drawing inferences about the assay results. For the specificity tests, the initial sample with initiator was spiked with 50% serum (Valley Biomedical, VA), and ~10 μM random staple sequences (~230 strands at 50 nM each). The analyses were run as for normal limit of detection experiments. The analyses were run in a similar manner to conventional limit of detection experiments explained previously. The analytical sensitivity was determined through the following

calculations for limit of blank (LoB), and limit of detection (LoD) (Armbruster and Pry 2008):

$$LoB = mean_{blank} + 1.645\,(SD_{blank}) \quad (1)$$

where LoB is the highest apparent analyte concentration found when a blank sample containing no analyte molecules was tested with replicates, and

$$LoD = LoB + 1.645\,(SD_{low\ concentration\ sample}) \quad (2)$$

where LoD is determined by summing the LoB and replicates of a sample with low analyte concentration (10 pM in our case).

A logarithmic curve was fitted to the data in each experiment, and the LoD value obtained from the above calculation was used to find the corresponding analyte molar concentration from the curve equation.

4.3 Results and Discussion

4.3.1 Demonstrating bulk, enzyme-free linear amplification of synthetic nucleic acid targets using strand displacement

Prior to performing *in situ* Hybridization Chain Reaction (HCR) on the nanoarray platform, we conducted bulk experiments in an agarose gel (Figure 19) to demonstrate polymerization in the presence of target (initiator, I_1) strands. Briefly, upon detection of an initiator, the amplification reaction proceeds through a cyclical strand-displacement process of fluorescently-labeled hairpin loops (H_1, H_2) until a detectable signal is obtained, or the hairpins are completely exhausted (schematic in Figure 20). Bulk experiments revealed a progressive shift towards higher molecular weight products as the I_1 concentration was decreased from the micromolar to the low nanomolar concentration regime. This observation, consistent with previous studies (Choi, Beck et al. 2014), is attributed to longer hairpin (polymer) chains being formed per probe-target interaction

due to the presence of progressively lesser I_1 for the same concentration of hairpins in solution (200 nM). It is worth noting that the negative control showed little to no polymerization in the absence of initiator strands, implying minimal non-specific interactions (leak) between hairpins. Gel-based experiments run with probe strands attached to DNA origami showed similarly promising results as is seen for origami with a varying number of initiator binding strands (18, 6, 1). The smears indicate polymerization and the resultant higher molecular weight products in the lanes with 0.05x I_1. In addition, a negative control without any hairpins shows no interactions in this gel result. Schematics depict both, the strand-based and *in situ* assay-based paradigms for isothermal HCR on the nanoarray platform.

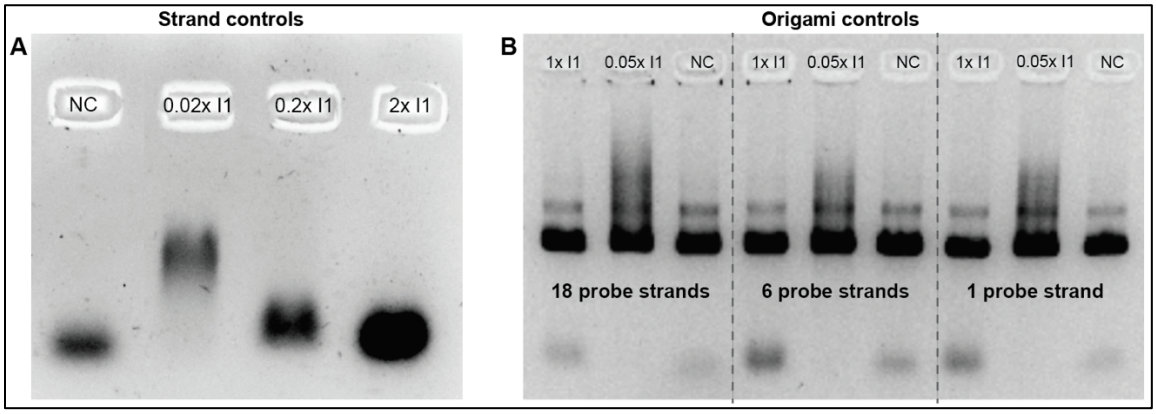

Figure 19: Bulk gel experiment. (A) Negative control (NC) indicates hairpins without initiator, I_1; 1x I_1 = 2 μM and hairpins were at 200 nM each. (B) Gel run with three different origami containing 18, 6, and 1 probe strand respectively. The first, second, and third lanes for each type of origami in the top image are with 1x (2 μM), 0.05x, and no target strand. Negative control indicates little to no leak in HCR reaction.

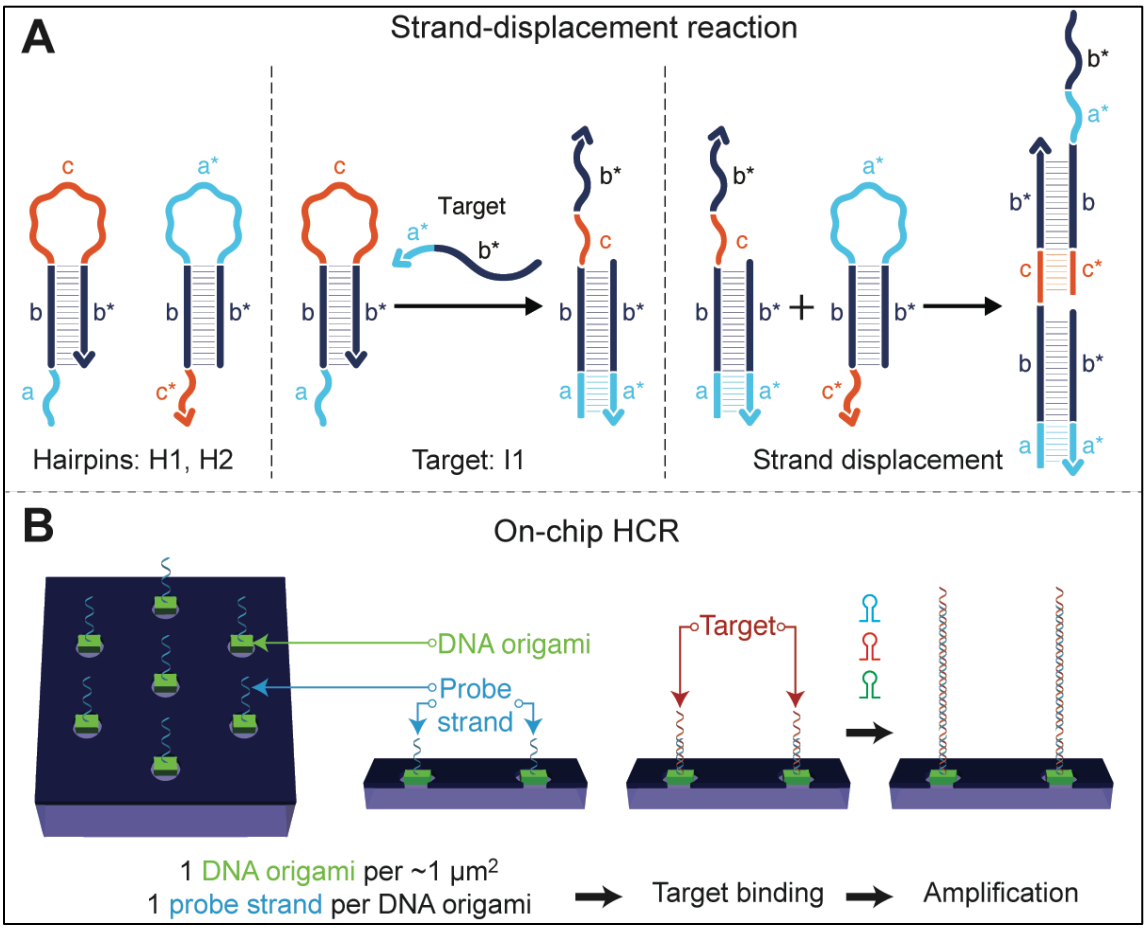

Figure 20: Enzyme-free, isothermal amplification paradigm for target amplification in a linear fashion (~ 1 fluorophore every 2 minutes). (A) Schematic representation of the strand displacement reaction through cyclical displacement of the hairpins on detection of a target (initiator, I_1) strand. (B) On-chip, in situ HCR on origami nanoarrays with each origami hosting a target-binding sequence.

4.3.2 Assessing the efficacy of background passivation strategies for surface-reactions

Surface-based hybridization (and other SME-) reactions are extremely susceptible to nonspecifically bound molecules confounding overall analysis of SME results (Cai and Wind 2016). With photon budget being the major currency of such experiments, background noise, or false positives can be detrimental if not addressed adequately, especially in digital-diagnostic applications. To test various passivation strategies, we ran negative controls (no I_1, 10 nM H_1, 10 nM H_2) on the glass surface, i.e. we did not expect

any amplification reaction to occur. Normalized counts are displayed on the Y-axis as a measure of passivation efficacy, with 1.0 indicating least efficient, and 0 indicating most efficient passivation strategy (Figure 21). We first assessed the performance of various Mg^{2+} concentrations from 40 mM-10 mM on an HMDS passivated, and origami patterned (400-nm pitch) chip surface. We then proceeded to add Tween-20 (0.05% v/v) to 40-, and 10-mM Mg^{2+} and repeated these experiments. We observed a significant reduction in nonspecifically bound fluorescent hairpins at 10 mM Mg^{2+} with Tween (Figure 21, N=3). We further explored the effect of adding 1mg/mL Bovine Serum Albumin (BSA), 2 μM unlabeled H_2 (20x excess), and 10 μM Poly (20)-T strands (100x excess) to the 10 mM Mg^{2+}-Tween solution as a means of competitive binding to the surface. Tween, a surfactant, has been popularly used as a reagent for surface passivation (Hua, Han et al. 2014, Cai and Wind 2016) and displays almost no autofluorescence. We quantified the number of nonspecifically bound molecules for each passivation strategy post-thresholding. It is worth noting that nearly all "real" signal on a positive control sample (indicating an amplification reaction) occurred at a higher intensity value than the threshold used here. Our results suggested that the H_2 "flood"-based competitive binding strategy with 10 mM Mg^{2+}-Tween provided optimum passivation of the glass surface, thereby boosting Signal to Noise Ratio (SNR). Another point worth noting is that the number of counts reported here are different from the number of molecules measured in limit of detection experiments, and so are the threshold values. In other words, surface passivation studies are purely a measure of efficacy of the passivation agent used and do not relate directly to the number of molecules detected in negative controls included in actual HCR experiments detailed below.

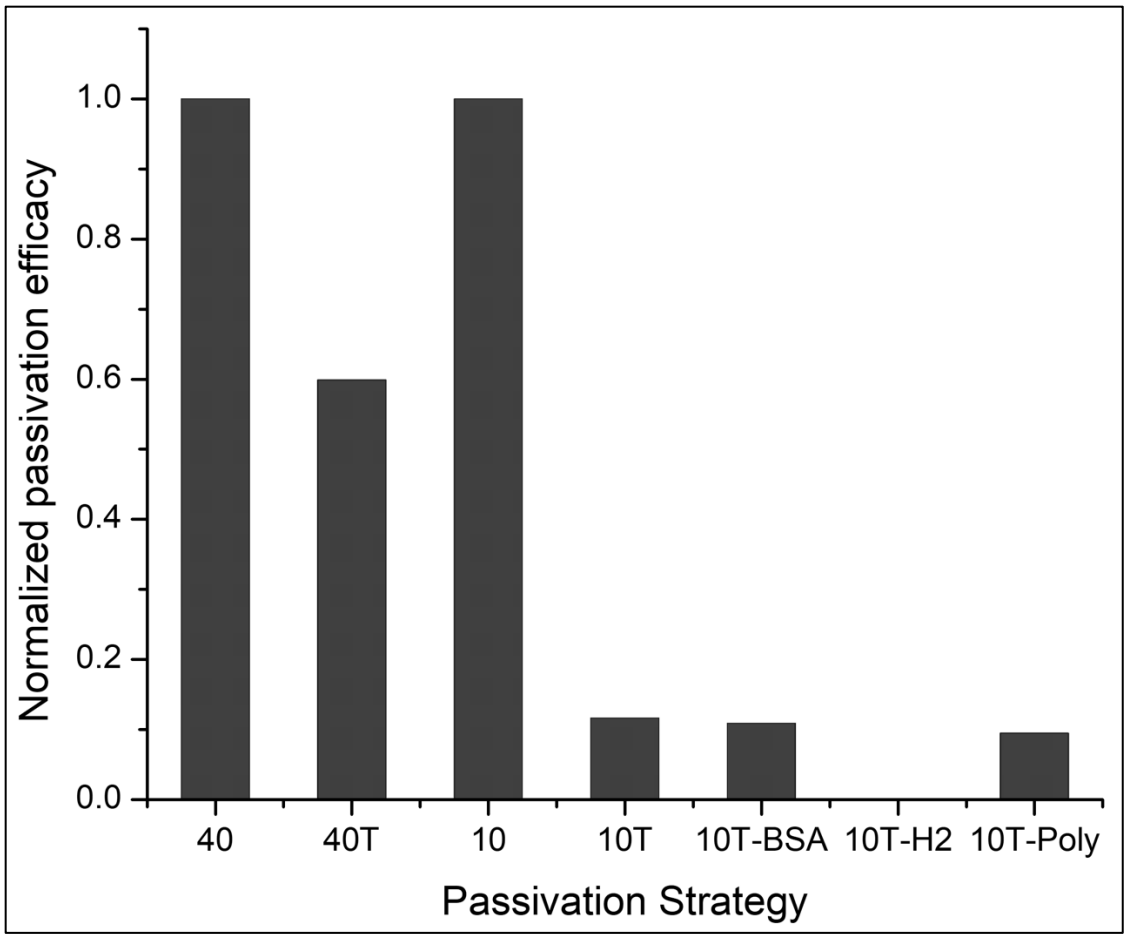

Figure 21: Surface passivation efficacy of various strategies: 10 and 40 mM Mg^{2+} concentrations, T indicates the presence of 0.05% v/v Tween-20; 10-T BSA (1 mg/mL); 10-T hairpins (2 μM); and 10-T PolyT (10 μM). Results indicate an extremely low background count with the hairpin "flood"-based strategy compared to others. The Y-axis min-max normalized with 10T-H2 displaying minimum counts, and 40, 10 displaying the maximum.

4.3.3 Determining a Limit-of-Detection and validating system specificity

Typical fluorescence-based assays are limited by background or non-specific interactions to a detection threshold of 1 pM for hybridization adsorption of DNA. Further, detection of a target concentration of 1 pM or lower is limited by both surface diffusion and adsorption kinetics (Lee, Wark et al. 2006). The primary determinants of a limit-of-detection for surface-based amplification reactions are the surface-passivation efficacy, and target diffusion kinetics. At optimal surface passivation, we are theoretically limited

to a detection limit of ~500 fM- 1 pM. Serial dilution of target concentration revealed an expected trend of reduction in the number of fluorescent binding events, indicating a steady decrease in the number of target strands captured on the underlying origami grid (Figure 22). This demonstrates the contrast between integration-based analog formats, and the counting-based digital assay format described in this work. Furthermore, while higher concentrations display evidence of hexagonal close-packing between binding events, there is potential for the known Fourier Transform (of 400-nm grids) to act as a denoising filter for the processing of lower concentration experimental data.

Theoretical estimation of the number of expected target molecules per field-of-view (FOV) for a 50 μL sample volume, and 8 mm x 8mm well size, suggested the presence of between approximately 190 - 1900 molecules in the 100 fM-1 pM regime (Figure 23). Previous studies on surface-based reactions (alluded to earlier) indicated a background-limited detection in this region, and we observed similar results with the negative control (no target molecules) counts falling between 100 fM – 1 pM (Figs. 24, 25). Based on calculations for 400-nm spacing between individual molecules on the nanoarray, it is known that the maximum number of probes available assuming exemplarily formed origami, and 100% occupancy of binding sites is 25,000 per FOV. A reasonable assumption based on the non-uniform light intensity profile of the camera (edge effects), and strand conjugation efficiency (Chapter 3), however, meant that the effective FOV had closer to ~12,000 binding sites. At the highest tested concentration of 10 nM, target molecules were abundantly available and consequently, all effective binding sites on the nanoarray were occupied (saturated at ~12000). We speculate that in the concentration regimes of 10 pM-1 nM, surface diffusion and adsorption kinetics play a role in lowering the number of counts observed in the limit of detection (LoD) experiments. This is true, especially at the picomolar concentrations where the number of target-probe interactions

over the entire surface area of the chip are dramatically reduced. Our calculations indicated that for the values obtained for the three replicates at each concentration of the target sequence, the analytical sensitivity was slightly higher than 25 pM.

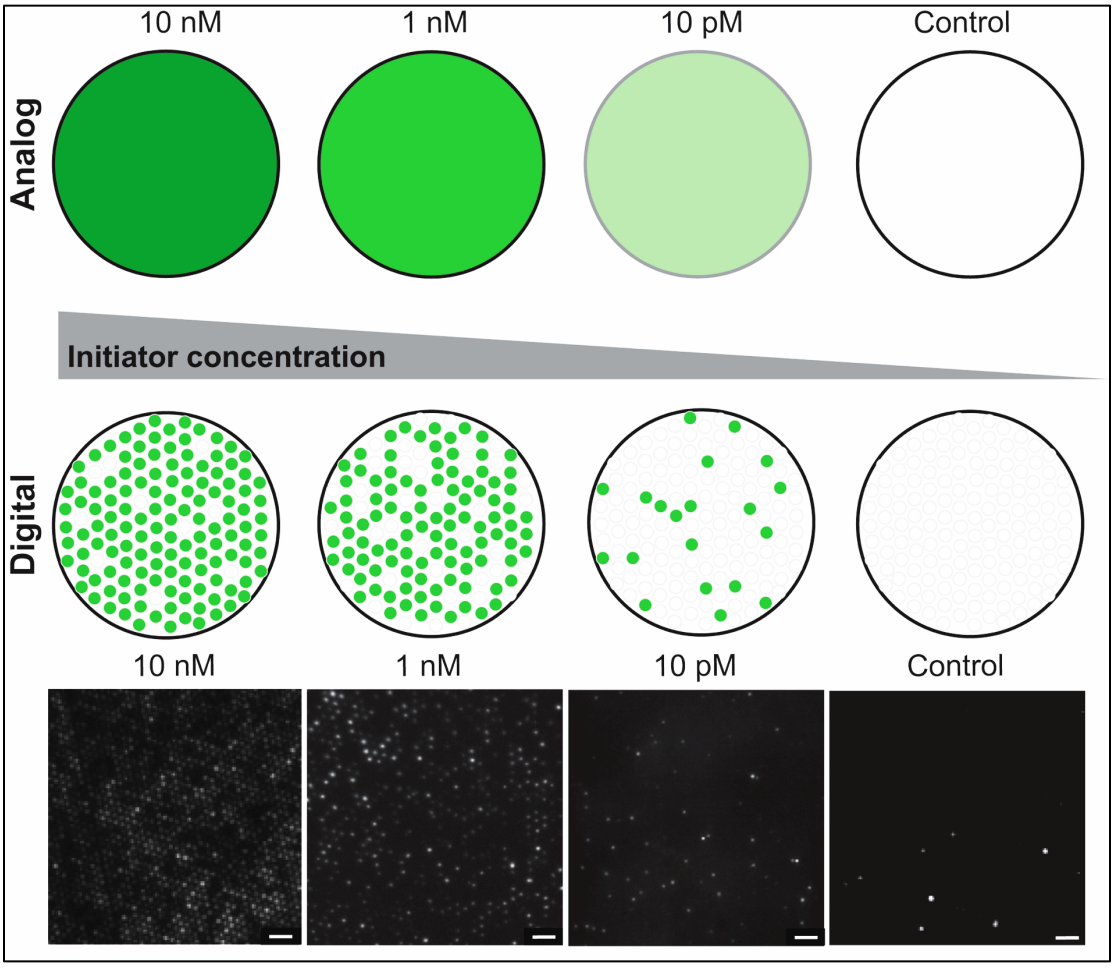

Figure 22: A comparison between "integration"-based analog assays, and "counting"-based digital assays. As target (initiator, I_1) concentration decreases, there is a reduction in total intensity in the analog format whereas digital detection is realized through the progressively lower counts of target binding events on the nanoarray. Scale bars are 1 μm.

Evidence of the "goodness" of surface-based experiments in the nanomolar concentrations can be extracted from classical single-molecule experiments. Most TIRF microscopy experiments are limited to the tens of nanomolar concentrations owing to the high background observed at higher abundance values of ligands and other molecules-of-

interest (Zhu and Craighead 2012, Dulin, Lipfert et al. 2013). However, higher concentrations are preferred to counteract the detrimental effects of slow diffusion, adsorption kinetics, and photobleaching on the speed of reaction time and data acquisition. For instance, DNA-PAINT experiments (reported in Chapter 3) display optimal duty cycles (ON:OFF blinking rates) at an imager concentration of ~ 5 nM for high density nanoarrays. This is also the reason why a highly sensitive digital ELISA approach decorates large, micrometer-sized beads in solution with a carpet of capture antibodies to significantly increase the surface area and consequently the number of probe-target collision events to drive the detection limit down (Walt 2014, Cohen, Hartman et al. 2017, Cohen and Walt 2017). We therefore conclude with reasonable certainty that the low number of molecules detected is most likely due to slow diffusion kinetics at the low I_1 (and H_1, H_2) concentration and incubation times of hybridization (2 hours) and/or amplification reactions (1.5 hours).

Assay robustness was validated using two approaches: human serum spiking-, and random oligo sequence spiking- of the initiator-containing sample solution. A change in the profile of the LoD curve and/or a shift in the detection limit to a lower concentration when compared with a blank sample might indicate spurious interactions (false positives) between the components of the human serum or random, short (~32-nt), staple sequences with origami nanoarray and their probes. Our results (Figure 25) indicated little to no change in the specificity of the assay under both testing conditions based on the profile and limit of detection. However, we noticed a similar trend of reduction in the number of counts at each initiator concentration value when validating with both methods. We hypothesize that in the case of excess oligos this is likely due to the blocking of certain origami probe strands by the large excess of staples and/or the non-specific interactions between the target strand and one or more of the 200 random sequences. The former

observation may be supported by the surface passivation data which suggests that excess random oligo sequences (hairpins, Poly-T) results in an overall reduction in the amount of non-specific binding to the surface but may also likely block certain specific interactions. It is also plausible that the staples added an extra layer of background screening and prevented non-specific binding of hairpin strands to the surface, as is indicated by the significantly lower negative control counts. For the latter observation, careful NUPACK analysis of each combination of staple-target strand sequence might reveal spurious interactions, but this was not pursued owing to the overall integrity in the LoD profile for these experiments. Excess, unbound molecules were washed away prior to hairpin-incubation and amplification reaction, and this might mean that there were even fewer than normal strands available for conjugation with probe strands on the origami nanoarray. In the case of 50% serum spiking, we posit that its components had a similar effect to the blocking properties of a passivation agent such as BSA, leading to the attenuation of specific interactions between probe and target. We ruled out the possibility of either the excess oligonucleotide sequences or the serum spiking lifting the origami off the nanoarrays by validating the presence of a well-formed grid post data collection for HCR reaction experiments as assessed through the Fourier transforms of each field-of-view. Varying the concentration of staples and the serum would help ascertain their effect on specific probe-target interactions when compared to a conventional Limit of Detection curve. However, the preservation of the detection limit and curve profile and the calculated limits of 24 pM (serum), and 35 pM (staples) in both cases was encouraging and suggest that the assay retained its sensitivity in biologically relevant fluids. This makes it a strong candidate for testing with real-world biomarkers following careful probe design. Table 4 summarizes the important characteristics of the digital assay format demonstrated on the nanoarray platform.

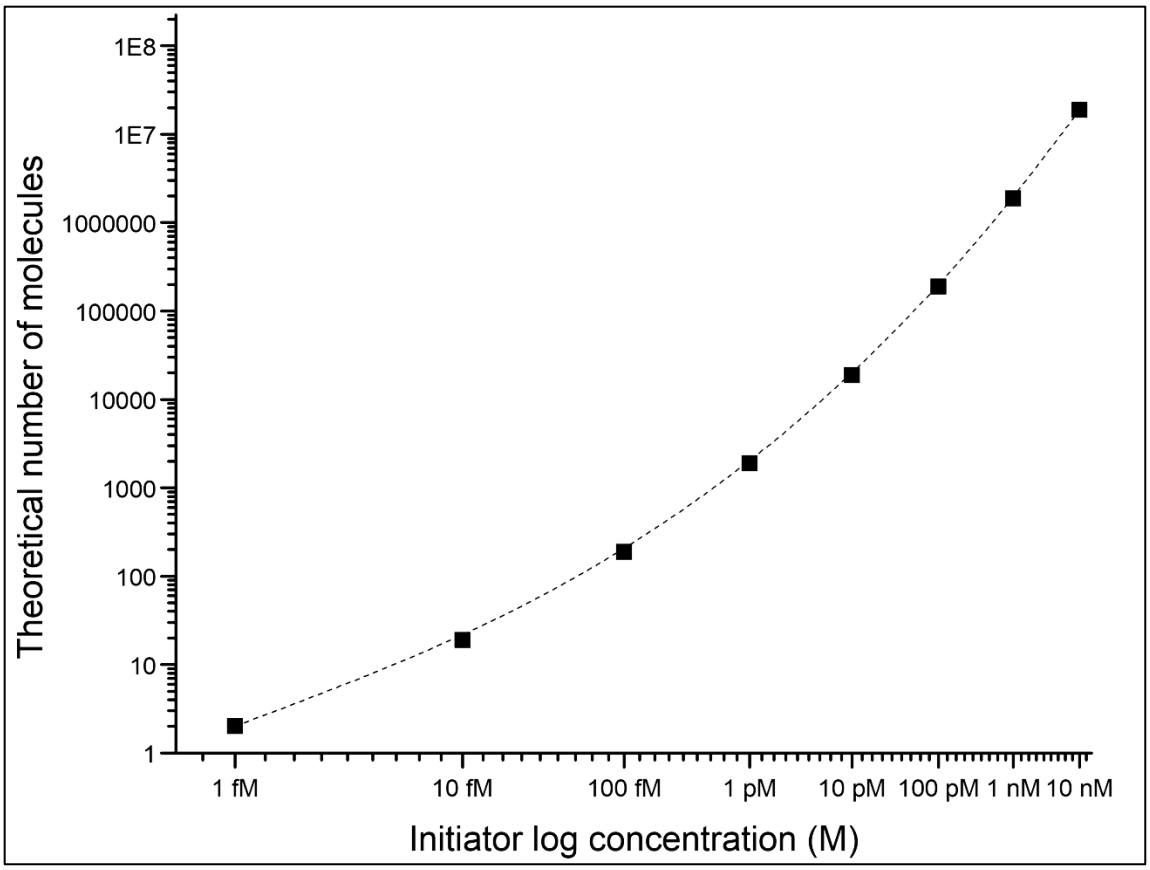

Figure 23: Theoretical estimation of the number of target molecules available per field-of-view (50 μm x 80 μm) in a 50 μL solution pipetted onto a single well of a large, 24 mm x 50 mm chip. Owing to non-specific binding/background noise, and slow diffusion/adsorption kinetics, it is expected that the detection limit is capped at 1 pM (~1880 molecules) for surface-based probe-target interactions. Both axes are log scale.

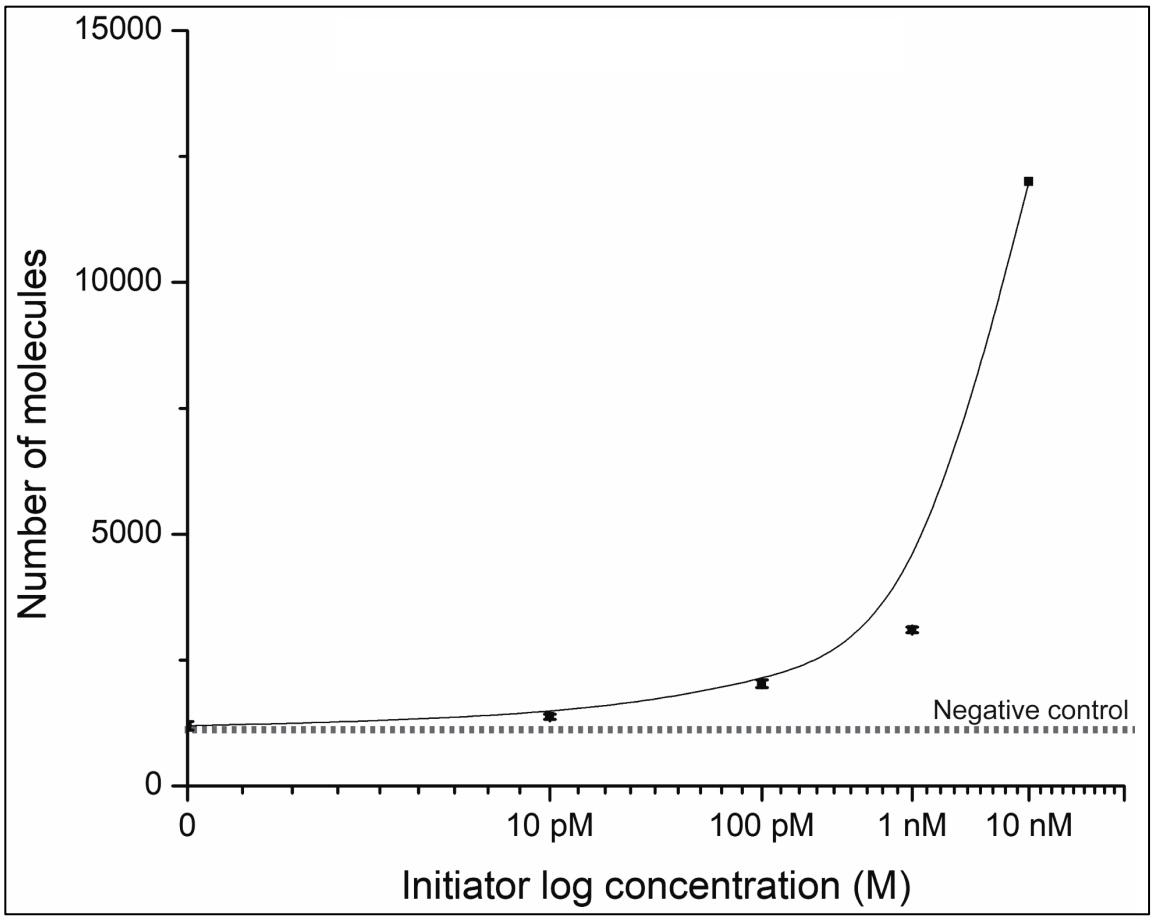

Figure 24: The limit of detection (LoD) of the surface-based HCR assay yields results as expected with the sensitivity being ~25 pM, i.e. the first concentration value calculated to be higher than the background (negative control) which can be definitively counted. Error bars are SEM.

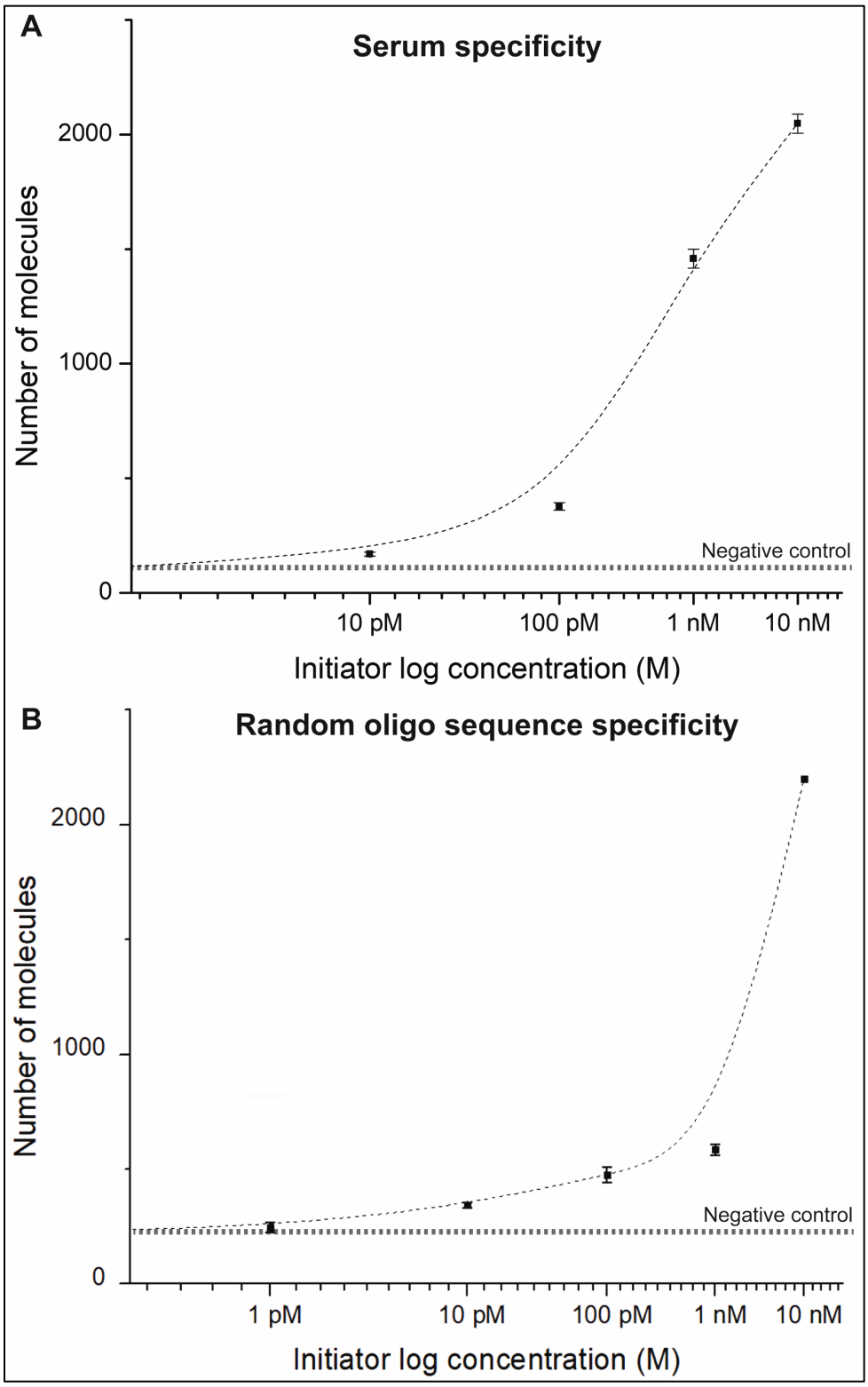

Figure 25: Specificity studies were conducted with (A) 50% serum spiked initiator solutions, and (B) ~200 random staple sequences. The limit of detection was ~25 pM in each case, exhibiting the robustness of the reaction. All error bars are SEM.

4.3.4 A low-cost imaging system for digital assay portability

Simplification of detection optics for a low-cost imaging setup comes at the cost of the inability to correct optical aberrations, a low numerical aperture, low excitation intensity and light collection efficiency, etc. and consequently leads to poor image resolution. The $1000 portable imaging setup we tested (Figure 26) has a maximum resolution of ~500-nm. This is larger than the spacing required to maintain a single-molecule occupancy higher than the Poisson limit as described in Chapter 2. This meant that HCR experiments on the nanoarray platform could only be performed at >500-nm spacing between individual probe molecules, and there were more than one probe strands per diffraction-limited binding spot. One of the advantages of using lower magnification objectives, and cheaper camera sensors with larger pixel sizes was the ability to scan larger FOVs and collect more photons. We describe preliminary results in Chapter 5 that show promise for utilizing the 400-nm spacing on the nanoarray platform for HCR-based biomarker detection.

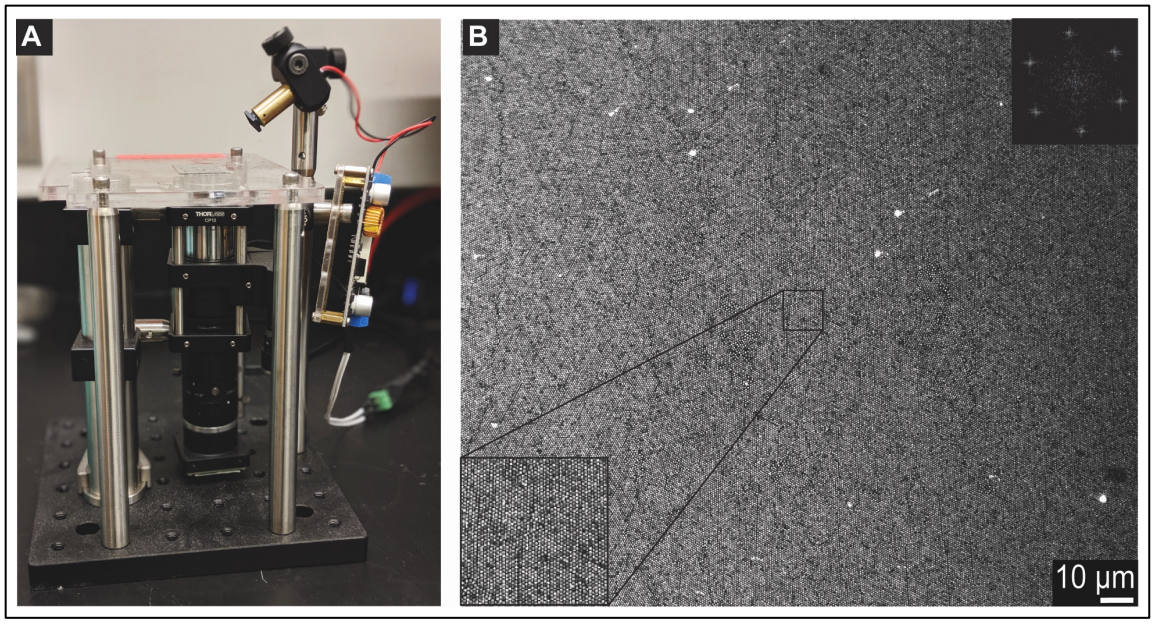

Figure 26: (A) The low-cost (~ $1,000) imaging setup from Stanford, and (B) A cropped image from an approximately 1 mm² FOV of HCR reactions conducted on a 700-nm pitch nanoarray, at a single occupancy below the Poisson limit.

Parameters	Characteristics
Biomarkers detected	*ss*DNA/RNA
Detection probe	*ss*DNA
Sample preparation	Pre-concentration, lysis/purification
Background-imposed limit of detection	500 fM- 1 pM
Experimental limit of detection	~25 pM
Turnaround time	~4 hours
Assay format	Digital
Detection format	Optical (fluorescence)
Sample volume	50 μL
Dynamic range	4-5 log
Minimum cost of microscope currently required	~ $30,000 - $50,000
Price of low-cost microscope setup for portability	~ $1000
Hands-on time	15-30 minutes
Chip cost	~ $1
Reagent cost per chip per assay	< $1
Storage requirements	Room temperature (aluminum foil)
Applications	Point-of-care (POC) diagnoses (Infectious diseases, Avian DNA sexing)
Estimated assay cost	< $10

Table 4: Characteristics of the benchtop nanoarray platform for synthetic nucleic-acid biomarker detection.

4.4 Conclusions

We describe the development of a novel digital assay based on enzyme-free, *in situ* isothermal amplification and counting of synthetic nucleic acid biomarkers bound to *ss*DNA probes on individual DNA origami molecules on the nanoarray chip platform. We report on the surface-passivation efficacy and discuss its direct role in imposing a detection limit of ~1 pM on any surface-adsorption based DNA hybridization assay. We find that a "flood-based" strategy of excess DNA sequences serves as a screen for non-specific binding of fluorescently-labeled hairpin molecules which generate the amplification signal. Further, we establish the system sensitivity to be 25 pM and find that it is significantly limited by non-specific binding, and slow diffusion and adsorption kinetics at low target concentrations. We also validate the robustness of the assay in the presence of 50% serum, and ~200 random target sequences spiked into the target sequence solution by detecting little to no change in the detection limit. This suggests assay compatibility with biofluids. Finally, we provide preliminary data for low-cost imaging on the nanoarray platform and foresee its potential as a point-of-care testing device for various molecular classes of biomarkers.

CHAPTER 5* FUTURE DIRECTIONS AND CONCLUDING REMARKS

5.1 Iterative size reduction

The nanoarray platform demonstrates significant advantages in terms of its simplicity, low-cost, accessibility, etc. over top-down lithography based single molecule nanoarray fabrication. However, a specific drawback of this technology in its current stage of development is the inability to separate adjacent molecules by arbitrarily large distances like EBL-DOP can. This limits the application of this technique on microscopy platforms to high-end optics, and specifically restricts its applicability in point-of-care settings. A 400-nm pitch is the minimum distance required to obtain non-Poisson limited single molecule occupancy of DNA origami molecules on the nanoarray. Nanospheres larger than this size will result in the creation of diffraction-limited binding sites where more than two probe molecules are likely to bind, with detrimental effects on the digital assay capabilities of the DNA nanoarray platform. To address this issue, we developed a process flow dubbed “iterative size reduction” which would enable the creation of single origami capture sites (Figure 27). The routine origami placement protocol is modified such that after the lift-off of the first layer of 1 μm nanospheres, amine-functionalized 200-nm nanospheres are incubated with the chip surface in the placement buffer. The pK_a of the silanol groups on the surface is ~8.3 and that of amine groups is ~9.2. A buffer pH of >8.3 ensures electrostatic interactions between the positively charged nanospheres and the negatively charged silanol groups on the surface. The placement buffer is used for the incubation, and the HMDS discourages positively charged nanospheres from immobilizing non-specifically on areas without binding sites.

* Some parts of this chapter appear in an unfunded NSF grant proposal

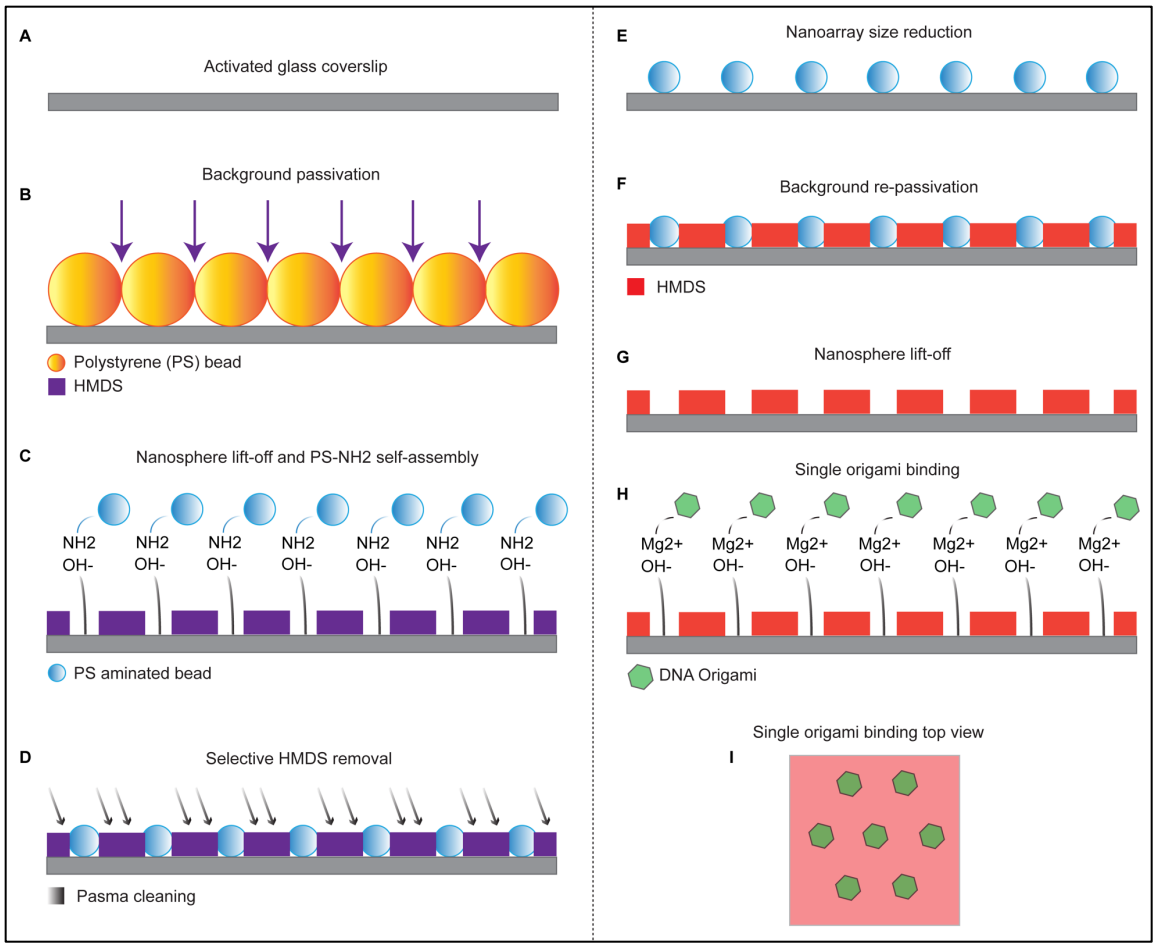

Figure 27: Iterative size reduction. A close-packed first layer of large, 1 µm nanospheres is used for binding site creation and smaller, NH_2 functionalized nanospheres are programmatically placed in these binding sites. These nanospheres act as a second mask layer for the re-passivation of the surface, bringing the ultimate binding site size within the footprint of DNA origami molecules, while maintaining the initial 1 µm pitch for simplified resolution of fluorescence events.

At this stage, all steps prior to re-passivation, second layer lift-off, and origami immobilization have been reproducibly achieved (Figure 32). Once the re-passivation is achieved, this would lead to the creation of ~60 nm binding sites for DNA origami to be immobilized on, while preserving the initial, 1 µm pitch set by the first layer of nanospheres. This would enable the straightforward resolution of HCR reactions on adjacent sites while maintaining or more likely, improving, the 63% single molecule occupancy currently obtained.

5.2 Zero Mode Waveguides

One of the exciting avenues the benchtop nanoarray platform opens up is the bottom-up nanofabrication of a variety of biophysical tools. Perhaps most promising among these is Zero Mode Waveguides (ZMWs). Optical observation of single-molecule dynamics suffers from the need to dilute fluorophore concentrations down to the pM or nM concentrations for isolation of individual molecules and events (e.g. Figure 28. a) (Levene, Korlach et al. 2003, Heucke, Baumann et al. 2014). A unique solution to conducting single-molecule experiments at physiologically relevant ligand concentrations (μM to mM) with microsecond temporal resolution was invented in 2003 (Levene, Korlach et al. 2003).This method achieves excellent background attenuation by reducing the observation volume by three orders of magnitude in metal nanoapertures, termed ZMWs. ZMW nanoholes in a thin (~100 nm) film of metal exhibit a cut-off wavelength above which no propagating modes of light exist within the waveguide. Hence, the (Zero-mode) nomenclature. Wavelengths over the cut-off value are evanescent and decay exponentially along the vertical axis of the waveguide. Arrays of ZMWs confine the observation volume to a few tens of nanometers of the sample volume (along the vertical axis), enabling parallel observation of kinetic events in single-molecules of interest within the field of excitation (Figure 28. b). As mentioned, they achieve this by significantly attenuating depth of field, and consequently fluorescent background.

For context, at zeptoliter (10^{-21} L) volumes routinely achievable with ZMWs, even tens of μM concentration of reacting species can be observed at roughly one molecule per waveguide (Zhu and Craighead 2012). This technique has utility in long-read length DNA sequencing, observing myosin motor dynamics, single molecule FRET, etc. (Foquet, Samiee et al. 2008, Korlach, Marks et al. 2008, Moran-Mirabal and Craighead 2008, Eid, Fehr et al. 2009, Uemura, Aitken et al. 2010, Teng, Lionberger et al. 2012, Elting, Leslie et

al. 2013, Pibiri, Holzmeister et al. 2014, Goldschen-Ohm, White et al. 2017) all at unprecedented Signal to Noise Ratios and temporal resolution. However, the cost of these ZMW chips is ~ $1,000. Using NSL-based fabrication, we developed strategies (Figs. 29, 30, 31, 32) for the cost-effective fabrication of this useful biophysical tool and present some preliminary data from these experiments (Figs. 29, 32).

While developing the rationale for bottom-up ZMW fabrication on an immobilized origami platform, we pursued a parallel, "quick and dirty" approach dubbed "self-assemble and etch". We aimed to determine the suitability of nanosphere micromachining for fabricating a hexagonally close-packed grid of point sources of light. This, we hoped, would help estimate ZMW diameters and metal layer thicknesses required for adequate light attenuation. We began with a process similar to the NP technique, i.e. tilted drop-casting of nanospheres onto an activated glass coverslip. We then etched these nanospheres isotropically in air plasma at ~18 W, for 70 minutes. Thereafter, a 100 nm layer of Aluminum was deposited onto the substrate, followed by nanosphere lift-off via dissolving in an appropriate solvent solution, or sticky tape. The metal nanoapertures were backlit in transmission mode in epi- as well as TIRF-fluorescence configurations with performances not being radically different. The process workflow is schematically depicted in Figure 29. The nanospheres resisted etching past a mean diameter of ~300 nm, and instead started deforming. As our results demonstrate, this size of nanoapertures is adequate for ZMW-like performance. It has been previously reported (Levene, Korlach et al. 2003) that: $d_C = 0.586\alpha_M$; where d_C is the cut-off diameter for (a perfect conductor as) the cladding material, and αM is the wavelength of the incident light in the medium of the material filling the ZMW. That is, the cut-off diameter d_C = 311.75 nm for 532 nm, and d_C = 375 nm for 640 nm incident light. The drawback of this technique, however, is that the

ZMWs (as seen from SEM images) are crudely shaped, which might lead to non-uniform illumination profiles within the nanoapertures and result in sub-par performance.

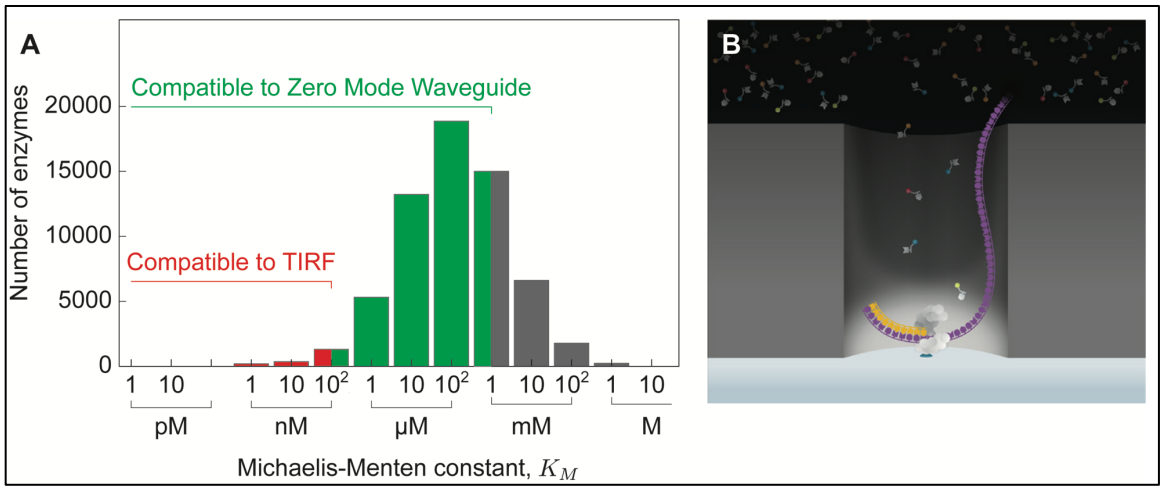

Figure 28: Zero Mode Waveguide (ZMW): structure and function. (A) Histogram of Michaelis-Menten constants K_M of 62 x 10^{23} enzymes taken from the Brenda database (http://www.brenda-enzymes.info). ZMWs (green) enable experiments at biologically-relevant K_M that are not accessible with TIRF microscopy (red). Histogram is adapted (Heucke, Baumann et al. 2014). (B) Geometry of a ZMW nanoaperture with excitation confinement in the 10^{-21} L regime to detect individual fluorescent deoxyribonucleoside triphosphates (dNTPs) against the bulk fluorescent background for incorporation into the DNA fragment by an immobilized polymerase. Schematic is adapted (Eid, Fehr et al. 2009).

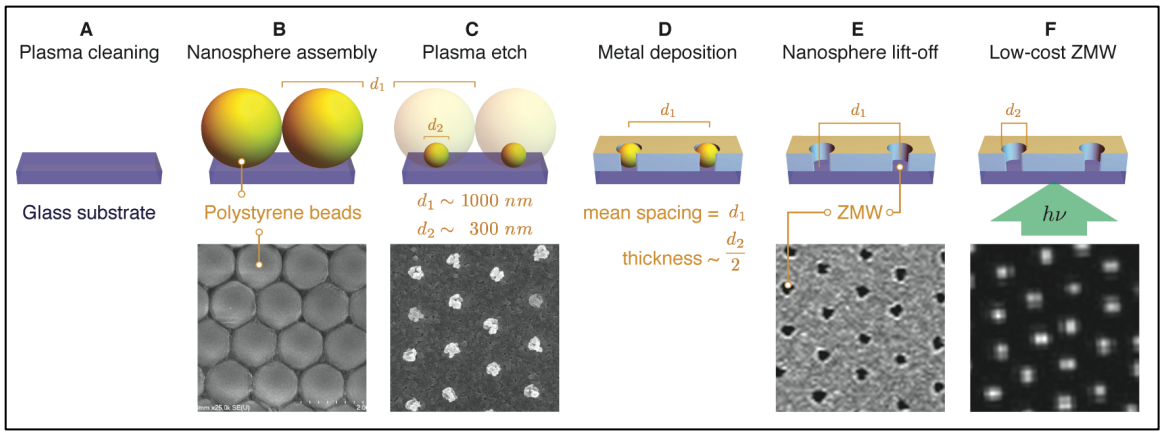

Figure 29: ZMW micromachining via a "self-assemble and etch" strategy. The workflow proceeds through nanosphere deposition (A, B) and isotropic plasma etching (C), followed by metal deposition (D), and nanosphere lift-off (E) to reveal low-cost ZMWs under transmission mode microscopy (F). Scanning electron micrographs demonstrate experimental results of this procedure.

Undoubtedly the most exciting bottom-up ZMW nanofabrication approach is where a single origami molecule is placed inside each nanoaperture prior to the ZMW itself being fabricated around the origami through bottom-up assembly. This approach requires an immobilized origami grid (created with the NSL technique; Figure 30) achieving >70%, non-Poisson limited single-molecule (origami) occupancy per binding site. ZMWs, similar to other top-down fabricated devices are restricted to a single molecule occupancy limited by Poisson statistics to a maximum of 37%. Rather than plugging these nanoapertures with origami nanoadapters post-fabrication (Pibiri, Holzmeister et al. 2014), we propose to build them around already bound functionalized origami. The origami will be modified to incorporate several amine-terminated linker strands on the side facing-up. Incubation with EDC-NHS activated, amine-reactive carboxylated nanospheres will result in the nanospheres covalently binding to the immobilized aminated-DNA origami (Bart, Tiggelaar et al. 2009, Gopinath and Rothemund 2014, Bugiel, Fantana et al. 2015). Each origami is intended to bind exactly one nanosphere. Once bound, this nanosphere will be used as a sacrificial mask layer to deposit a chosen thickness of aluminum. Post metal-deposition, the nanosphere will be dissolved in Tetrahydrofuran, or another such solvent in which the origami is stable. A second, possibly more straightforward approach to nanosphere-origami binding is that of electrostatically attaching the carboxylated nanospheres to aminated-origami under the right pH, and Mg^{++} concentration conditions. A third alternative is to attach streptavidin-coated nanospheres to biotinylated strands extending from DNA origami. The final device will boast a high-density grid of already occupied and functional metal nanoapertures that will serve as ZMWs. The significance of the proposed method is two-fold: First, it overcomes Poisson- limited loading of single-molecules via the NSL-based benchtop origami placement technique. Second, the built-in origami can subsequently serve to recruit other biological molecules of interest for single-

molecule experiments in the μM-to-mM concentration regime. Thus, the single-molecule origami baseplates serve to build-up ZMWs while also being built into them, overcoming the long-standing Poisson-limited single-molecule occupancy in such devices.

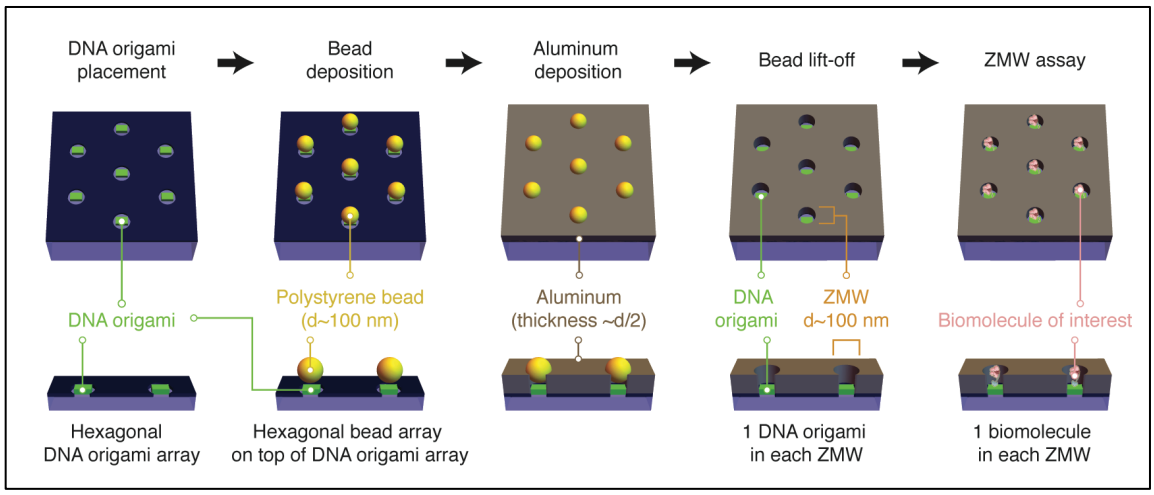

Figure 30: Schematic representation of a bottom-up paradigm for ZMW fabrication with one origami per ZMW. This workflow proceeds through routine benchtop DNA origami placement with each origami being functionalized for bead recruitment via EDC-NHS, electrostatic, or biotin-streptavidin chemistry. Aluminum is then deposited on the beads to act as a mask prior to bead removal and Poisson de-limited single molecule (origami) occupancy.

The foreseeable shortcomings of this technique are the metal deposition step that needs to be performed in an electron-beam evaporator in a cleanroom, and the minimum achievable diameter of the final aperture, which will be directly related to the diameter of the nanosphere. It is recommended to maintain at least a 2:1 (sacrificial layer: deposited layer) clearance for complete (nanosphere) lift-off. AFM, and SEM will enable structural characterization of this process. We are interested in the fabrication of ZMWs in the range of 50–200 nm, and in characterizing the optical performance of each corresponding grid in terms of light attenuation, and Point Spread Functions (PSFs) to validate device performance prior to providing experimental proof-of-concept. Finally, in an attempt at developing a workflow for origami placement at more relaxed distances from each other

for easier resolution with simplified optical setups (described in the previous section), we also developed a process for ZMW fabrication (Figure 31), preliminary results for which are presented here (Figure 32). This “iterative size reduction” technique requires the programmed placement of a second layer of appropriately-sized nanospheres in the binding sites created by a first layer of larger nanospheres. This is achievable under optimal incubation conditions using electrostatic interactions. Once in place, these nanospheres are used as a mask for the deposition of aluminum. A lift-off process leaves nanosphere-sized ZMWs on the chip surface. The entire process apart from the metal deposition step can be performed on a laboratory benchtop and is expected to cost under $10, a reduction of 100x compared to commercially available ZMW devices. This significantly lowers the barrier-of-adoption for ZMW devices to be used in biophysical experiments across the world.

5.3 Metalenses and amplification-free strategies for biomarker detection

Subwavelength-spaced scatterers enable the fabrication of metalenses which, in the future, may facilitate small footprint, low-weight wearable optical devices (Khorasaninejad and Capasso 2017). These lenses will replace bulky, heavy, and expensive refractive lenses currently used in microscope objectives and allow unprecedented flexibility in design. They overcome spherical aberrations through clever phase manipulation while being able to achieve diffraction-limited resolution with a high numerical aperture. The fabrication of these lenses is compatible with traditional semiconductor industry technology, and they can be produced with high efficiency to enable easy optical alignment and packaging in camera modules (She, Zhang et al. 2018). Such a compact system could spark a revolution in point-of-care imaging systems based on fluorescence or optical imaging due to their size and cost-efficiency. It is plausible that

the current low-cost imaging system can be upgraded using metalenses acquired from researches at Sandia National Laboratory in the near future (Aiello, Backer et al. 2019).

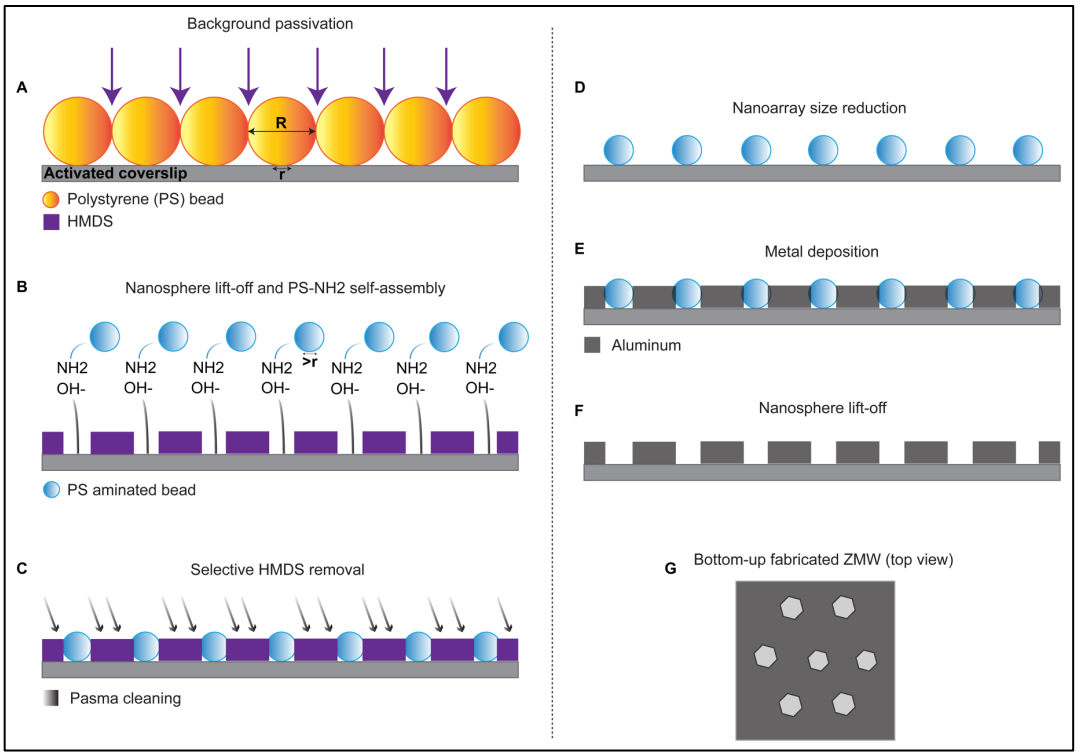

Figure 31: Iterative size reduction process for ZMW fabrication. This workflow proceeds through the creation of binding sites (A, B) using an HMDS layer and the consequent electrostatic programmable placement of smaller functionalized nanospheres size-matched with the binding sites (B), and HMDS removal (C). Aluminum deposition (E) and lift-off result in the creation of ZMWs (F, G) where DNA origami molecules can be placed if required for steric hindrance-based single molecule placement (Pibiri, Holzmeister et al. 2014).

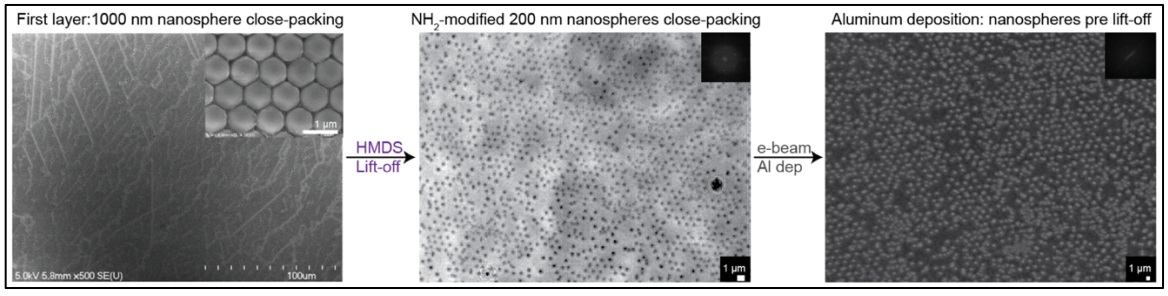

Figure 32: The iterative size-reduction approach towards bottom-up ZMW nanofabrication. This process proceeds through the close-packing of large, 1000 nm nanospheres and HMDS passivation for the creation of ~250 nm binding sites. Amine-modified, 200-nm nanospheres are then incubated under the appropriate conditions to form a close-packed layer of smaller beads (separated by 1000 nm) which can be used as a mask for Aluminum deposition. The final step will be lift-off of the smaller nanospheres.

Amplification-free strategies for biomarker detection based on kinetic fingerprinting or molecular dynamics (Hayward, Lund et al. 2018, Schickinger, Zacharias et al. 2018) rather than amplification (protein-, or nucleic-acid based) have several advantages: 1) Differentiation between background or non-specific binding and "real" signal is relatively straightforward due to the kinetic footprint of dynamic events which are different from aggregation of molecules on a surface. 2) There are fewer failure modes to analyze because of lesser number of components being involved, i.e. biases and errors can be reduced. 3) Time-to-detection can be much shorter than with amplification-based strategies. However, such strategies can suffer from reduced sensitivity and the inability for binding events to generate a significant enough signal to be detected accurately. Using dark-field microscopy, gold nanoparticles, and other alternatives have the potential to circumvent such problems. One such approach uses a tethered multifluorophore (TMF)-based assay with an immobile and a reporter origami unit (Schickinger, Zacharias et al. 2018). The open state of the reporter unit is noticeably different from its closed state in response to the binding of a target molecule. This can lead to the facile digital detection of analytes on the nanoarray platform by immobilizing the two origami units on the origami baseplate on each binding site and implementing single molecule tracking to reveal dynamics correlated to binding events without the need for amplification.

5.4 Concluding remarks

The work in this dissertation is the first demonstration of a benchtop method for DNA origami, and by extension, single molecule nanoarray fabrication with high efficiency (~2x the Poisson limit) single molecule immobilization in diffraction-limited areas. It is broadly aimed at democratizing the highest-throughput single molecule biophysics experiments and low-cost digital diagnostics for point-of-care applications. During the course of this work we have (1) optimized a bottom-up, DNA origami immobilization paradigm through the creation of long-range, hexagonally-close packed (HCP), self-assembled binding sites; (2) validated the robustness, shelf-life, and biophysical relevance of this "nanoarray" platform via high-throughput experiments probing *ss*DNA counting; (3) highlighted the potential of DNA origami nanoarrays as a diagnostic platform for low-cost, quantitative biomarker detection.

The platform developed in this work employs cleanroom-free, bottom-up fabrication of DNA nanoarrays on a bench-top without the need for sophisticated infrastructure or training. This extensively characterized technique enables the highest density of diffraction-limited experimental data to be collected at a fraction of the cost of current top-down fabrication-based DNA Origami Placement (DOP) methods. It utilizes NSL-assisted surface passivation for DOP in predetermined binding sites and exhibits two times the single molecule placement efficiency achievable with conventional, stochastic loading techniques. We demonstrated the utility of deterministic single molecule experiments in comparison to classical, stochastic approaches in terms of throughput, and efficacy. Further, we validated the performance of the platform for digital synthetic nucleic acid detection at a limit of 25 pM. Experimental testing helped determine the suitability of DNA origami nanoarrays as an affordable, and easily fabricated single molecule dynamics and quantitative detection platform. In the future, through integration with low-

cost imaging setups and innovative assay design, this platform could be a portable diagnostic tool for POC disease detection of various molecular classes of biomarkers. As outlined in this chapter, the platform is uniquely placed to develop bottom-up nanofabrication processes for heretofore expensive biophysical tools such as zero mode waveguides.

REFERENCES

Acuna, G. P., F. M. Möller, P. Holzmeister, S. Beater, B. Lalkens and P. Tinnefeld (2012). "Fluorescence Enhancement at Docking Sites of DNA-Directed Self-Assembled Nanoantennas." Science **338**: 506-510.

Aiello, M. D., A. S. Backer, A. J. Sapon, J. Smits, J. D. Perreault, P. Llull and V. M. Acosta (2019). "Achromatic varifocal metalens for the visible spectrum." Biorxiv **arXiv:1903.03930v2**.

Armbruster, D. A. and T. Pry (2008). "Limit of Blank, Limit of Detection and Limit of Quantitation." Clin Biochem Rev **29**: 49-52.

Axelrod, D. (2001). "Total Internal Reflection Fluorescence Microscopy in Cell Biology." Traffic **2**: 764-774.

Axelrod, D., T. P. Burghardt and N. L. Thompson (1984). "Total Internal Reflection Fluorescence." Annu Rev Biophys Bioeng. **13**: 247-268.

Bald, I. and A. Keller (2014). "Molecular processes studied at a single-molecule level using DNA origami nanostructures and atomic force microscopy." Molecules **19**(9): 13803-13823.

Bart, J., R. Tiggelaar, M. Yang, S. Schlautmann, H. Zuilhof and H. Gardeniers (2009). "Room-temperature intermediate layer bonding for microfluidic devices." Lab Chip **9**(24): 3481-3488.

Basu, A. (2017). "Digital Assays Part I: Partitioning Statistics and Digital PCR." SLAS Technology.

Basu, A. (2017). "Digital Assays Part II- Digital Protein and Cell Assays." SLAS Technology.

Bi, S., M. Chen, X. Jia, Y. Dong and Z. Wang (2015). "Hyperbranched Hybridization Chain Reaction for Triggered Signal Amplification and Concatenated Logic Circuits." Angew Chem Int Ed Engl **54**(28): 8144-8148.

Brassat, K., S. Ramakrishnan, J. Bürger, M. Hanke, M. Doostdar, J. K. N. Lindner, G. Grundmeier and A. Keller (2018). "On the Adsorption of DNA Origami Nanostructures in Nanohole Arrays." Langmuir.

Breitschwerdt, E. B. (2011). "Serological and Molecular Diagnosis of Infectious Diseases." World Small Animal Veterinary Association World Congress Proceedings.

Bugiel, M., H. Fantana, V. Bormuth, A. Trushko, F. Schiemann, J. Howard, E. Schäffer and A. Jannasch (2015). "Versatile microsphere attachment of GFP-labeled motors and other tagged proteins with preserved functionality." Journal of Biological Methods **2**(4).

Bui, H., C. Onodera, C. Kidwell, Y. Tan, E. Graugnard, W. Kuang, J. Lee, W. B. Knowlton, B. Yurke and W. L. Hughes (2010). "Programmable periodicity of quantum dot arrays with DNA origami nanotubes." Nano Lett **10**(9): 3367-3372.

Cai, H. and S. J. Wind (2016). "Improved Glass Surface Passivation for Single-Molecule Nanoarrays." Langmuir **32**(39): 10034-10041.

Caliendo, A. M., D. N. Gilbert, C. C. Ginocchio, K. E. Hanson, L. May, T. C. Quinn, F. C. Tenover, D. Alland, A. J. Blaschke, R. A. Bonomo, K. C. Carroll, M. J. Ferraro, L. R. Hirschhorn, W. P. Joseph, T. Karchmer, A. T. MacIntyre, L. B. Reller, A. F. Jackson and A. Infectious Diseases Society of (2013). "Better tests, better care: improved diagnostics for infectious diseases." Clin Infect Dis **57 Suppl 3**: S139-170.

Chang, C. C., C. C. Chen, S. C. Wei, H. H. Lu, Y. H. Liang and C. W. Lin (2012). "Diagnostic devices for isothermal nucleic acid amplification." Sensors (Basel) **12**(6): 8319-8337.

Choi, H. M. T., V. A. Beck and N. A. Pierce (2014). "Next-Generation *in Situ* Hybridization Chain Reaction- Higher Gain, Lower Cost, Greater Durability." ACS Nano **8**(5): 4284-4294.

Choi, H. M. T., M. Schwarzkopf, M. E. Fornace, A. Acharya, G. Artavanis, J. Stegmaier, A. Cunha and N. A. Pierce (2018). "Third-generation in situ hybridization chain reaction: multiplexed, quantitative, sensitive, versatile, robust." Development **145**(12).

Cloherty, G., A. Talal, K. Coller, C. Steinhart, J. Hackett, Jr., G. Dawson, J. Rockstroh and J. Feld (2016). "Role of Serologic and Molecular Diagnostic Assays in Identification and Management of Hepatitis C Virus Infection." J Clin Microbiol **54**(2): 265-273.

Coelho, M., N. Maghelli and I. M. Tolic-Norrelykke (2013). "Single-molecule imaging in vivo: the dancing building blocks of the cell." Integr Biol (Camb) **5**(5): 748-758.

Cohen, L., M. R. Hartman, A. Amardey-Wellington and D. R. Walt (2017). "Digital direct detection of microRNAs using single molecule arrays." Nucleic Acids Res **45**(14): e137.

Cohen, L. and D. R. Walt (2017). "Single-Molecule Arrays for Protein and Nucleic Acid Analysis." Annu Rev Anal Chem **10**: 345-363.

Colson, P., R. Cloots and C. Henrist (2011). "Experimental design applied to spin coating of 2D colloidal crystal masks: a relevant method?" Langmuir **27**(21): 12800-12806.

Colson, P., C. Henrist and R. Cloots (2013). "Nanosphere Lithography: A Powerful Method for the Controlled Manufacturing of Nanomaterials." Journal of Nanomaterials **2013**: 1-19.

Cong, H., B. Yu, J. Tang, Z. Li and X. Liu (2013). "Current status and future developments in preparation and application of colloidal crystals." Chem Soc Rev **42**(19): 7774-7800.

Craighead, H. G. and P. M. Mankiewich (1982). "Ultra-small metal particle arrays produced by high resolution electron-beam lithography." Journal of Applied Physics **53**(11): 7186-7188.

Craighead, H. G. and G. A. Niklasson (1984). "Characterization and optical properties of arrays of small gold particles." Applied Physics Letters **44**(12): 1134-1136.

Cybulski, J. S., J. Clements and M. Prakash (2014). "Foldscope: origami-based paper microscope." PLoS One **9**(6): e98781.

Daems, D., W. Pfeifer, I. Rutten, B. Sacca, D. Spasic and J. Lammertyn (2018). "Three-Dimensional DNA Origami as Programmable Anchoring Points for Bioreceptors in Fiber Optic Surface Plasmon Resonance Biosensing." ACS Appl Mater Interfaces **10**(28): 23539-23547.

Dai, M., R. Jungmann and P. Yin (2016). "Optical imaging of individual biomolecules in densely packed clusters." Nat Nanotechnol **11**(9): 798-807.

Deckman, H. W. (1983). "Applications of surface textures produced with natural lithography." Journal of Vacuum Science & Technology B: Microelectronics and Nanometer Structures **1**(4).

Deniz, A. A., S. Mukhopadhyay and E. A. Lemke (2008). "Single-molecule biophysics: at the interface of biology, physics and chemistry." J R Soc Interface **5**(18): 15-45.

Denkov, N. D., O. D. Velev, P. A. Kralchevsky, I. B. Ivanov, H. Yoshimura and K. Nagayama (1992). "Mechanism of Formation of Two-Dimensional Crystals from Latex Particles on Substrates." Langmuir **8**: 3183-3190.

Derr, N. D., B. S. Goodman, R. Jungmann, A. E. Leschziner, W. M. Shih and S. L. Reck-Peterson (2012). "Tug-of-War in Motor Protein Ensembles Revealed with a Programmable DNA Origami Scaffold." Science **338**: 662-666.

Ding, B., Z. Deng, H. Yan, S. Cabrini and R. N. Zuckermann (2010). "Gold Nanoparticle Self-Similar Chain Structure Organized by DNA Origami." J Am Chem Soc **132**(10): 1-16.

Ding, B., Z. Deng, H. Yan, S. Cabrini, R. N. Zuckermann and J. Bokor (2010). "Gold Nanoparticle Self-Similar Chain Structure Organized by DNA Origami." J Am Chem Soc **132**: 3248-3249.

Dirks, R. M. and N. A. Pierce (2004). "From The Cover: Triggered amplification by hybridization chain reaction." Proceedings of the National Academy of Sciences **101**(43): 15275-15278.

Dirks, R. M. and N. A. Pierce (2004). "Triggered amplification by hybridization chain reaction." Proc Natl Acad Sci U S A **101**(43): 15275-15278.

Dulin, D., J. Lipfert, M. C. Moolman and N. H. Dekker (2013). "Studying genomic processes at the single-molecule level: introducing the tools and applications." Nat Rev Genet **14**(1): 9-22.

Dutta, P. K., R. Varghese, J. Nangreave, S. Lin, H. Yan and Y. Liu (2011). "DNA-directed artificial light-harvesting antenna." J Am Chem Soc **133**(31): 11985-11993.

Eid, J., A. Fehr, J. Gray, K. Luong, J. Lyle, G. Otto, P. Peluso, D. Rank, P. Baybayan, B. Bettman, A. Bibillo, K. Bjornson, B. Chaudhuri, F. Christians, R. Cicero, S. Clark, R. Dalal, A. Dewinter, J. Dixon, M. Foquet, A. Gaertner, P. Hardenbol, C. Heiner, K. Hester, D. Holden, G. Kearns, X. Kong, R. Kuse, Y. Lacroix, S. Lin, P. Lundquist, C. Ma, P. Marks, M. Maxham, D. Murphy, I. Park, T. Pham, M. Phillips, J. Roy, R. Sebra, G. Shen, J. Sorenson, A. Tomaney, K. Travers, M. Trulson, J. Vieceli, J. Wegener, D. Wu, A. Yang, D. Zaccarin, P. Zhao, F. Zhong, J. Korlach and S. Turner (2009). "Real-time DNA sequencing from single polymerase molecules." Science **323**(5910): 133-138.

Elting, M. W., S. R. Leslie, L. S. Churchman, J. Korlach, C. M. McFaul, J. S. Leith, M. J. Levene, A. E. Cohen and J. A. Spudich (2013). "Single-molecule fluorescence imaging of processive myosin with enhanced background suppression using linear zero-mode waveguides (ZMWs) and convex lens induced confinement (CLIC)." Opt Express **21**(1): 1189-1202.

Foquet, M., K. T. Samiee, X. Kong, B. P. Chauduri, P. M. Lundquist, S. W. Turner, J. Freudenthal and D. B. Roitman (2008). "Improved fabrication of zero-mode waveguides for single-molecule detection." Journal of Applied Physics **103**(3): 034301.

Fu, J., M. Liu, Y. Liu, N. W. Woodbury and H. Yan (2012). "Interenzyme substrate diffusion for an enzyme cascade organized on spatially addressable DNA nanostructures." J Am Chem Soc **134**(12): 5516-5519.

Gardner, S. N., C. J. Jaing, K. S. McLoughlin and T. R. Slezak (2010). "A microbial detection array (MDA) for viral and bacterial detection." BMC genomics **11**(1): 668.

Ge, Z., M. Lin, P. Wang, H. Pei, J. Yan, J. Shi, Q. Huang, D. He, C. Fan and X. Zuo (2014). "Hybridization chain reaction amplification of microRNA detection with a tetrahedral DNA nanostructure-based electrochemical biosensor." Anal Chem **86**(4): 2124-2130.

Geng, C., T. Wei, X. Wang, D. Shen, Z. Hao and Q. Yan (2014). "Enhancement of light output power from LEDs based on monolayer colloidal crystal." Small **10**(9): 1668-1686.

Geng, C., T. Wei, X. Wang, D. Shen, Z. Hao and Q. Yan (2014). "Enhancement of Light Output Power from LEDs Based on Monolayer Colloidal Crystal." Small **10**(9): 1668-1686.

George M. Whitesides, J. P. M., Christopher T. Seto (1991). "Molecular Self-Assembly and Nanochemistry- A Chemical Strategy for the Synthesis of Nanostructures." Science **254**: 1312-1319.

Gerling, T., M. Kube, B. Kick and H. Dietz (2018). "Sequence-programmable covalent bonding of designed DNA assemblies." Science Advances **4**.

Godonoga, M., T.-Y. Lin, A. Oshima, K. Sumitomo, M. S. L. Tang, Y.-W. Cheung, A. B. Kinghorn, R. M. Dirkzwager, C. Zhou, A. Kuzuya, J. A. Tanner and J. G. Heddle (2016). "A DNA aptamer recognising a malaria protein biomarker can function as part of a DNA origami assembly." Scientific Reports **6**(1).

Godonoga, M., T. Y. Lin, A. Oshima, K. Sumitomo, M. S. Tang, Y. W. Cheung, A. B. Kinghorn, R. M. Dirkzwager, C. Zhou, A. Kuzuya, J. A. Tanner and J. G. Heddle (2016). "A DNA aptamer recognising a malaria protein biomarker can function as part of a DNA origami assembly." Sci Rep **6**: 21266.

Goldschen-Ohm, M. P., D. S. White, V. A. Klenchin, B. Chanda and R. H. Goldsmith (2017). "Observing Single-Molecule Dynamics at Millimolar Concentrations." Angew Chem Int Ed Engl **56**(9): 2399-2402.

Gopinath, A., E. Miyazono, A. Faraon and P. W. Rothemund (2016). "Engineering and mapping nanocavity emission via precision placement of DNA origami." Nature **535**(7612): 401-405.

Gopinath, A. and P. W. K. Rothemund (2014). "Optimized Assembly and Covalent Coupling of Single-Molecule DNA Origami Nanoarrays." ACS Nano **8**(12): 12030-12040.

Gopinath, A., C. Thachuk, A. Mitskovets, H. A. Atwater, D. Kirkpatrick and P. W. K. Rothemund (2018). "Absolute and arbitrary orientation of single molecule shapes." Biorxiv.

Gopinath, A., C. Thachuk, A. Mitskovets, H. A. Atwater, D. Kirkpatrick and P. W. K. Rothemund (2018). "Absolute and arbitrary orientation of single molecule shapes." arXiv:1808.04544[physics.app-ph].

Grandidier, J., R. A. Weitekamp, M. G. Deceglie, D. M. Callahan, C. Battaglia, C. R. Bukowsky, C. Ballif, R. H. Grubbs and H. A. Atwater (2013). "Solar cell efficiency enhancement via light trapping in printable resonant dielectric nanosphere arrays." physica status solidi (a) **210**(2): 255-260.

Greene, E. C., S. Wind, T. Fazio, J. Gorman and M.-L. Visnapuu (2010). DNA Curtains for High-Throughput Single-Molecule Optical Imaging. Single Molecule Tools: Fluorescence Based Approaches, Part A**:** 293-315.

Ha, T. (2001). "Single-molecule fluorescence resonance energy transfer." Methods **25**(1): 78-86.

Hariadi, R. F., M. Cale and S. Sivaramakrishnan (2014). "Myosin lever arm directs collective motion on cellular actin network." Proc Natl Acad Sci U S A **111**(11): 4091-4096.

Hariadi, R. F., R. F. Sommese and S. Sivaramakrishnan (2015). "Tuning myosin-driven sorting on cellular actin networks." Elife **4**.

Hawker, C. J. and T. P. Russell (2005). "Block Copolymer Lithography- Merging “Bottom-Up” with “Top-Down” Processes." MRS Bulletin **30**: 952-965.

Hayward, S. L., P. E. Lund, Q. Kang, A. Johnson-Buck, M. Tewari and N. G. Walter (2018). "Ultraspecific and Amplification-Free Quantification of Mutant DNA by Single-Molecule Kinetic Fingerprinting." J Am Chem Soc **140**(37): 11755-11762.

Heller, M. J. (2002). "DNA microarray technology: devices, systems, and applications." Annu Rev Biomed Eng **4**: 129-153.

Heucke, S. F., F. Baumann, G. P. Acuna, P. M. Severin, S. W. Stahl, M. Strackharn, I. H. Stein, P. Altpeter, P. Tinnefeld and H. E. Gaub (2014). "Placing individual molecules in the center of nanoapertures." Nano Lett **14**(2): 391-395.

Heydarian, H., F. Schueder, M. T. Strauss, B. van Werkhoven, M. Fazel, K. A. Lidke, R. Jungmann, S. Stallinga and B. Rieger (2018). "Template-free 2D particle fusion in localization microscopy." Nature Methods.

Hua, B., K. Y. Han, R. Zhou, H. Kim, X. Shi, S. C. Abeysirigunawardena, A. Jain, D. Singh, V. Aggarwal, S. A. Woodson and T. Ha (2014). "An improved surface passivation method for single-molecule studies." Nature Methods **11**(12): 1233-1236.

Huang, B., M. Bates and X. Zhuang (2009). "Super-resolution fluorescence microscopy." Annu Rev Biochem **78**: 993-1016.

Hulteen, J. C. and R. P. V. Duyne "Nanosphere lithography- A materials general fabrication process for periodic particle array surfaces." Journal of Vacuum Science & Technology A: Vacuum, Surfaces, and Films **13**(3): 1553-1558.

Isa, L., K. Kumar, M. Muller, J. Grolig, M. Textor and E. Reimhult (2010). "Particle Lithography from Colloidal SelfAssembly at Liquid Liquid Interfaces." ACS Nano **10**: 5665-5670.

John, A. S. and C. P. Price (2014). "Existing and Emerging Technologies for Point-of-Care Testing_Review article." Clin Biochem Rev **35**(3): 155-167.

Jungmann, R., M. S. Avendano, M. Dai, J. B. Woehrstein, S. S. Agasti, Z. Feiger, A. Rodal and P. Yin (2016). "Quantitative super-resolution imaging with qPAINT." Nat Methods **13**(5): 439-442.

Ke, Y., S. Lindsay, Y. Chang, Y. Liu and H. Yan (2008). "Self-Assembled Water-Soluble Nucleic Acid Probe Tiles for Label-Free RNA Hybridization Assays." Science **319**: 180-183.

Kershner, R. J., L. D. Bozano, C. M. Micheel, A. M. Hung, A. R. Fornof, J. N. Cha, C. T. Rettner, M. Bersani, J. Frommer, P. W. Rothemund and G. M. Wallraff (2009). "Placement and orientation of individual DNA shapes on lithographically patterned surfaces." Nat Nanotechnol **4**(9): 557-561.

Khorasaninejad, M. and F. Capasso (2017). "Metalenses: Versatile multifunctional photonic components." Science **358**(6367).

Kim, H., S. P. Surwade, A. Powell, C. O'Donnell and H. Liu (2014). "Stability of DNA Origami Nanostructure under Diverse Chemical Environments." Chemistry of Materials **26**(18): 5265-5273.

Ko, S. H., K. Du and J. A. Liddle (2013). "Quantum-dot fluorescence lifetime engineering with DNA origami constructs." Angew Chem Int Ed Engl **52**(4): 1193-1197.

Korlach, J., P. J. Marks, R. L. Cicero, J. J. Gray, D. L. Murphy, D. B. Roitman, T. T. Pham, G. A. Otto, M. Foquet and S. W. Turner (2008). "Selective aluminum passivation for targeted immobilization of single DNA polymerase molecules in zero-mode waveguide nanostructures." Proceedings of the National Academy of Sciences **105**(4): 1176-1181.

Kozel, T. R. and A.R.Burnham-Marusich (2017). "Point-of-Care Testing for Infectious Diseases- Past, Present, and Future." Journal of Clinical Microbiology **55**(8): 2313-2320.

Kralchevsky, P. A. and N. D. Denkov (2001). "Capillary forces and structuring in layers of colloid particles." Current Opinion in Colloid and Interface Science **6**: 383-401.

Kuhler, P., E. M. Roller, R. Schreiber, T. Liedl, T. Lohmuller and J. Feldmann (2014). "Plasmonic DNA-origami nanoantennas for surface-enhanced Raman spectroscopy." Nano Lett **14**(5): 2914-2919.

Kuzuya, A., Y. Sakai, T. Yamazaki, Y. Xu and M. Komiyama (2011). "Nanomechanical DNA origami 'single-molecule beacons' directly imaged by atomic force microscopy." Nat Commun **2**: 449.

Kuzyk, A., R. Schreiber, Z. Fan, G. Pardatscher, E. M. Roller, A. Hogele, F. C. Simmel, A. O. Govorov and T. Liedl (2012). "DNA-based self-assembly of chiral plasmonic nanostructures with tailored optical response." Nature **483**(7389): 311-314.

Leake, M. C. (2012). "The physics of life: one molecule at a time." Philosophical Transactions of the Royal Society B: Biological Sciences **368**(1611): 20120248-20120248.

lee, H. J., A. W. Wark and R. M. Corn (2006). "Creating Advanced Multifunctional Biosensors with Surface Enzymatic Transformations." Langmuir **22**(12): 5241-5250.

Levene, M. J., K. Korlach, S. W. Turner, M. Foquet, H. G. Craighead and W. W. Webb (2003). "ZMW for single-molecle analysis at high concentrations." Science **299**: 682-686.

Li, J.-R., K. L. Lusker, J.-J. Yu and J. C. Gamo (2009). "Engineering the Spatial Selectivity of Surfaces at the Nanoscale Using Particle Lithography Combined with Vapor Deposition of Organosilanes." ACS Nano **3**(7): 2023-2035.

Lizardi, P. M., X. Huang, Z. Zhu, P. Bray-Ward, D. C. Thomas and D. C. Ward (1998). "Mutation detection and single-molecule counting using isothermal rolling-circle amplification." Nature Genetics **19**: 225-232.

Lizardi, P. M., Z. Huang, Z. Zhu, P. Bray-Ward, D. C. Thomas and D. C. Ward (1998). "Mutation detection and single-molecule counting using isothermal rolling-circle amplification." Nature Genetics **19**(3): 225-232.

Lotito, V. and T. Zambelli (2017). "Approaches to self-assembly of colloidal monolayers: A guide for nanotechnologists." Adv Colloid Interface Sci **246**: 217-274.

Mattheyses, A. L., S. M. Simon and J. Z. Rappoport (2010). "Imaging with total internal reflection fluorescence microscopy for the cell biologist." J Cell Sci **123**(Pt 21): 3621-3628.

Maune, H. T., S. P. Han, R. D. Barish, M. Bockrath, W. A. Goddard, III, P. W. Rothemund and E. Winfree (2010). "Self-assembly of carbon nanotubes into two-dimensional geometries using DNA origami templates." Nat Nanotechnol **5**(1): 61-66.

Micheletto, R., H.Fukuda and M.Ohtsu (1995). "A Simple Method for the Production of a Two-Dimensional, Ordered Array of Small Latex Particles " Langmuir **11**: 3333-3336.

Mijatovic, D., J. C. Eijkel and A. van den Berg (2005). "Technologies for nanofluidic systems: top-down vs. bottom-up--a review." Lab Chip **5**(5): 492-500.

Moran-Mirabal, J. M. and H. G. Craighead (2008). "Zero-mode waveguides: sub-wavelength nanostructures for single molecule studies at high concentrations." Methods **46**(1): 11-17.

Nallur, G., C. Luo, L. Fang, S. Cooley, V. Dave, J. Lambert, K. Kukanskis, S. Kingsmore, R. Lasken and B. Schweitzer (2001). "Signal amplification by rolling circle amplification on DNA microarrays." Nucleic Acids Res **29**(23).

Nayak, S., N. R. Blumenfeld, T. Laksanasopin and S. K. Sia (2017). "Point-of-Care Diagnostics: Recent Developments in a Connected Age." Anal Chem **89**(1): 102-123.

Nickels, P. C., H. C. Hoiberg, S. S. Simmel, P. Holzmeister, P. Tinnefeld and T. Liedl (2016). "DNA origami seesaws as comparative binding assay." ChemBioChem **17**: 1093-1096.

Nickels, P. C., B. Wunsch, P. Holzmeister, W. Bae, L. M. Kneer, D. Grohmann, P. Tinnefeld and T. Liedl (2016). "Molecular force spectroscopy with a DNA origami–based nanoscopic force clamp." Science **354**(6310): 305-307.

Notomi, T., H.Okayama, H. Masubuchi, T. Yonekawa, K. Watanabe, N. Amino and T. Hase (2000). "Loop-mediated isothermal amplification of DNA." Nucleic Acids Res **28**(12).

Ochmann, S. E., C. Vietz, K. Trofymchuk, G. P. Acuna, B. Lalkens and P. Tinnefeld (2017). "Optical Nanoantenna for Single Molecule-Based Detection of Zika Virus Nucleic Acids without Molecular Multiplication." Anal Chem **89**(23): 13000-13007.

Pal, S., Z. Deng, B. Ding, H. Yan and Y. Liu (2010). "DNA-origami-directed self-assembly of discrete silver-nanoparticle architectures." Angew Chem Int Ed Engl **49**(15): 2700-2704.

Pei, H., X. Zuo, D. Pan, J. Shi, Q. Huang and C. Fan (2013). "Scaffolded biosensors with designed DNA nanostructures." NPG Asia Materials **5**(6): e51-e51.

Pibiri, E., P. Holzmeister, B. Lalkens, G. P. Acuna and P. Tinnefeld (2014). "Single-molecule positioning in zeromode waveguides by DNA origami nanoadapters." Nano Lett **14**(6): 3499-3503.

Pinheiro, A. V., D. Han, W. M. Shih and H. Yan (2011). "Challenges and opportunities for structural DNA nanotechnology." Nat Nanotechnol **6**(12): 763-772.

Primiceri, E., M. S. Chiriaco, F. M. Notarangelo, A. Crocamo, D. Ardissino, M. Cereda, A. P. Bramanti, M. A. Bianchessi, G. Giannelli and G. Maruccio (2018). "Key Enabling Technologies for Point-of-Care Diagnostics." Sensors (Basel) **18**(11).

Puren, A., J. L. Gerlach, B. H. Weigl, D. M. Kelso and G. J. Domingo (2010). "Laboratory operations, specimen processing, and handling for viral load testing and surveillance." J Infect Dis **201 Suppl 1**: S27-36.

Rao, S. and K. D. Costa (2014). Atomic Force Microscopy (AFM) in biomedical research. Biomedical Imaging**:** 41-64.

Ritort, F. (2006). "Single-molecule experiments in biological physics: methods and applications." J Phys Condens Matter **18**(32): R531-583.

Rothemund, P. W. (2006). "Folding DNA to create nanoscale shapes and patterns." Nature **440**(7082): 297-302.

Roy, R., S. Hohng and T. Ha (2008). "A practical guide to single-molecule FRET." Nat Methods **5**(6): 507-516.

Schickinger, M., M. Zacharias and H. Dietz (2018). "Tethered multifluorophore motion reveals equilibrium transition kinetics of single DNA double helices." Proc Natl Acad Sci U S A **115**(32): E7512-E7521.

Schnitzbauer, J., M. T. Strauss, T. Schlichthaerle, F. Schueder and R. Jungmann (2017). "Super-resolution microscopy with DNA-PAINT." Nat Protoc **12**(6): 1198-1228.

Seeman, N. C. (2010). "Nanomaterials based on DNA." Annu Rev Biochem **79**: 65-87.

Selnihhin, D., S. M. Sparvath, S. Preus, V. Birkedal and E. S. Andersen (2018). "Multifluorophore DNA Origami Beacon as a Biosensing Platform." ACS Nano **12**(6): 5699-5708.

She, A., S. Zhang, S. Shian, D. R. Clarke and F. Capasso (2018). "Large area metalenses: design, characterization, and mass manufacturing." Opt Express **26**(2): 1573-1585.

Shrestha, P., T. Emura, D. Koirala, Y. Cui, K. Hidaka, W. J. Maximuck, M. Endo, H. Sugiyama and H. Mao (2016). "Mechanical properties of DNA origami nanoassemblies are

determined by Holliday junction mechanophores." Nucleic Acids Research **44**(14): 6574-6582.

Skandarajah, A., C. D. Reber, N. A. Switz and D. A. Fletcher (2014). "Quantitative Imaging with a Mobile Phone Microscope." PLoS One **9**(5).

Stehr, F., J. Stein, F. Schueder, P. Schwille and R. Jungmann (2019). "Flat-top TIRF illumination boosts DNA-PAINT imaging and quantification." Nat Commun **10**(1): 1268.

Strauss, M. T., F. Schueder, D. Haas, P. C. Nickels and R. Jungmann (2018). "Quantifying absolute addressability in DNA origami with molecular resolution." Nature Communications **9**(1).

Sun, D. and T. Y. Hu (2018). "A low cost mobile phone dark-field microscope for nanoparticle-based quantitative studies." Biosens Bioelectron **99**: 513-518.

Takabayashi, S., S. Kotani, J. Flores-Estrada, E. Spears, J. E. Padilla, L. C. Godwin, E. Graugnard, W. Kuang, S. Sills and W. L. Hughes (2018). "Boron-Implanted Silicon Substrates for Physical Adsorption of DNA Origami." Int J Mol Sci **19**(9).

Tang, Y.-W., G. W. Procop and D. H. Persing (1997). "Molecular diagnostics of infectious diseases." Clinical Chemistry **43**(11): 2021-2038.

Taylor, Z. R., K. Patel, T. G. Spain, J. C. Keay, J. D. Jernigen, E. S. Sanchez, B. P. Grady, M. B. Johnson and D. W. Schmidtke (2009). "Fabrication of protein dot arrays via particle lithography." Langmuir **25**(18): 10932-10938.

Tee, Y. H., T. Shemesh, V. Thiagarajan, R. F. Hariadi, K. L. Anderson, C. Page, N. Volkmann, D. Hanein, S. Sivaramakrishnan, M. M. Kozlov and A. D. Bershadsky (2015). "Cellular chirality arising from the self-organization of the actin cytoskeleton." Nat Cell Biol **17**(4): 445-457.

Teng, C. H., T. A. Lionberger, J. Zhang, E. Meyhofer and P. C. Ku (2012). "Fabrication of nanoscale zero-mode waveguides using microlithography for single molecule sensing." Nanotechnology **23**(45): 455301.

Thissen, J. B., K. McLoughlin, S. Gardner, P. Gu, S. Mabery, T. Slezak and C. Jaing (2014). "Analysis of sensitivity and rapid hybridization of a multiplexed Microbial Detection Microarray." J Virol Methods **201**: 73-78.

Tsang, C. A., S. M. Anderson, S. B. Imholte, L. M. Erhart, S.Chen, B. J. Park, C. Christ, K. K. Komatsu, T. Chiller and R. H. Sunenshine (2010). "Enhanced Surveillance of Coccidioidomycosis, Arizona, USA, 2007-2008." Emerging Infectious Diseases **16**(11): 1738-1744.

Tsekouras, K., T. C. Custer, H. Jashnsaz, N. G. Walter and S. Presse (2016). "A novel method to accurately locate and count large numbers of steps by photobleaching." Mol Biol Cell **27**(22): 3601-3615.

Uemura, S., C. E. Aitken, J. Korlach, B. A. Flusberg, S. W. Turner and J. D. Puglisi (2010). "Real-time tRNA transit on single translating ribosomes at codon resolution." Nature **464**(7291): 1012-1017.

Ullman, G., M. Wallden, E. G. Marklund, A. Mahmutovic, I. Razinkov and J. Elf (2013). "High-throughput gene expression analysis at the level of single proteins using a microfluidic turbidostat and automated cell tracking." Philos Trans R Soc Lond B Biol Sci **368**(1611): 20120025.

Vemula, S. V., J. Zhao, J. Liu, X. Wang, S. Biswas and I. Hewlett (2016). "Current Approaches for Diagnosis of Influenza Virus Infections in Humans." Viruses **8**(4): 96.

Vernon-Parry, K. D. (2000). "Scanning Electron Microscopy: An introduction." Analysis III-Vs Review **13**(4): 40-44.

Vogel, N., M. Retsch, C. A. Fustin, A. Del Campo and U. Jonas (2015). "Advances in colloidal assembly: the design of structure and hierarchy in two and three dimensions." Chem Rev **115**(13): 6265-6311.

Vogel, N., C. K. Weiss and K. Landfester (2012). "From soft to hard: the generation of functional and complex colloidal monolayers for nanolithography." Soft Matter **8**(15): 4044-4061.

Voigt, N. V., T. Torring, A. Rotaru, M. F. Jacobsen, J. B. Ravnsbaek, R. Subramani, W. Mamdouh, J. Kjems, A. Mokhir, F. Besenbacher and K. V. Gothelf (2010). "Single-molecule chemical reactions on DNA origami." Nat Nanotechnol **5**(3): 200-203.

Walt, D. R. (2013). "Optical methods for single molecule detection and analysis." Anal Chem **85**(3): 1258-1263.

Walt, D. R. (2014). "Protein measurements in microwells." Lab Chip **14**(17): 3195-3200.

Wang, P., T. A. Meyer, V. Pan, P. K. Dutta and Y. Ke (2017). "The Beauty and Utility of DNA Origami." Chem **2**(3): 359-382.

Whitesides, G. (2002). "Self-Assembly at All Scales." Science **295**: 2418-2422.

Wu, Y., C. Zhang, Y. Yuan, Z. Wang, W. Shao, H. Wang and X. Xu (2013). "Fabrication of wafer-size monolayer close-packed colloidal crystals via slope self-assembly and thermal treatment." Langmuir **29**(46): 14017-14023.

Xu, A., J. N. Harb, M. A. Kostiainen, W. L. Hughes, A. T. Woolley, H. Liu and A. Gopinath (2017). "DNA origami: The bridge from bottom to top." MRS Bulletin **42**(12): 943-950.

Xu, H., C. Xue, R. Zhang, Y. Chen, F. Li, Z. Shen, L. Jia and Z.-S. Wu (2017). "Exponential rolling circle amplification and its sensing application for highly sensitive DNA detection of tumor suppressor gene." Sensors and Actuators B: Chemical **243**: 1240-1247.

Xuan, F. and I. M. Hsing (2014). "Triggering hairpin-free chain-branching growth of fluorescent DNA dendrimers for nonlinear hybridization chain reaction." J Am Chem Soc **136**(28): 9810-9813.

Yang, J., S. Jiang, X. Liu, L. Pan and C. Zhang (2016). "Aptamer-Binding Directed DNA Origami Pattern for Logic Gates." ACS Appl Mater Interfaces **8**(49): 34054-34060.

Ye, X. and L. Qi (2011). "Two-dimensionally patterned nanostructures based on monolayer colloidal crystals: Controllable fabrication, assembly, and applications." Nano Today **6**(6): 608-631.

Zadegan, R. M. and M. L. Norton (2012). "Structural DNA nanotechnology: from design to applications." Int J Mol Sci **13**(6): 7149-7162.

Zhang, L., B. Ding, Q. Chen, Q. Feng, L. Lin and J. Sun (2017). "Point-of-care-testing of nucleic acids by microfluidics." TrAC Trends in Analytical Chemistry **94**: 106-116.

Zhang, L. and Y. Xiong (2007). "Rapid self-assembly of submicrospheres at liquid surface by controlling evaporation and its mechanism." J Colloid Interface Sci **306**(2): 428-432.

Zhu, P. and H. G. Craighead (2012). "Zero-mode waveguides for single-molecule analysis." Annu Rev Biophys **41**: 269-293.

APPENDIX A

GUIDE TO TROUBLESHOOTING BINDING SITE CREATION AND ORIGAMI PLACEMENT

Problem	Likely cause	Solution
Nanosphere pellet absent	Spin speed too low to precipitate beads out of suspension	Spin speed/time required for pellet formation is inversely proportional to nanosphere size and should be adjusted accordingly
Nanospheres do not stick to the glass surface	1. Improper plasma activation 2. Improper ethanol concentration. 3. Low nanosphere concentration	Contact angle measurements should delineate a difference between "inactive" and "active" glass surfaces Start at a nominal, 25% ethanol, but 50% should be okay.
No nanosphere close-packing observed	1. Some amount of surfactant in the original solution prevents agglomeration of nanospheres in the bottle 2. Final ethanol suspension might have surfactant due to improper washing	Centrifuge a minimum of 2 times and resuspend in pure water before preparing a final suspension in 25% ethanol at the appropriate concentration Always be careful to aspirate supernatant from the end opposite to the pellet on the Eppendorf tube
Nanospheres do not come off on sonication and/or nanospheres form an amorphous layer on the chip preventing the creation of defined binding sites *Alternative:*	1. Sonication intensity may be low 2. Dehydration bake temperature may be too high	Use an 80x40 mm Pyrex® petri dish (#3140) for sonication and leave the dish in the bath for >5 mins if necessary The glass transition temperature (T_g) of polystyrene nanospheres is ~80°C and should not be exceeded to prevent nanospheres from losing their integrity

Chips can be inserted in a petri dish containing an organic solvent such as Tetrahydrofuran (THF, # 401757, Sigma) heated to 60°C for 5-15 mins to dissolve beads. Care must be taken when handling THF, and to reduce evaporation owing to its volatility.		
Binding site variability is observed over the surface of the chip	1. Insufficient dehydration bake time results in "water puddles" around the nanosphere "footprints" preventing HMDS from depositing all around the circumference 2. Nanospheres not NIST-standards approved, i.e. high standard deviation in nanosphere size	Increase initial dehydration bake time to 10 minutes Check with manufacturer to confirm SD from nominal size of nanospheres
Binding sites are hard to find using AFM	1. AFM tapping force under threshold value 2. Scanned area devoid of nanosphere close-packing	Proceed to origami placement to simplify AFM imaging. Origami nanostructures provide better contrast Sample at least one area from each quadrant of the chip to determine the source of the issue conclusively
Impurities on the surface	4 Improper cleaning 5 Unclean plasma chamber 6 Failure to perform "descum" plasma step, which can leave particulate matter in the interstitial spaces	More aggressive cleaning required (RCA) Clean plasma cleaner chamber with isopropanol and let dry

		Filter all buffers used during wash steps Ensure petri dishes are clean Sterilize peristaltic pump tubing by running boiling hot water through it first, followed by a gradient of 100%, 75%, and 50% ethanol in pure water, and finally placement buffer just before use
Origami bound non-specifically all over the surface	1. Poor HMDS quality 2. Bake step for HMDS stabilization accidentally skipped 3. Improper washing and failure to remove weakly bound origami from HMDS background - new buffers may be required	Dehydrate the wafer by baking before *and* after HMDS monolayer formation. Keep pH<9 preferably in the range 8.3–8.5. Reduce Mg^{++} concentration, and compensate by increasing origami concentration/incubation time Keep incubation between 30 and 90 minutes. Remove weakly bound origami with more aggressive Tween-20 washes (0.08%, 10-20 minutes)
Site occupancy low	1. Old chip with inactive sites 2. Low origami concentration 3. Short incubation time 4. Low pH, or Mg^{2+} concentration	Sites remain optimally active for ~4 hours post-plasma cleaning

		Optimize origami concentration (e.g. 4 chips, 200-400 pM for 400-nm spacing). Use higher origami concentration, prepare fresh dilutions, and use immediately Check buffer pH (8.3-8.5), prepare fresh if necessary, with ≥35 mM Mg^{++} Add a verification step to ascertain appropriate binding site diameter post nanosphere lift-off using AFM
High multiple binding	1. High origami concentration 2. Long incubation time 3. Oversized features	Optimize origami concentration if fresh stock prepared Use an incubation time between 30-90 minutes Check buffer conditions Add a verification step to ascertain appropriate binding site diameter post nanosphere lift-off using AFM
High background binding: Origami (balled-up [white "blobs"] or otherwise)	If HMDS passivation is good, origami cannot bind flush against the surface, and improper washing can lead origami to come off partially. Subsequent ethanol washing leads to any origami not bound completely to ball up and appear as white blobs during AFM imaging	Dehydrate the chip before and after HMDS monolayer formation taking care to keep first dehydration step below T_g of polystyrene nanospheres Keep placement buffer pH between 8.3-8.5

		Remove weakly bound origami with longer Tween-20 wash and/or increasing Tween concentration (<0.1% to prevent origami in binding sites from falling off)
Origami fall off during ethanol drying	Too much time spent in dilute ethanol (<80%)	Move quickly from low to high % ethanol
Origami ball up into site during ethanol drying and corners are double height	Origami project partially onto non-sticky HMDS surface	Hydrolyze HMDS surface before drying by washing in pH 8.9-9.0 buffer to mitigate background binding
Binding sites are filled up, but no defined origami shapes observed	1. Staple excess may be present 2. Scaffold purity might be a problem	Check origami integrity using gel electrophoresis post-purification

APPENDIX B

LIST OF MODIFIED STAPLE STRANDS FOR SINGLE MOLECULE EXPERIMENTS

Experiment	Description	Sequence
Photobleaching	P1 (9-nt) *P4*	/5AmMC6/ GTAGATTGATTAGATGTAT
	P1P4-A12-H3base128	ATACATCTAGATCAATCTACTTTTCGGAACGGCACCAACCTAAAACGGCGACCTG
	P1P4-B4-H3base256	ATACATCTAGATCAATCTACTTTTCAAGCCCAGGCGGATAAGTGCCGCCTGCCT
	P1P4-H7-H14base303	ATACATCTAGATCAATCTACTTTTAATGAAAGCCCAATAATAAGAGTAAGCAGA
	P1P4-H10-H14base79	ATACATCTAGATCAATCTACTTTTCATTTTGCAACTAAAGTACGGAGAGTACC
	P1P4-G11-H25base128	ATACATCTAGATCAATCTACTTTTCGCACTTACACTGGTGTGTTCCGTTTTCA
	P1P4-H3-H25base256	ATACATCTAGATCAATCTACTTTTAAATCCTTTGGCAAATCAACAGTCGGTCAG
PAINT (45-nm, 6 primary vertices)	P1(10-nt) *	CTAGATGTAT/3AmMO/
	9-nt P1 docking site	ATACATCTATTTT-Strand
	G11-H25base128-HCR-PAINT-large-P1P4-10mer	ATACATCTAGATCAATCTACTTTTCGCACTTACACTGGTGTGTTCCGTTTTCA
	H3-H25base256-HCR-PAINT-large-P1P4-10mer	ATACATCTAGATCAATCTACTTTTAAATCCTTTGGCAAATCAACAGTCGGTCAG
	A12-H3base128-HCR-PAINT-	ATACATCTAGATCAATCTACTTTTCGGAACGGCACCAACCTAAAACGGCGACCTG

	large-P1P4-10mer	
	B4-H3base256-HCR-PAINT-large-P1P4--10mer	ATACATCTAGATCAATCTACTTTTCAAGCCCAGGCGGATAAGTGCCGCCTGCCT
	H7-H14base303-HCR-PAINT-large-P1P4-10mer	ATACATCTAGATCAATCTACTTTTCAAGCCCAGGCGGATAAGTGCCGCCTGCCT
	H10-H14base79-HCR-PAINT-large-P1P4-10mer	ATACATCTAGATCAATCTACTTTTCATTTTGCAACTAAAGTACGGAGAGTACC
	B7-H4base143-PAINT-Large-P1P4-10mer-3P	ATACATCTAGATCAATCTACTTTTCTACGAAGAGGGTAGCAACGGCTACCACGCAT
	F5-H23base128-PAINT-Large-P1P4-10mer-3P	ATACATCTAGATCAATCTACTTTTAAAAAAAGAGCCTCCGGCCAGAGCGCAGGCGC

PAINT (45-nm, 12 secondary vertices)	B10-H4base239-PAINT-Large-P1P4-10mer-3P	ATACATCTAGATCAATCTACTTTTGTTGATATACCACCCTCATTTTCACAGTACAAACTACAA C
	F9-H23base256-PAINT-Large-P1P4-10mer-3P	ATACATCTAGATCAATCTACTTTTCGGGAGAATCCTGATTGTTTGGTCGTATT
	B12-H5base128-PAINT-Large-P1P4-10mer-3P	ATACATCTAGATCAATCTACTTTTCTCCATGTCATAGGCTGGCTGACCTAATTTCA
	G3-H24base143-PAINT-Large-P1P4-10mer-3P	ATACATCTAGATCAATCTACTTTTCGCTGGCCCGCACAGGCGGCCTTAGCCGCCA
	C4-H5base256-PAINT-Large-P1P4-10mer-3P	ATACATCTAGATCAATCTACTTTTATTTCGGACAGAATGGAAAGCGCACCACCC
	G6-H24base239-PAINT-Large-	ATACATCTAGATCAATCTACTTTTCTGAATAATACAGTAACAGTACCGGAAACAG

	P1P4-10mer-3P	
	G11-H13base288-PAINT-Large-P1P4-10mer-3P	ATACATCTAGATCAATCTACTTTTGAGTTAAATAGCAGCCTTTACAGTCTTACCA
	H3-H13base96-PAINT-Large-P1P4-10mer-3P	ATACATCTAGATCAATCTACTTTTAGTTTCATGGTCAATAACCTGTTTGCTAAATC
	A1-H15base288-PAINT-Large-P1P4-10mer-3P	ATACATCTAGATCAATCTACTTTTACGCTAACGCTTATCCGGTATTCTTATCATTC
	A5-H15base96-PAINT-Large-P1P4-10mer-3P	ATACATCTAGATCAATCTACTTTTGGTTGTACAACCCTCATATATTTTAGATCTAC
PAINT (35-nm, 6 vertices)	H4-H14base111-PAINT-small-P1P4-10mer	ATACATCTAGATCAATCTACTTTTCGCAAATTCCATATAACAGTTGCCGGAAGC
	H6-H14base271-	ATACATCTAGATCAATCTACTTTTACATAAAAATCAGAGAGATAACCCGAAACCGA

	PAINT-small-P1P4-10mer	
	E9-H22base143-PAINT-small-P1P4-10mer	ATACATCTAGATCAATCTACTTTTCGGGAACGGATTAAGTTGGGTAACGTGTAGAT
	E12-H22base239-PAINT-mall-P1P4-10mer	ATACATCTAGATCAATCTACTTTTACATAAATAAGACGCTGAGAAGAGGTTTGAA
	C9-H6base143-PAINT-small-P1P4-10mer	ATACATCTAGATCAATCTACTTTTACCAGGCGTACTTAGCCGGAACGATAATGCCA
	C12-H6base239-PAINT-small-P1P4-10mer	ATACATCTAGATCAATCTACTTTTAATTTACCTAAACAGTTAATGCCCTCGAGAGG
Origami labeling	PolyA-Cy3b	/5AmMC6/AAAAAAAAAAAAAAAAAAAA
HCR	I1P1*P4*	CCTCAACCTACCTCCAACTCTCACCATATTCGCTTCTTGTAGATTGATTAGATGTAT
	H1	GAAGCGAATATGGTGAGAGTTGGAGGTAGGTTGAGGCACATTTAAGACCTCAACCTACCTCCAACTCTCAC /C9-dye-3'/
	H2	CCTCAACCTACCTCCAACTCTCACCATATTCGCTTCGTGAGAGTTGGAGGTAGGTTGAGGTCTGTAAATGTG

	P1P4-A12-H3base128	ATACATCTAGATCAATCTACTTTTCGGAACGGCACCAACCTAAAACGGCGACCTG

APPENDIX C

LOW-COST MICROSCOPE PARTS LIST

Part #	Description	Qty	Price	Total	Vendor
MV-CB060-10UM-C	Hikvision 6 MP 1/1.8" CMOS Board Level USB3.0 Camera (Monochrome)	1	$185.00	$185.00	Aegis Electronic Group
MVL-HF5028M-6MP	1/1.8" 50mm F2.8 Manual Iris C-Mount Lens, 6 Megapixel	1	$125.00	$125.00	
PA40X-INF-V300	40X Infinity-corrected Plan Microscope Objective (Spring)	1	$75.99	$75.99	Amscope
ET570lp	ET570lp 25mm Dia Mounted	1	$325.00	$325.00	Chroma
SM1A3	Adapter with External SM1 Threads and Internal RMS Threads	1	$17.44	$17.44	Thorlabs
SM1A25	SM1A25 - Adapter with External M25.5 x 0.5 Threads and Internal SM1 Threads	1	$19.79	$19.79	
SM1Z	Z-Axis Translation Mount, 30 mm Cage Compatible	1	$193.80	$193.80	

SM1L03	SM1 Lens Tube, 0.30" Thread Depth, One Retaining Ring Included	2	$12.16	$24.32	
CMT2	C-Mount (1.00"-32) Coupler, External Threads, 0.5" Long	1	$20.30	$20.30	
ER3-P4	Cage Assembly Rod, 3" Long, Ø6 mm, 4 Pack	1	$25.08	$25.08	
CP12	30 mm Cage Plate with Ø1.2" Bore	2	$20.81	$41.62	
TR1.5	Ø1/2" Optical Post, SS, 8-32 Setscrew, 1/4"-20 Tap, L = 1.5"	2	$4.97	$9.94	
RA90RS	Right-Angle Ø1" to Ø1/2" Post Clamp	2	$26.78	$53.56	
RS6P8E	Ø1" Pedestal Pillar Post, 8-32 Taps, L = 6"	1	$43.86	$43.86	
MB6	Aluminum Breadboard 6" x 6" x 1/2", 1/4"-20 Taps	1	$49.98	$49.98	
TR6	Ø1/2" Optical Post, SS, 8-32 Setscrew, 1/4"-20 Tap, L = 6"	4	$6.91	$27.64	

TR8	Ø1/2" Optical Post, SS, 8-32 Setscrew, 1/4"-20 Tap, L = 8"	1	$8.28	$8.28	
SWC	Rotating Clamp for Ø1/2" Posts, 360° Continuously Adjustable, 3/16" Hex	1	$23.56	$23.56	
RA90	Right-Angle Clamp for Ø1/2" Posts, 3/16" Hex	1	$9.76	$9.76	
	10-20 mW 532nm green laser pointer	1	$12.88	$12.88	Laserland
180051US	DC-DC converter	1	$10.47	$10.47	Amazon
TOTAL				$1303.27	